INTERATOMIC INTERACTIONS AND DYNAMICS OF ATOMIC AND DIATOMIC LATTICES

by

Khaled Awni Touqan

B.E. American University of Beirut
(1977)

M.S. University of Michigan
(1978)

Submitted to the Department of
Nuclear Engineering
in Partial Fulfillment of the
Requirements of the
Degree of

DOCTORATE IN PHILOSOPHY

at the

MASSACHUSETTS INSTITUTE OF TECHNOLOGY

May 1982

Signature of Author _____
Department of Nuclear Engineering
May 19, 1982

Certified by _____
Thesis Supervisor

Certified by _____
Thesis Supervisor

Accepted by _____
Chairman, Departmental Committee on Graduate Students

INTERATOMIC INTERACTIONS AND DYNAMICS OF ATOMIC AND DIATOMIC LATTICES

by

Khaled Awni Touqan

Submitted to the Department of Nuclear Engineering on May 19, 1982 in partial fulfillment of the requirements for the Degree of Doctor of Philosophy in Nuclear Engineering

ABSTRACT

A study of interatomic interactions in the halogen crystals is carried out using two models. A lattice dynamical model based on central force pair interactions between atoms is proposed. The force constants are derived by fitting the model to observed Raman and infrared frequencies at the zone center. In the case of iodine, phonon dispersion relations are calculated along the symmetry directions [010] and [001]. Agreement between the theoretical calculations and phonon frequencies measured by neutron scattering is within 10%. For the cases of chlorine and bromine where neutron data is not available, phonon dispersion curves along [001] are predicted. The eigenvectors of all the modes at the zone center are presented to clarify the existing ambiguity in the symmetry assignment in the literature. A simple procedure for evaluating the slopes of the acoustic modes at the zone center is given based on a second order perturbation theory. The elastic constants along the [001] direction for the three halogens are given.

An interatomic potential model for halogen crystals based on central dispersion-repulsion forces and noncentral electrostatic charge interactions is also proposed. The electronic charge around each atom is represented by a dipole and the molecule as a whole acts like a quadrupole. The ten potential parameters are determined by fitting the model to the observed static and dynamic properties for each of chlorine, bromine and iodine. The static properties include the equilibrium conditions for a given atom in the crystal and the cohesive energy of the lattice. The dynamic properties constitute nine experimental zone center frequencies determined by Raman and infrared measurements. Phonon dispersion relations are then calculated along the symmetry directions [100], [010] and [001]. In the case of iodine, agreement between the calculations and measured phonon frequencies is good along the [001] direction and less so along the [010] direction. For the cases of chlorine and bromine, phonon dispersion curves along [100], [010] and [001] are predicted. Values of the quadrupole moments for each of the halogens are calculated using the determined potential parameters. The elastic constants along the [001] direction for the three halogens are given.

The determination of minimum free energy structures for atomic lattices is carried out using computer molecular dynamics with periodic flexible boundary conditions at constant pressure. The application of this technique to a two dimensional Lennard-Jones crystal structure correctly predicts the triangular lattice as the most stable one. A transition from a square lattice to a triangular one is successfully observed by applying this technique.

Thesis Supervisor: Dr. Sow-Hsin Chen
Title: Professor of Nuclear Engineering

Thesis Supervisor: Dr. Sidney Yip
Title: Professor of Nuclear Engineering

TABLE OF CONTENTS

TO MY PARENTS

AWNI AND NAHIDA

List of Tables

List of Figures

List of Figures (continued)

List of Figures (continued)

Acknowledgement

I would like to thank my thesis supervisors, Professor Sow-Hsin Chen and Professor Sidney Yip for their guidance and encouragement throughout the course of this work. Their financial support during my stay at the Massachusetts Institute of Technology is greatly appreciated.

I also would like to express my gratitude to colleagues H. Ettouney, R. Jishi and my brother, Majed, for fruitful discussions during the course of this work. Thanks are due to Ms. Donna Dutton for typing the thesis.

I wish to thank the Department of Nuclear Engineering at the Massachusetts Institute of Technology for the Theos J. Thompson Memorial Fellowship granted for the academic year of 1980-81.

This research is supported by the National Science Foundation.

Chapter 1

INTRODUCTION

I. BACKGROUND

An important branch of solid state physics is the representation of interatomic and intermolecular interactions by appropriate potential functions. Given a proper Hamiltonian one may in principle compute static properties determined explicitly by the potential such as crystal structure, cohesive energy, and P-V data as well as phonon dispersion curves and all dynamic dependent properties such as specific heat and thermal expansion. This ambitious route is one which contemporary theory treads with limited success even on simple systems as ideal as solid nitrogen. Of course, for the great majority of observables experimental precision is far greater than theory can achieve with reasonable cost and labor. It is not the function of theory in those cases to improve upon existing numerical data, but rather to produce a valid coherent physical structure consistent with known data and from this to compute other interesting properties that have not been prescribed adequately, if at all, by experiment. Since a quantum mechanical calculation for the interaction energy of many electron systems is formidable even for simple systems such as the inert gases, phenomenological potentials are therefore invariably used.

Historically the quantitative study of potential functions was initiated by Mie in 1906, by Grüneisen in 1912

and by Born and coworkers in connection with the study of solids. In 1924 Lennard-Jones began the serious study of gas properties, extended later to include both solid and liquid properties. In the 1940's De Boer and coworkers and Hirschfelder and coworkers made extensive contributions. By the beginning of the 1960's the "Lennard-Jones 6:12 potential" and the "exp-6" potential were widely used for representing data, and generally regarded as satisfactory quantitative representation of real potentials.

The simplest systems that were initially investigated were the monoatomic inert gas solids. In general, one starts by assuming that the potential energy U corresponding to a given configuration of N nuclei specified by their position vectors $\vec{r}_1,\ldots,\vec{r}_N$ is given by

$$U(\vec{r}_1\ldots\vec{r}_N) = \sum_{i<j=1}^{N} U_2(\vec{r}_i,\vec{r}_j) + \sum_{i<j<k=1}^{N} U_3(\vec{r}_i,\vec{r}_j,\vec{r}_k)+\ldots \quad (1.1)$$

in which U_2, U_3 are pair and triplet potential functions, and the series is in principle an infinite one. The pair potential depends only on the internuclear distance and may be written as $U(R_{ij})$. The triplet potential U_3 approaches zero whenever one of the atoms becomes very far away from the other in the set. In the case of inert gases, the three body potentials contribute appreciably (about 7% of the cohesive energy of crystalline argon (1)). Higher

terms appear to be negligible at the present level of experimental and computational accuracy. In the discussion of the inert gases, we will specifically concentrate on argon because most of the techniques for studying potential functions have been developed using argon, for which more extensive experimental data are available.

The "traditional" potential for argon was the 6:12 potential with parameters $\frac{\varepsilon}{k} = 119.8^{o}K$, $\sigma = 3.405$ Å, determined by Michels, Wijker and Wijker (2) from second virial coefficients at temperatures above $273^{o}K$. Guggenheim and McGlashan (3) pointed out the error of a factor of about 2 in the long-range R^{-6} term, and reanalyzed solid state data, neglecting many-body interactions, and derived a piece-wise analytic potential with $\frac{\varepsilon}{k} \sim 138^{o}K$ and approximately correct long-range behavior. Barker, Fock and Smith (4) showed that the Guggenheim and McGlashan potential did not agree well with experimental viscosities due to inadequacies in the repulsive region, and used second virial coefficients and viscosities to derive a Kihara potential which was surprisingly close to the best modern estimates. This potential also gave a good value for the long-range coefficient of R^{-6}. However, it did not reproduce the experimental solid cohesive energy, suggesting that many-body interactions were present. Further refinements were done for the potential of argon, the most noteworthy of which is the potential derived by Barker, Fisher and Watts

(5). Work on krypton, xenon, neon and helium proceeded in parallel to the study of argon.

The second phase of the potential study was to consider the next simplest systems which constituted the diatomic molecular solids. Analytical forms were also developed for the intermolecular potential. This offered the advantage of making possible the calculation of a wide range of crystal properties from the same intermolecular potential such as the crystal structure, the thermodynamic and several dynamical properties. The intermolecular forces are normally classified in terms of their interaction radius as short, medium and long range forces or, on the basis of their nature, as repulsive, dispersion, induction, electrostatic and polarization forces. The term Van der Waals includes the short range repulsive, dispersion and induction forces. A direct calculation of the Van der Waals energy from the knowledge of the electronic structure of the molecules is a formidable task even for small molecules and has been actually performed only for very simple systems such as hydrogen. Phenomenological potentials are therefore used in the static and dynamic crystal calculations. Theoretically constructed potential functions for the crystal have invariably been based on the pair approximation, i.e. it is assumed that the total potential energy may be written as a sum of terms representing only the interaction between different pairs of molecules. Within the pair

potential framework two main approaches have been taken. On the one hand the molecule is regarded as an entity and the intermolecular interactions are treated accordingly. In the second approach the intermolecular potential is further dissected into a sum of atom-atom potentials, each depending on interatomic separation R_{ij}. The first approach will be discussed in the case of nitrogen. The second approach is the one which we shall use for the halogens. The nearest intermolecular interatomic distance is smaller than the Van der Waals diameter in all three halogens which makes the treatment of the molecule as a separate entity not realistic.

We will first dwell on the case of nitrogen. The intermolecular potential of nitrogen is not satisfactorily understood despite a large number of forays each of which can claim some success. Experimental data exist to subject any trial potentials to critical examination and under this scrutiny all so far proposed fail in varying degrees. The essential difference between molecular solids and atomic solids such as argon is the presence of anisotropic terms in the intermolecular potential of the former governing orientational ordering and librational vibrations. Various analytical forms of the intermolecular potential have been employed. Following preliminary calculations by Jansen and De Wette (6), Kohin (7) performed the first elaborate computation on the low-temperature low-pressure phase of

nitrogen in 1960. The potential adopted by Kohin to represent the interaction between nitrogen molecules consists of three parts: (a) a molecular quadrupole-quadrupole interaction, (b) a dipole-dipole dispersive attraction, (c) a parametric short-range repulsion representing exchange and overlap. Calculation of the crystal energy at $0^{o}K$ fitted the experimental value to 2.2%. Nonetheless, many other quantities computed with this potential are found to be in very poor agreement with experiment. For example, librational frequencies calculated in the small-angle harmonic approximation are too large by almost a factor of two, and the order parameter describing molecular orientation is much higher than the experimental value. Kjems and Dolling (8) performed inelastic neutron scattering measurements to determine translational and librational lattice modes in a single crystal of solid nitrogen in the cubic α-phase at $15^{o}K$. Calculations based on a general potential function which includes Lennard-Jones or exp-6 interactions as well as electric quadrupole forces, gave good agreement between both the observed frequencies and intensities and their calculated counterparts. Further work to account for other experimental data is expected in this field.

In the case of halogens, the intermolecular potential is taken as the sum of the interatomic interactions (9,10). The main assumption is the additivity of atomic contributions in the molecule-molecule interaction. A number of analytical

functions have been proposed in the literature to represent the atom-atom potential. The most widely used are the Lennard-Jones and exp-6 potential. The atom-atom potential is undoubtedly a simple and crude approximation. Despite this, it has been used often to represent the total intermolecular interaction and in many cases, specially for molecules containing only hydrogen and carbon atoms, it has been found that it works extremely well in reproducing crystal structures, energies and vibrational frequencies. The central nature of the atom-atom potential has as a consequence an isotropy of the interaction around the atom, that is clearly unrealistic for atoms linked by chemical bonds or for atoms with lone pairs or involved in delocalized π electron systems. Attempts to obtain anisotropic atom-atom potentials have been made very recently. The simplest solution is the use of atom-atom coefficients including an angular dependence.

Another important contribution to the intermolecular potential is the electrostatic interaction between the charge distributions of the molecules. Two main approaches have been used to represent this type of interaction. The first is to localize charge, fractions of charge or even dipoles on the atoms or in the bonds. The second is to represent the charge distribution by an expansion in terms of point multipoles at the center of charges. Both approaches have their advantages and disadvantages. The use of discrete

charges is for instance simple, but there is no unique way of partitioning the charge distribution and this introduces a considerable amount of uncertainty in the problem. Furthermore, serious problems of convergence rise in the lattice sums. Similar considerations can be made for the point dipoles localized on the atoms or in the bonds. In this case the convergence problem is less serious, but the uncertainty in the values of these formal dipoles remain a major problem. The multipole expansion has the advantage that a precise functional form is furnished by the theory and that the molecular multipoles are often available as experimental quantities or, if not, can be calculated with sufficient accuracy. It has however the drawback of being not valid for close-packed neighboring molecules whose charge distributions overlap.

In our study of halogens, the intermolecular potential is taken as the sum of central potentials and electrostatic interactions. The intramolecular interaction being of the order of magnitude as the intermolecular counterpart makes such approach more appropriate. The electrostatic charge is represented by dipoles localized in the vicinity of the nuclear centers. Other work in the literature adopted the same approach though different patterns of potentials and charges have been used (11,12). Attempts so far to produce all the known properties of the halogens are fair to good. On the one hand, work has been done to reproduce the known

Ccmb structure starting with a given potential by minimizing the static energy of the lattice (13,14). On the other hand, the measured dynamic properties of the crystals, infrared and Raman active zone-center frequencies in addition to phonon dispersion curves have been studied using different sets of potentials (10-12). In our work we started with the given structure of the crystal and derived the cohesive energy and phonon dispersion curves using an interatomic potential model.

The determination of the structure of the crystal is an interesting topic to discuss. Thus far the stable structure of the crystal is the one that minimizes the lattice energy. This inherently assumes that one is working at $0^{o}K$. However, in most of these studies, the experimental data available is always at some higher temperatures. In the case of halogens, the present data is in the temperature range of $70\text{-}110^{o}K$. In such cases, where one is focusing on studying both static and dynamic properties, minimization of the free energy rather than the lattice energy should be undertaken. Computer molecular dynamics offers such a technique. A molecular simulation may be carried out at the given temperature using flexible boundary conditions to seek the minimum free energy structure. The term flexible boundary is used here to indicate that the boundary can change volume as well as shape, as opposed to a fixed rigid boundary. This technique offers the advantage of carrying out the simulation isobarically. Our work has focused on testing the applicability of this technique

to determine minimum energy structures. Two dimensional crystal lattices are investigated.

Our study may be divided into three major parts. In the first part a general study of the validity of central force potentials for halogens is undertaken. Force constants are derived from a given central force potential and fitted to zone-center frequencies. The agreement between the fitted and calculated frequencies at the zone-center and finite $|\vec{q}|$ looks to be very good indicating that central potentials may still be applied as a major component in the development of a potential for the halogens. The actual development of a potential to fit the static and dynamic properties of the crystal is done in the second part. Morse, Buckingham and electrostatic charge interactions are employed to calculate lattice energies and measured phonon dispersion curves for the halogens. Agreement between the calculated properties and the experimental ones is fair to good. In the last part a scheme to study minimum free energy structures using computer molecular dynamics is constructed. An isobaric, flexible boundary simulation is carried out to study minimum energy structures for two dimensional systems. The scheme is successful in predicting such structures where a thorough investigation of thermodynamic properties is possible.

II. REFERENCES

1. Barker, J.A. and Pompe, A. 1968 Aust. J. Chem. 21, 1683.

2. Michele, A., Wijker, Hk. and Wijker, Hub. 1949 Physica 15, 627.

3. Guggenheim, E.A. and McGlashan, M.L. 1960 Proc. Roy. Soc. London A255, 456.

4. Barker, J.A., Fock, W. and Smith F. 1964 Phys. Fluids 7, 897.

5. Barker, J.A., Fisher, R.A. and Watts, R.O. 1971 Mol. Phys. 21, 657.

6. Jansen, L. and De Wette, F.W. 1955 Physica 21, 83.

7. Kohin, B.C. 1960 J. Chem. Phys. 33, 882.

8. Kjems, J.K. and Dolling, G. 1975 Phys. Rev. B11, 1639.

9. Toukan, K. and Chen, S.H. 1981 Mol. Phys. 44, 693.

10. Dumas, G.G., Vovelle, F. and Viennot, J.P. 1974 Mol. Phys. 28, 1345.

11. Pasternak, A., Anderson, A. and Leech, J.W. 1977 J. Phys. C: Solid St. Phys. 10, 3261.

12. Pasternak, A., Anderson, A. and Leech, J.W. 1978 J. Phys. C: Solid St. Phys. 11, 1563.

13. Nyburg, S.C. 1964 J. Chem. Phys. 40, 2493.

14. Nyburg, S.C. and Wong-Ng, W. 1979 Proc. Roy. Soc. Lond. A. 367, 29.

Chapter 2

LATTICE DYNAMICS OF HALOGEN CRYSTALS

I. INTRODUCTION

The solid halogens, chlorine, bromine and iodine form an interesting group of isomorphic molecular crystals. Their crystal structure is relatively simple: the lattice is one-face-centered orthorhombic, space-group Ccmb (D_{2h}^{18}), with two diatomic molecules per primitive unit cell stacked in a planar arrangement as shown in Figure 2-1 (a). Collin (1) has measured the structure of chlorine at 38°K. The structure of bromine and iodine has been measured by Vonnegut and Warren (2) and Van Bolhuis et al. (3) at 123°K and 110°K respectively. The nearest intermolecular atom-atom distance is smaller than the Van der Waals diameter in all three crystals: by 0.8 A° in iodine, 0.6 A° in bromine and 0.25 A° in chlorine. This indicates that solid halogens depart from the ideal picture of molecular crystals. The internal and external vibrations of the crystalline halogens have been extensively studied by Raman scattering and infrared absorption at the zone-center (4,5). Comparison of the two sets of measurements shows that they have some disagreement with regard to the assignment of the observed Raman active frequencies in chlorine and bromine. Anderson et al. (4) assign the highest frequency mode to a B_{3g} mode while Suzuki et al. (5)

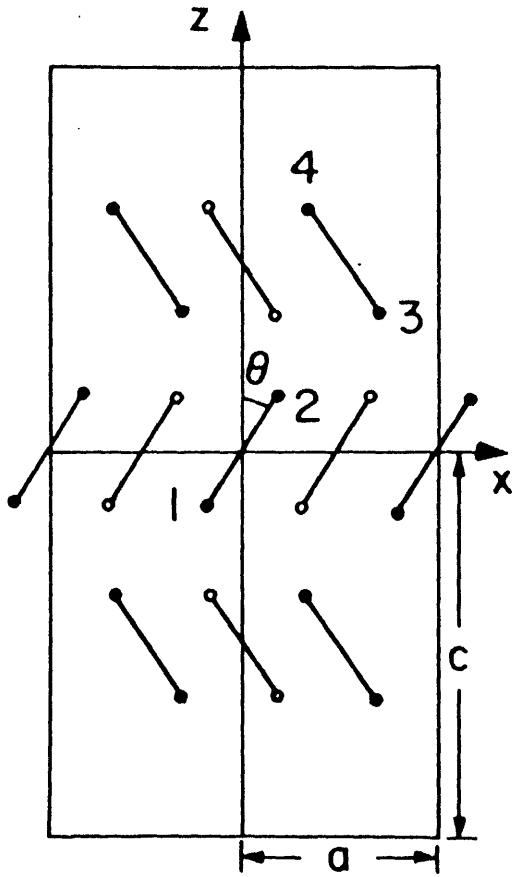

(a)

Figure 2-1(a). Structure of the halogen crystals. Full circles indicate atoms at y = 0; open circles indicate atoms at $y = \pm\frac{b}{2}$.

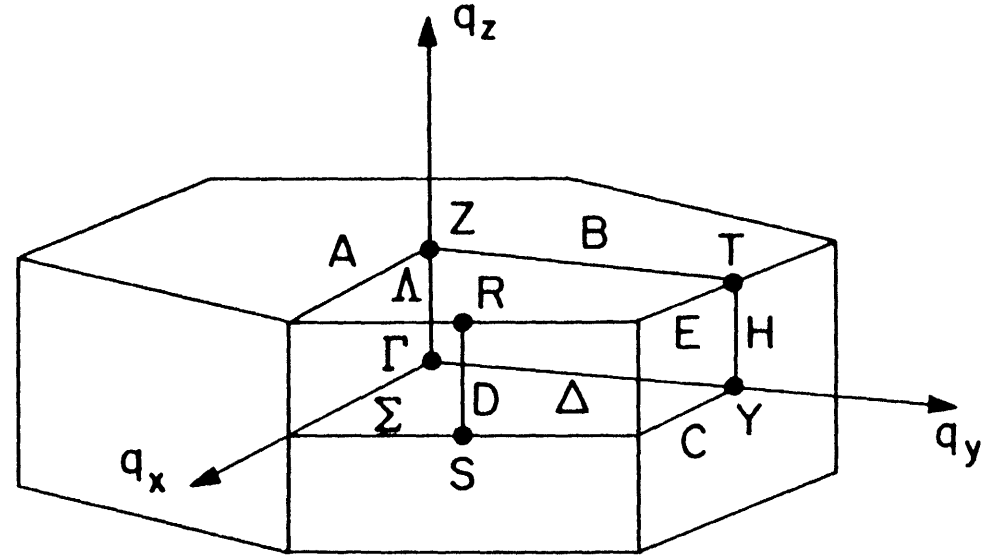

(b)

Figure 2-1(b). The Brillouin zone for the one-face centered orthorhombic lattice (a < b).

assign it to an A_g mode. Smith et al. (6,7) have measured the phonon dispersion curves of iodine at 77°K along [010] and [001] directions using inelastic neutron scattering. The latter workers have made a lattice dynamics calculation based on rigid diatomic molecules interacting through two atom-atom potential energy functions of the Buckingham-six type. The results give only a qualitative agreement with the experimental measurements.

Extensive theoretical studies have shown that the inclusion of Lennard-Jones and Buckingham interactions alone in the lattice dynamical calculations leads to mode instabilities (8-11). Pasternak, Anderson and Leech (12, 13) have suggested a simple bond-charge potential for the three halogens. The potential employed is the sum of the electrostatic interaction between nuclei and electrons, and the electronic kinetic energy. Mode instabilities of previous models are absent in their calculations, however discrepancies with the experimental lattice vibrational frequencies still exist. The calculated A_u mode in iodine differs from the experimental one by 23%, the calculated B_{1u} mode in bromine differs from the observed one by 21%. The lower phonon branches in iodine show poor agreement with the experimental neutron data in [001] direction.

Since the lattice dynamical models based on atom-atom potentials have not been successful in predicting the available experimental data on the halogens, we used a general

central force model to test the applicability of the central potentials in these systems. The measured zone-center frequencies for iodine, bromine and chlorine are reproduced to an accuracy of 1%. The availability of the force constants of the model may make the construction of such potentials easier. At the same time this model could also be used to predict the dynamic structure factor necessary for the assignment of phonon groups as measured by inelastic neutron scattering in the three halogens. Applications of this model to predict phonon dispersion relations along [010] and [001] directions in iodine gives 10% agreement between the theoretical calculations and the experimental measurements performed by Smith et al. (6,7). This indicates that the central force model is a good description of the type of interactions that exist in the halogen crystals contrary to earlier conclusions by Suzuki et al. (8).

In Section II, we develop the central force model used. The dynamical matrix is written in terms of ten parameters at the zone-center. In Section III, we give analytical expressions for the eigenvalues and eigenvectors at the zone-center. The numerical values of the ten paramters are obtained by fitting the eigenvalues to the nonzero experimental frequencies for each of the three halogens. Our results confirm the symmetry assignment of Suzuki et al. (5). In Section IV we develop a general method for evaluating the elastic constants along any symmetry direction in a given crystal. The method employs the eigenvectors of the dynamical

matrix at the zone-center to evaluate the elastic constants using second order perturbation theory. The elastic constants C_{33}, C_{44} and C_{55} for [001] direction are evaluated in all three halogens. In Sective V, we compare the phonon dispersion curves for iodine with the neutron inelastic scattering data. We predict the phonon dispersion curves for chlorine and bromine in [001] direction. Table 2-5 gives in detail the character tables for the points Γ, Δ and Z of the Brillouin zone.

II. A LATTICE DYNAMICS MODEL FOR HALOGEN CRYSTALS

The lattice dynamical model assumes a two body central potential between a given pair of atoms $\begin{pmatrix} l & l' \\ k & k' \end{pmatrix}$ of the form $V_{kk'}(r)$ which depends only on the magnitude of the separation between the atoms. The force constants for a pair of atoms $\begin{pmatrix} l & l' \\ k & k' \end{pmatrix}$ is (14),

$$\Phi_{\alpha\beta}\begin{pmatrix} l & l' \\ k & k' \end{pmatrix} = -\left[\frac{1}{r} V'_{kk'}(r)\left\{\delta_{\alpha\beta} - \frac{r_\alpha r_\beta}{r^2}\right\} + \frac{r_\alpha r_\beta}{r^2} V''_{kk'}(r)\right]$$

where $\vec{r}\begin{pmatrix} l & l' \\ k & k' \end{pmatrix} = r\begin{pmatrix} l \\ k \end{pmatrix} - \vec{r}\begin{pmatrix} l' \\ k' \end{pmatrix}$, is the vector joining atoms $\begin{pmatrix} l \\ k \end{pmatrix}$ and $\begin{pmatrix} l' \\ k' \end{pmatrix}$

$$r = \left|\vec{r}\begin{pmatrix} l & l' \\ k & k' \end{pmatrix}\right| \tag{2.1}$$

It is observed that the force constants are characterized by two parameters, namely, the first and second derivatives

of the pair potential. Also it is noted that if two atoms are coplanar, i.e. either r_α or $r_\beta = 0$, then

$$\Phi_{\alpha\beta}\begin{pmatrix} l & l' \\ k & k' \end{pmatrix} = \Phi_{\alpha\alpha}\,\delta_{\alpha\beta} \tag{2.2}$$

The four atoms forming the basis of a primitive unit cell are designated by numbers 1 to 4 in Figure 2-1(a). The primitive lattice translation vectors are given by,

$$\begin{aligned} \vec{t}_1 &= \frac{1}{2}(a\vec{i} + b\vec{j}) \\ \vec{t}_2 &= a\vec{i} \\ \vec{t}_3 &= c\vec{k} \end{aligned} \tag{2.3}$$

where a, b, c are the orthorhombic unit cell dimensions. The Brillouin zone and associated symmetry directions and symmetry points on its surface are given in Figure 2-1(b).

The dynamical matrix is written according to the definition,

$$D_{\alpha\beta}\begin{pmatrix} \vec{q} \\ k & k' \end{pmatrix} = \frac{1}{M}\sum_{l'} \Phi_{\alpha\beta}\begin{pmatrix} l & l' \\ k & k' \end{pmatrix} \exp\left\{ i\vec{q} \cdot \left[\vec{r}\begin{pmatrix} l' \\ k' \end{pmatrix} - \vec{r}\begin{pmatrix} l \\ k \end{pmatrix} \right] \right\} \tag{2.4}$$

where $\vec{q}$ is the wave vector, M is the atomic mass. The Λ-direction in this lattice is a special symmetry direction. Within the central-force model up to the second nearest

$$
\begin{bmatrix}
\alpha & 0 & \beta_1 & -\alpha_1-\Delta_1\tau & 0 & -\beta_1 & -\alpha_2-\Delta_2\tau & 0 & 0 & -\alpha_3-\Delta_3\tau & 0 & 0 \\
0 & \gamma & 0 & 0 & -\gamma_1-\phi_1\tau & 0 & 0 & -\gamma_2-\phi_2\tau & 0 & 0 & -\gamma_3-\phi_3\tau & 0 \\
\beta_1 & 0 & \zeta & -\beta_1 & 0 & -\zeta_1-\eta_1\tau & 0 & 0 & -\zeta_2-\eta_2\tau & 0 & 0 & -\zeta_3-\eta_3\tau \\
-\alpha_1-\Delta_1\tau & 0 & -\beta_1 & \alpha & 0 & \beta_1 & -\alpha_3-\Delta_3\tau & 0 & 0 & -\alpha_2-\Delta_2\tau & 0 & 0 \\
0 & -\gamma_1-\phi_1\tau & 0 & 0 & \gamma & 0 & 0 & -\gamma_3-\phi_3\tau & 0 & 0 & -\gamma_2-\phi_2\tau & 0 \\
-\beta_1 & 0 & -\zeta_1-\eta_1\tau & \beta_1 & 0 & \zeta & 0 & 0 & -\zeta_3-\eta_3\tau & 0 & 0 & -\zeta_2-\eta_2\tau \\
-\alpha_2-\Delta_2\tau & 0 & 0 & -\alpha_3-\Delta_3\tau & 0 & 0 & \alpha & 0 & -\beta_1 & -\alpha_1-\Delta_1\tau & 0 & \beta_1 \\
0 & -\gamma_2-\phi_2\tau & 0 & 0 & -\gamma_3-\phi_3\tau & 0 & 0 & \gamma & 0 & 0 & -\gamma_1-\phi_1\tau & 0 \\
0 & 0 & -\zeta_2-\eta_2\tau & 0 & 0 & -\zeta_3-\eta_3\tau & -\beta_1 & 0 & \zeta & \beta_1 & 0 & -\zeta_1-\eta_1\tau \\
-\alpha_3-\Delta_3\tau & 0 & 0 & -\alpha_2-\Delta_2\tau & 0 & 0 & -\alpha_1-\Delta_1\tau & 0 & \beta_1 & \alpha & 0 & -\beta_1 \\
0 & -\gamma_3-\phi_3\tau & 0 & 0 & -\gamma_2-\phi_2\tau & 0 & 0 & -\gamma_1-\phi_1\tau & 0 & 0 & \gamma & 0 \\
0 & 0 & -\zeta_3-\eta_3\tau & 0 & 0 & -\zeta_2-\eta_2\tau & \beta_1 & 0 & -\zeta_1-\eta_1\tau & -\beta_1 & 0 & \zeta
\end{bmatrix} \tag{2.5}
$$

$\alpha = \alpha_1 + \alpha_2 + \alpha_3 + \Delta_0\tau$

$\gamma = \gamma_1 + \gamma_2 + \gamma_3 + \phi_0\tau$

$\zeta = \zeta_1 + \zeta_2 + \zeta_3 + \eta_0\tau$

$\tau = 1 - \cos\left(\frac{qb}{2}\right)$

neighbor for a given pair of the atomic basis, the dynamical matrix in the Λ-direction can be written in terms of the same ten parameters used in constructing the dynamical matrix at the zone-center. The zone boundary Z is an interesting high symmetry point (see Table 2-5(c) in Section V). where owing to the time reversal symmetry, all branches are doubly degenerate. Other symmetry directions are more complicated. For example, in the Δ-direction the dynamical matrix, within the same model, has to be written in terms of 22 parameters. The twenty-two parameters include the ten parameters determined at the zone-center in addition to twelve others. We give the complete dynamical matrix for the Δ direction in (2.5).

III. EVALUATION OF THE DYNAMICAL MATRIX

The eigenvalues and eigenvectors of the dynamical matrix are determined explicity at the zone-center by solving the secular equation

$$\text{Det } |\bar{D}(0) - \omega^2 \bar{I}| = 0 \qquad (2.6)$$

Table 2-1(a) lists the analytical expressions for the eigenvalues of the dynamical matrix at the zone-center. The experimental frequencies of iodine, bromine and chlorine are listed (13). Table 2-1(b) lists the corresponding expressions for the eigenvectors. The nine nonzero eigenvalues are matched to the squares of the corresponding experimental frequencies. The matching is done by identifying each eigenvector with the corresponding symmetry element of

Table 2-1(a) Calculated and observed phonon frequencies for iodine, bromine, and chlorine at the zone-center (cm^{-1}).

Eigenvalues	I_2		Br_2		CL_2	
	Exp.	Calc.	Exp.	Calc.	Exp.	Calc.
$\omega^2\ (B_{3u}^1) = 0.0$	------	0.0	------	0.0	------	0.0
$\omega^2\ (B_{2u}) = 0.0$	------	0.0	------	0.0	------	0.0
$\omega^2\ (B_{1u}^1) = 0.0$	------	0.0	------	0.0	------	0.0
$\omega^2\ (A_u) = 2\ (\gamma_2 + \gamma_3)$	30.67	30.69	------	32.99	------	47.49
$\omega^2\ (B_{1u}^2) = 2\ (\alpha_2 + \alpha_3)$	40.00	40.00	49.00	48.99	62.00	61.99
$\omega^2\ (B_{1g}) = 2\ (\gamma_1 + \gamma_2)$	41.67	41.69	51.50	51.49	80.00	80.00
$\omega^2\ (B_{3g}) = 2\ (\gamma_1 + \gamma_3)$	57.67	57.69	70.50	70.49	96.00	95.97
$\omega^2\ (B_{3u}^2) = 2\ (\zeta_2 + \zeta_3)$	65.33	65.29	74.00	73.99	90.00	89.99
$\omega^2\ (A_g^1) = \alpha_1 + \alpha_2 + \zeta_1 + \zeta_3 - \sqrt{(\alpha_1 + \alpha_2 - \zeta_1 - \zeta_3)^2 + 4\beta_1^2}$	75.33	75.31	81.50	81.58	96.00	95.99
$\omega^2\ (B_{2g}^1) = \alpha_1 + \alpha_3 + \zeta_1 + \zeta_2 - \sqrt{(\alpha_1 + \alpha_3 - \zeta_1 - \zeta_2)^2 + 4\beta_1^2}$	87.33	87.40	95.00	95.07	112.00	111.97
$\omega^2\ (B_{2g}^2) = \alpha_1 + \alpha_3 + \zeta_1 + \zeta_2 + \sqrt{(\alpha_1 + \alpha_3 - \zeta_1 - \zeta_2)^2 + 4\beta_1^2}$	180.67	180.69	296.00	295.97	538.00	537.99
$\omega^2\ (A_g^2) = \alpha_1 + \alpha_2 + \zeta_1 + \zeta_3 + \sqrt{(\alpha_1 + \alpha_2 - \zeta_1 - \zeta_3)^2 + 4\beta_1^2}$	189.33	189.31	301.00	300.97	539.00	538.99

Table 2-1(b)

Eigenvectors of the dynamical matrix at the zone-center.

B_{3u}^1	B_{2u}	B_{1u}^1	A_u	B_{1u}^2	B_{1g}	B_{3g}	B_{3u}^2	A_g^1	B_{2g}^1	B_{2g}^2	A_g^2
1/2	0	0	0	1/2	0	0	0	$1/N_1$	$-1/N_2$	$1/N_3$	$-1/N_4$
0	1/2	0	1/2	0	1/2	-1/2	0	0	0	0	0
0	0	1/2	0	0	0	0	1/2	X_1/N_1	X_2/N_2	X_3/N_3	X_4/N_4
1/2	0	0	0	1/2	0	0	0	$-1/N_1$	$1/N_2$	$-1/N_3$	$1/N_4$
0	1/2	0	1/2	0	-1/2	1/2	0	0	0	0	0
0	0	1/2	0	0	0	0	1/2	$-X_1/N_1$	$-X_2/N_2$	$-X_3/N_3$	$-X_4/N_4$
1/2	0	0	0	-1/2	0	0	0	$-1/N_1$	$-1/N_2$	$1/N_3$	$1/N_4$
0	1/2	0	-1/2	0	-1/2	-1/2	0	0	0	0	0
0	0	1/2	0	0	0	0	-1/2	X_1/N_1	$-X_2/N_2$	$-X_3/N_3$	X_4/N_4
1/2	0	0	0	-1/2	0	0	0	$1/N_1$	$1/N_2$	$-1/N_3$	$-1/N_4$
0	1/2	0	-1/2	0	1/2	1/2	0	0	0	0	0
0	0	1/2	0	0	0	0	-1/2	$-X_1/N_1$	X_2/N_2	X_3/N_3	$-X_4/N_4$

$$X_1 = \frac{(\zeta_1 + \zeta_3 - \alpha_1 - \alpha_2) - \sqrt{(\zeta_1 + \zeta_3 - \alpha_1 - \alpha_2)^2 + 4\beta_1^2}}{2\beta_1}$$

$$X_2 = \frac{-(\zeta_1 + \zeta_2 - \alpha_1 - \alpha_3) + \sqrt{(\zeta_1 + \zeta_2 - \alpha_1 - \alpha_3)^2 + 4\beta_1^2}}{2\beta_1}$$

$$X_3 = \frac{(\zeta_1 + \zeta_2 - \alpha_1 - \alpha_3) + \sqrt{(\zeta_1 + \zeta_2 - \alpha_1 - \alpha_3)^2 + 4\beta_1^2}}{2\beta_1}$$

$$X_4 = \frac{-(\zeta_1 + \zeta_3 - \alpha_1 - \alpha_2) - \sqrt{(\zeta_1 + \zeta_3 - \alpha_1 - \alpha_2)^2 + 4\beta_1^2}}{2\beta_1}$$

$$N_i = 2\sqrt{1 + X_i^2} \qquad i = 1,2,3,4$$

the group D_{2h}^{18}, Table 2-5. A strong intramolecular bond is assumed to exist between the atoms of a single molecule compared to other intermolecular bonds. Thus, for the atomic pair (1, 2) one can write,

$$\left.\frac{\partial V_{12}(r)}{\partial r}\right|_{r = R_{12}} = 0 \qquad (2.7)$$

henceforth,

$$\frac{\alpha_1}{\zeta_1} = \tan^2 \theta$$

where θ is the angle that the molecule subtends with the Z axis, Figure 2-1(a). Determination of the ten parameters appearing in the dynamical matrix at the zone-center, is done by solving explicitly for the squares of the nine nonzero zone-center frequencies in addition to the ratio $\left(\frac{\alpha_1}{\zeta_1}\right)$. The discrepancy between the calculated frequencies and the observed ones is less than 1% for all modes in all three halogens. Table 2-2 lists the ten parameters for each of the three halogens.

The dynamical matrix for iodine is solved in the Δ direction, Figure 2-1(b), and fitted to the experimental neutron data (6, 7) in order to determine the interplanar constants. Table 2-3 lists these constants for the case of iodine.

Table 2-2 The ten parameters for each of iodine, bromine and chlorine as determined at the zone-center. ($X10^4 cm^{-2}$)

	α_1	α_2	α_3	γ_1	γ_2	γ_3	ζ_1	ζ_2	ζ_3	β_1
I_2	0.5391	-0.0450	0.1250	0.1031	-0.0162	0.0633	1.3593	-0.0089	0.2221	0.5227
Br_2	1.3285	-0.0641	0.1842	0.1633	-0.0307	0.0852	3.3216	-0.0023	0.2761	1.7440
CL_2	4.1519	-0.04945	0.2416	0.3340	-0.0140	0.1268	10.5920	0.1131	0.2918	6.1612

Table 2-3 Interplanar constants for iodine ($X10^4 cm^{-2}$)

$\Delta_0 = 0.02$	$\phi_0 = 0.1104$	$\eta_0 = 0.0088$
$\Delta_1 = 0.0$	$\phi_1 = -0.0366$	$\eta_1 = 0.0$
$\Delta_2 = 0.0$	$\phi_2 = 0.0013$	$\eta_2 = 0.0$
$\Delta_3 = 0.0$	$\phi_3 = -0.0167$	$\eta_3 = -0.025$

IV. CALCULATION OF THE ELASTIC CONSTANTS

The method that we will use in this section is simple and quite general. It can be applied to any crystal structure of any group symmetry. This method is numerically convenient when the symmetry of the q-group is low and the dynamical matrix cannot be factorized analytically. The convenience of the method lies in the fact that one has only to know the eigenvectors at the zone-center in addition to an explicit form of the dynamical matrix for the symmetry direction under consideration. It is simple because it avoids the complicated formalism of the long wave method developed by Born and Huang (15) for evaluating the elastic constants.

The slopes of the acoustic branches are solved for by expanding $\bar{\bar{D}}(q_\alpha)$, where q_α refers to any symmetry direction in the Brillouin zone, in linear and quadratic terms in q_α around the zone-center. Defining the perturbation matrix $\bar{\bar{D}}'(q_\alpha)$ as:

$$\bar{\bar{D}}'(q_\alpha) = \bar{\bar{D}}(q_\alpha) - \bar{\bar{D}}(0) \tag{2.8}$$

one can write

$$q_\alpha^2 \left(\frac{d\omega_A}{dq_\alpha}\right)^2 = \langle A|\bar{\bar{D}}'(q_\alpha)|A\rangle - \sum_{M\neq A} \frac{|\langle A|\bar{\bar{D}}'(q_\alpha)|M\rangle|^2}{\omega_M^2} \tag{2.9}$$

where |A> represents an eigenvector of the acoustic mode considered, and the summation over |M> covers all other modes at the zone-center. The summation over |M> is nonzero only for the modes which are coupled to the particular acoustic mode considered. This is dictated by the group symmetry of the crystal. In the case of halogens with D_{2h}^{18} symmetry, the B_{3u} acoustic mode is coupled to the A_g, B_{1g} and B_{2g} optical modes. The elastic constants are then written as

$$C_{ii} = \zeta \left(\frac{d\omega_A}{dq_\alpha} \right)^2 \qquad (2.10)$$

where C_{ii} refers to the elastic constant for a given acoustic wave in the lattice and ζ is the density at the particular temperature considered. The eigenvectors at the zone-center being factored out numerically, are used to evaluate the matrix elements in equation (2.9). One thus determines the slope of the acoustic mode and evaluates the elastic constant using equation (2.10).

The elastic constants C_{33}, C_{55} and C_{44}, Figure 2-3, have been calculated using first and second order perturbation theory. Table 2-4 lists the calculated elastic constants for chlorine, iodine and bromine. The lowest C_{44} value corresponds to a transverse interplanar wave indicating that the interplanar force constants are the weakest. C_{55} corresponds to a transverse wave propagating in the Z direction with a displacement in the X direction. C_{33} corresponds to a longitudinal

Table 2-4 Elastic Constants for chlorine, bromine and iodine.

Elastic Constants X 10" dyne cm^{-2}	I_2	Br_2	CL_2
C_{44}	0.51	0.35	0.48
C_{55}	1.84	1.59	1.08
C_{33}	4.72	3.31	2.71

wave propagating in the Z direction. The lower value of C_{55} as compared to C_{33} is due to the smaller value of the force constant α_1 as compared to the force constant ζ_1, the molecule being tilted more towards the Z axis.

V. DISCUSSION

The interatomic central force potential is a good description of the type of interaction that exists in halogen crystals. The experimental Raman frequencies measured at the zone-center, for all three crystals, have been reproduced with good accuracy. Figure 2-2 compares the calculated phonon dispersion curve for iodine with the experimental points as measured by Smith et al. (6,7) for the Λ and Δ directions. The overall fit looks good for both directions except for the $\Lambda_1(B_{1u})$ branch. The experimental points of this branch depict an irregular pattern and show a large discrepancy from the calculations. The discrepancy might be attributed to the presence of impurities in the crystal rather than representing a true physical behavior. In Figure 2-3, phonon dispersion curves in the Λ direction are plotted for chlorine, bromine and iodine. The symmetry notation adopted for the Γ, Λ and Z points are given in Table 2-5. The strength of the intramolecular bond decreases as one shifts from chlorine to iodine, being strongest in chlorine. Another noteworthy aspect is the relative decrease in the intermolecular bond strength from chlorine to bromine to iodine. The B_{2g} mode has a frequency

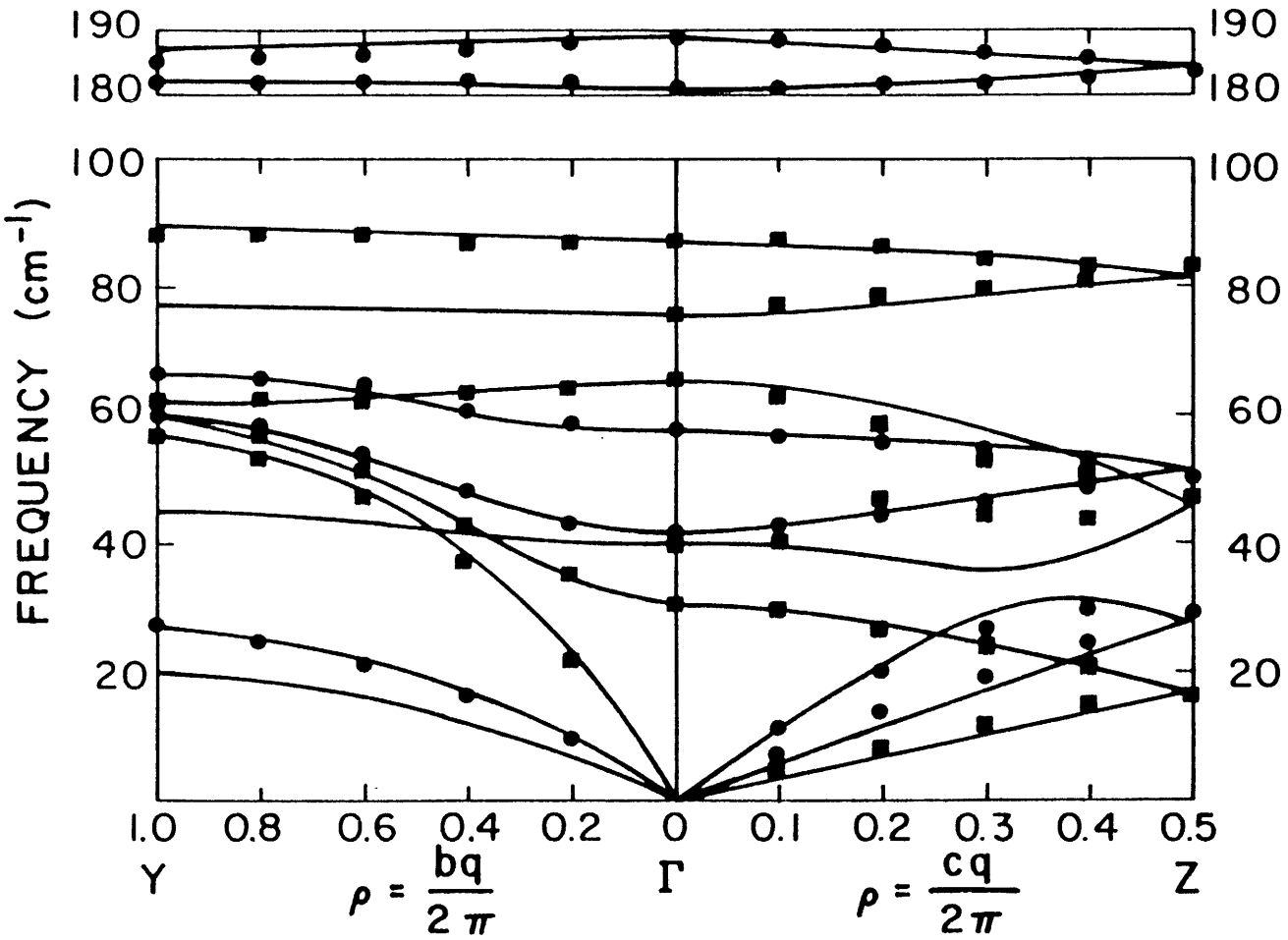

Figure 2-2. Dispersion curves for the Λ and Δ directions in iodine. Experimental points are indicated by black squares and circles ●, ■. Full curves indicate theoretical calculations.

Table 2-5 Character tables for points Γ, Λ, and Z

(a) Γ (0,0,0)

	E	$\{\overline{xy}z\|\frac{1}{2}0\frac{1}{2}\}$	$\{\overline{x}y\overline{z}\|000\}$	$\{x\overline{yz}\|\frac{1}{2}0\frac{1}{2}\}$	$\{\overline{xyz}\|000\}$	$\{xy\overline{z}\|\frac{1}{2}0\frac{1}{2}\}$	$\{x\overline{y}z\|000\}$	$\{\overline{x}yz\|\frac{1}{2}0\frac{1}{2}\}$	χ
Ag	1	1	1	1	1	1	1	1	2
B_1g	1	1	-1	-1	1	1	-1	-1	1
B_2g	1	-1	1	-1	1	-1	1	-1	2
B_3g	1	-1	-1	1	1	-1	-1	1	1
Au	1	1	1	1	-1	-1	-1	-1	1
B_1u	1	1	-1	-1	-1	-1	1	1	2
B_2u	1	-1	1	-1	-1	1	-1	1	1
B_3u	1	-1	-1	1	-1	1	1	-1	2

(b) $\Lambda\ (0,0,\frac{2\pi}{c}\mu)$, $-\frac{1}{2} \leq \mu \leq \frac{1}{2}$

	E	$\{\overline{xy}z\|\frac{1}{2}0\frac{1}{2}\}$	$\{\overline{x}yz\|\frac{1}{2}0\frac{1}{2}\}$	$\{x\overline{y}z\|000\}$	χ
Λ_1	1	$e^{i\pi\mu}$	$e^{i\pi\mu}$	1	4
Λ_2	1	$-e^{i\pi\mu}$	$e^{i\pi\mu}$	-1	4
Λ_3	1	$e^{i\pi\mu}$	$-e^{i\pi\mu}$	-1	2
Λ_4	1	$-e^{i\pi\mu}$	$-e^{i\pi\mu}$	1	2

(c) $Z\ (0,0,\frac{\pi}{c})$

	E	$\{\overline{xy}z\|\frac{1}{2}0\frac{1}{2}\}$	$\{\overline{x}y\overline{z}\|000\}$	$\{x\overline{yz}\|\frac{1}{2}0\frac{1}{2}\}$	$\{\overline{xyz}\|000\}$	$\{xy\overline{z}\|\frac{1}{2}0\frac{1}{2}\}$	$\{x\overline{y}z\|000\}$	$\{\overline{x}yz\|\frac{1}{2}0\frac{1}{2}\}$	χ
Z_1	$\begin{pmatrix}1&0\\0&1\end{pmatrix}$	$\begin{pmatrix}1&0\\0&-1\end{pmatrix}$	$\begin{pmatrix}0&1\\1&0\end{pmatrix}$	$\begin{pmatrix}0&-1\\1&0\end{pmatrix}$	$\begin{pmatrix}0&1\\1&0\end{pmatrix}$	$\begin{pmatrix}0&-1\\1&0\end{pmatrix}$	$\begin{pmatrix}1&0\\0&1\end{pmatrix}$	$\begin{pmatrix}1&0\\0&-1\end{pmatrix}$	4
Z_2	$\begin{pmatrix}1&0\\0&1\end{pmatrix}$	$\begin{pmatrix}-1&0\\0&1\end{pmatrix}$	$\begin{pmatrix}0&-1\\-1&0\end{pmatrix}$	$\begin{pmatrix}0&-1\\1&0\end{pmatrix}$	$\begin{pmatrix}0&1\\1&0\end{pmatrix}$	$\begin{pmatrix}0&1\\-1&0\end{pmatrix}$	$\begin{pmatrix}-1&0\\0&-1\end{pmatrix}$	$\begin{pmatrix}1&0\\0&-1\end{pmatrix}$	2

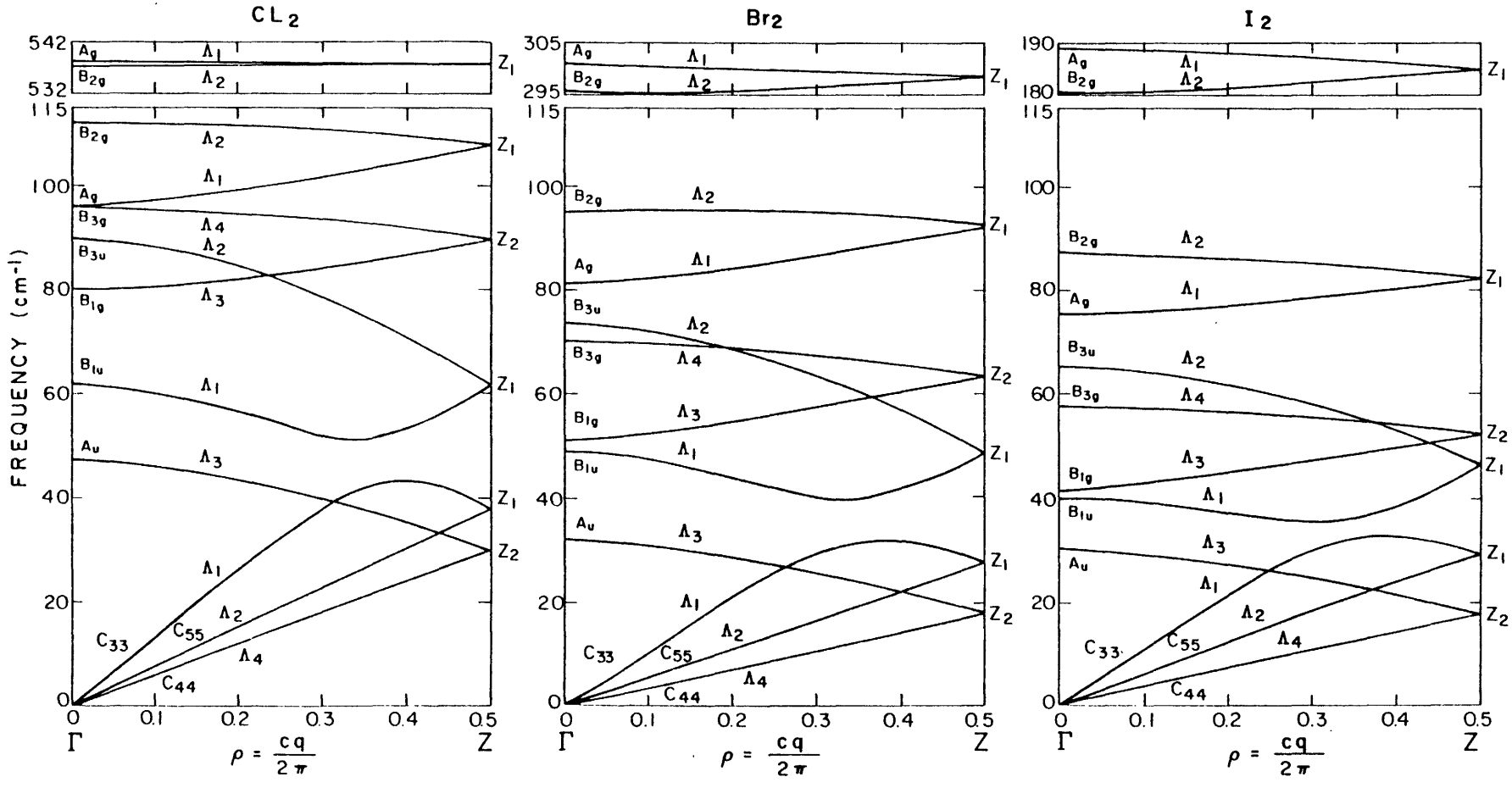

Figure 2-3. Dispersion curves for the Λ direction in chlorine, bromine and iodine. Symmetry assignments are given in detail in Table 2-5.

of 112 cm^{-1} in chlorine, compared to 95 cm^{-1} in bromine and 87.4 cm^{-1} in iodine.

The eigenvectors at the zone-center are listed in Table 2-1 (b). Figure 2-4 shows the relative phase of motion of each atom with respect to the other atoms forming the basis of the unit cell. The modes are listed in ascending order of energy. The lowest acoustic B_{3u}, B_{2u} and B_{1u} modes correspond to pure translational motion of the whole crystal in the X, Y and Z directions respectively. This is to be compared with the optical A_u, B_{1u} and B_{3u} modes in which the atoms of each molecule move in phase relative to each other but with 180^{o} phase difference relative to the atoms of the other molecule. Four librational modes are present. The B_{1g} mode corresponds to symmetrical rotation about the Z axis. Each molecule rotates alternately anticlockwise and then clockwise about a Z axis passing through its center of mass. The B_{3g} mode corresponds to an alternate anticlockwise then clockwise rotation about an X axis passing through the center of mass of each molecule. The lower A_g mode corresponds to antisymmetrical rotations about the Y axis, while the lower B_{2g} mode corresponds to symmetrical rotations about the Y axis.

There are two intramolecular stretching modes, the B_{2g} mode corresponding to antisymmetrical stretch versus the A_g mode corresponding to a symmetrical stretching

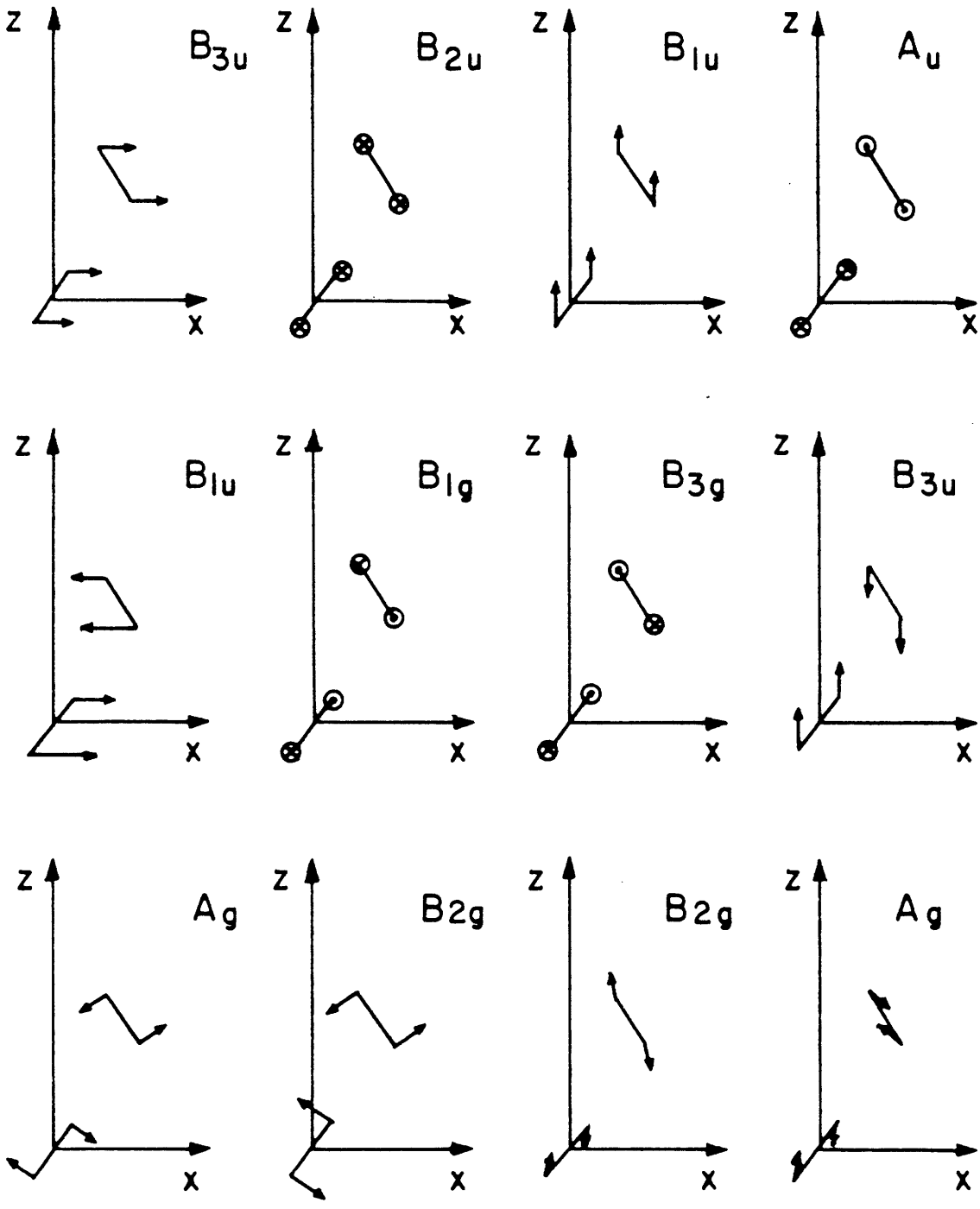

Figure 2-4. The motion of the atomic basis for each of the zone-center modes is shown. Arrows indicate the direction of motion in the xz plane. Crossed circles ⊗ indicate motion in the positive y direction, dotted circles ⊙ indicate motion in the negative y direction.

mode. One notes that the two stretching modes are associated with a small rotation of 3^{o} suggesting that the motion of the two molecules is coupled to each other and hence cannot be treated as rigid rotators. The anti-symmetrical B_{2g} mode has a lower energy as compared to the symmetrical A_g mode. This is to be expected because in the latter case, the electronic clouds of the two molecules tend to overlap and thus be in a higher energy state as compared to the former case. This confirms the experimental symmetry assignment of Suzuki et al. (5) while it is contrary to the assignment of Anderson et al. (4) who reversed the assignment of the intramolecular experimental modes.

VI. CONCLUSIONS

The calculation based on a general pair atom central force model reproduces all the available phonon frequencies at the zone-center for bromine, chlorine and iodine. It also gives phonon frequencies along two symmetry directions in iodine within the experimental error of the measurements. This implies that it may be possible to find a set of central atom-atom potential functions which will describe all the static and dynamic properties of the halogen crystals satisfactorily. So far attempts along this direction have not produced satisfactory results. What is clearly needed is to generate more information in terms of phonon frequencies and intensities for chlorine and

bromine. For iodine phonon dispersion measurements along [100] direction will serve to further refine the lattice dynamics model. We present a simple method based on perturbation theoretic technique for calculation of the elastic constants. It will be of great interest to pursue elastic constant measurements in iodine by Brillouin scattering experiments.

VII. REFERENCES

1. Collins, R.L. 1956 Acta. Crystallogr. 9, 537.
2. Vonnegut, B., and Warren, B.E. 1936 J. Am. Chem. Soc. 58, 2459-61.
3. Van Bolhuis, F., Koster, P.B., and Migchelsen, T. 1967 Acta. Crystallogr. 23, 90-1.
4. Anderson, A. and Sun, T.S. 1970 Chem. Phys. Lett. 6, 611-6.
5. Suzuki, M., Yokoyamma, T. and Ito, M. 1969 J. Chem. Phys. 51, 1929-31.
6. Smith, H.G., Nielson, M. and Clark, C.B. 1975 Chem. Phys. Lett. 33, 75-8.
7. Smith, H.G., Nielson, M. and Clark, C.B. 1974 ORNL-5028, 109-110.
8. Suzuki, M., Yokoyamma, T. and Ito, M. 1969 J. Chem. Phys. 50, 3392-98.
9. English, P.S. and Leech, J.W. 1973 Chem. Phys. Lett. 23, 24-7.
10. Dumas, G.G., Vovelle, F. and Viennot, J.P. 1974 Molec. Phys. 28, 1345-57.
11. Leech, J.W. and Pawely, G.S. 1976 Molec. Phys. 31, 1663-68.

12. Pasternak, A., Anderson, A., and Leech, J.W. 1977 J. Phys. C: Solid St. Phys. 10, 3261-71.

13. Pasternak, A., Anderson, A., and Leech, J.W. 1978 J. Phys. C: Solid St. Phys. 11, 1563-72.

14. Venkataraman, G., Feldkamp, L.A., and Sahni, V.C. 1975 Dynamics of Perfect Crystals (M.I.T. Press).

15. Born, M. and Huang, K. 1954 Dynamical Theory of Crystal Lattices (Oxford, Clarendon Press).

Chapter 3

AN INTERATOMIC POTENTIAL MODEL FOR HALOGEN CRYSTALS

I. INTRODUCTION

Several potential models have been introduced for the study of lattice vibrations of halogen crystals. These potentials covered a wide range of functions including Lennard-Jones, Buckingham, charge transfer and quadrupolar interactions. Nyburg (1) postulated a molecular model in which the molecule has a charge concentration at its outer ends in addition to a charge concentration at its center. This charge distribution applied in conjunction with a Lennard-Jones 12-6 potential correctly predicts the Ccmb space group structure and the orientation of the molecules in the unit cell for chlorine, though the cubic Pa3 is more stable. In a more recent work, Nyburg et al. (2) replaced the spherical atom-atom potential by one which is flattened at the atomic pole and equator. As a result, the Ccmb had the lowest lattice energy structure, and the crystal was free from internal stress. Suzuki et al. (3, 4) assumed a Lennard-Jones 12-6 potential for the chlorine crystal. They concluded that a central force field is inadequate for the chlorine crystal and noncentral forces must be taken into account to reproduce the observed frequencies. English et al. (5) further studied the Lennard-Jones 12-6 interaction by applying it to chlorine and iodine. A Lennard-Jones potential failed to produce

a real frequency for the A_u mode. A combination of Lennard-Jones and quadrupolar interactions still produced an imaginary frequency for the A_u mode. A charge transfer interaction produced a real frequency for the A_u mode but it was not possible to achieve good agreement with the experimental frequencies. Dumas et al. (6) tried a combination of three different central force potentials; a Morse potential for the intramolecular bond, a Buckingham-6 plus a charge transfer term for the nearest intermolecular interaction and a second Buckingham-6 potential for further intermolecular interactions, was applied for chlorine and bromine. Substantial improvement over other central force potentials was achieved where mode instabilities of previous models were absent. Smith et al. (7,8) tried a different set of central force potentials. A set of three Buckingham-6 potential functions with a rigid molecule was assumed. The nearest intermolecular interaction was represented by a set of potential parameters, the second nearest by a second set and all the more distant interactions by a third set. Moderate agreement was obtained between the observed and calculated phonon dispersion curves for iodine.

Leech et al. (9) outlined a simple method for identifying potential functions designed to reproduce given normal mode frequencies, equilibrium conditions and other constraints. They applied it to solid chlorine and a family

of potentials satisfying fourteen constraints was found. However, their potential functions had some implausible features as having imaginary phonon frequencies for certain $|\vec{q}|$ values and none of the potential curves appeared to have a wholly realistic shape. Pasternak et al. (10,11) assumed a simple bond charge for the three halogens, chlorine, bromine and iodine. In this model the charge distribution in the crystal is accounted for by placing a negative charge "-q" at the center of the intramolecular bond. Another negative charge "-q'" is placed at the center of the shortest intermolecular bond. Nuclear charges of magnitude $Z = q' + \frac{q}{2}$ ensure overall charge neutrality. Interatomic interactions are represented by a set of two Lennard-Jones 12-6 potentials, one for the shortest intermolecular bond and the other for further neighbors. No mode instabilities are present in their calculations, however some of the calculated modes are interchanged when compared with the observed experimental values.

In a previous work (12), we proposed a general pair atom central force model for the three halogens - chlorine, bromine and iodine. Force constants were determined by fitting them to the zone-center frequencies for the three halogens. Agreement between the calculated phonon frequencies at finite $|\vec{q}|$ and the observed ones was very good. In the present work we go a step further by trying to construct an actual potential model for the halogen crystals rather

than working with a force constant model. We propose a potential model for the halogens incorporating interatomic and electrostatic charge interactions. To each atom in the crystal is associated a dipole which represents the charge distribution of its valence electrons. A Morse potential is used to represent the intramolecular bond. The intermolecular interactions are represented by a Buckingham-6 potential in addition to the electrostatic dipole-dipole interaction. This potential model still retains part of the central interatomic interaction in agreement with the force constant model proposed in our previous work. However, the resultant interatomic force constants in this case are the superposition of central dispersion-repulsion and noncentral electronic electrostatic interactions. The static and dynamic properties for the three halogens have been calculated using this potential. The cohesive energies and equilibrium conditions are reproduced within the experimental error. The calculated zone-center frequencies are in good agreement with the experimental infrared and Raman frequencies for the three halogens. The results indicate that this potential model provides a good description of the dynamics of the halogen crystals.

The same type of potential model has been applied to the azabenzene crystals. Recently Gamba et al. (13) proposed a potential model which they called the distributed dipole model. The molecular charge distributions are

represented by dipoles placed near the nitrogen atoms and on the C-H bonds. Their model reproduces very well the electrical multipoles obtained from ab intio calculations for this series of molecules. The calculated zone-center frequencies are in good agreement with the experimental values.

In Section II we give a theoretical treatment of the potential model. The origin of such a model is discussed as well as some of the theories which have been suggested to explain the electronic charge configuration of the halogen molecules. In Section III, static and dynamic properties are calculated and compared with the observed experimental values for the three halogens. The static properties include equilibrium conditions in addition to the cohesive energies. The dynamic properties include the infrared and Raman-active zone-center frequences which have been measured for the three halogen crystals. In Section IV, phonon dispersion curves are calculated along the [001], [010] and [100] directions for the three halogens. Available experimental results along [010] and [001] for iodine are compared with the predicted theoretical curves constructed with the potential model. Table 3-5 gives in detail the group character tables for symmetry points Δ , Σ and Y of the Brillouin zone. The character tables for the points Γ, Λ and Z are already given in our previous work (12).

II. POTENTIAL MODEL

The basic feature of our model is that one associates a dipole with each atom to represent its electronic charge configuration. The halogen molecule will act as a quadrupole with two dipoles sitting antiparallel to each other close to the centers of its constituent atoms. The dipoles are placed antiparallel to each other to comply with the inversion symmetry around the center of mass of the molecule. The dipole model could be understood in terms of the charge migration of the molecular electronic cloud. If one considers a free halogen molecule, point-charge migration is thought to take place in the molecule. The molecule as a whole will have two centers of positive charge closer to its center and two centers of negative charge closer to its outer ends. Figure 3-1 shows the axial distribution of charge in a free halogen molecule. One possible cause of the charge separation is the repulsion between the nonbonding P_x and P_y orbitals of the two atoms leading to a drift in the electronic charge towards the outer ends of the free molecule. Simple models to account for point-charge migration in the free halogen molecules have been proposed by Nyburg (1,2). The electrostatic interaction between two atoms in the halogen crystal would consist of the different interactions between the localized positive and negative charges centered around each atom. Expansion of the interaction energy in terms of the interatomic distance "r"

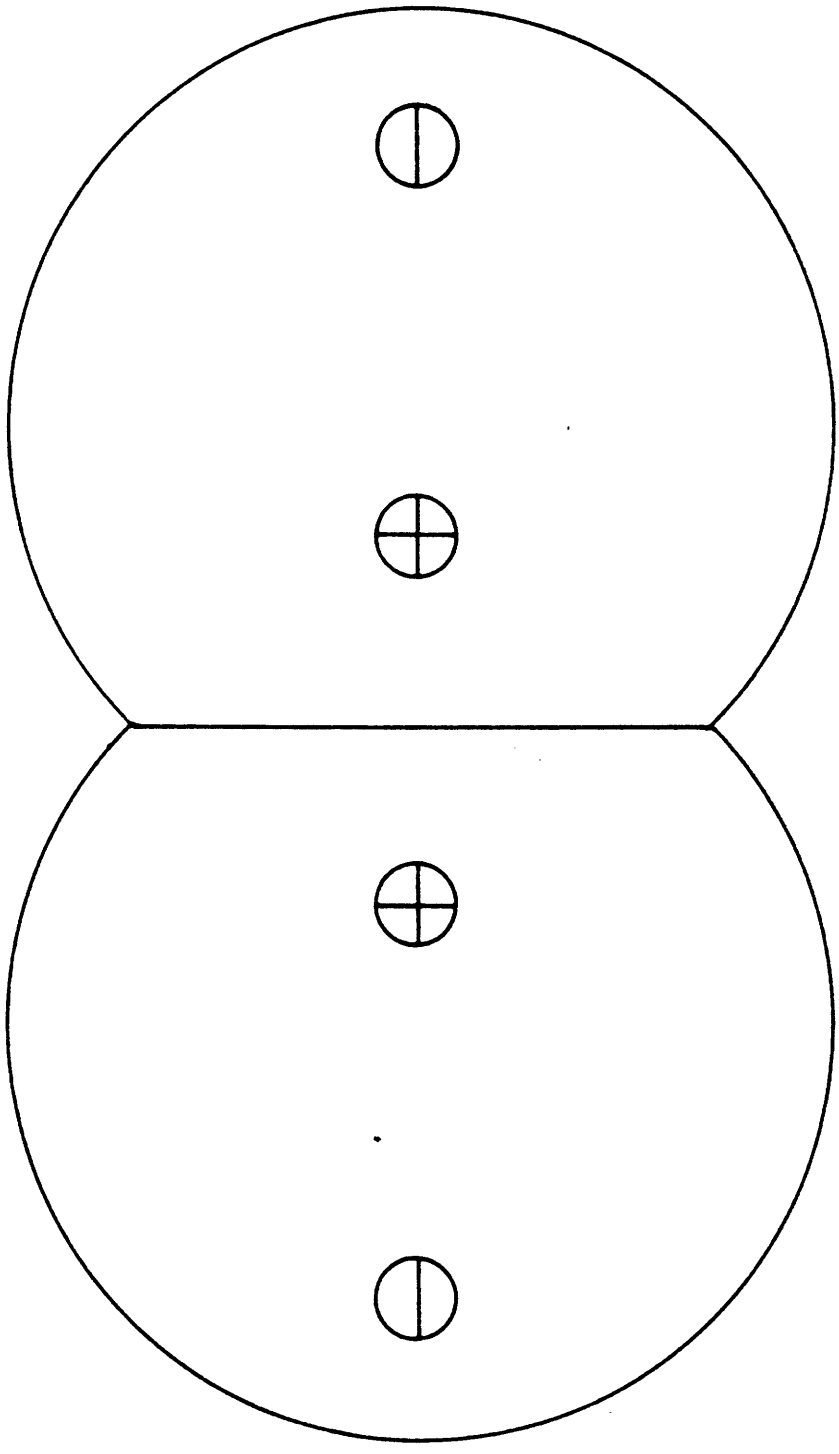

Figure 3-1. Point-charge migration model for a free halogen molecule.

would lead to dipole, quadrupole, octopole and higher order terms. In our potential model we have taken account only of the dipole-dipole interaction, ($1/r^3$) terms, and neglected all higher order terms. Thus the electronic charge of each atom is represented by a dipole located in the vicinity of the atomic center. Future work might involve the inclusion of all electrostatic interactions by solving for the separate localized charges centered around each atom to improve on the accuracy of the dipole model.

Thus far we have considered charge migration in a free halogen molecule in which charge separation takes place along the molecular axis. However, molecular charge separation is expected to be different in the halogen crystal. Polarization of the charge of one molecule by the adjacent charges of neighboring molecules is expected to take place. The net effect is an off-axial charge drift in the electronic molecular cloud. The potential model that we will consider for the halogen crystal is based on an interatomic interaction which is the superposition of electrostatic dipole-dipole interactions and dispersion-repulsion forces. The distribution of these dipoles in the lattice is clarified by considering the atomic basis for a halogen crystal. Figure 3-2 shows the atomic basis with the associated dipole charge distribution. The first feature of the model is that the dipoles are coplanar with the XZ plane. This is a consequence of the planar symmetry of the Ccmb structure. The

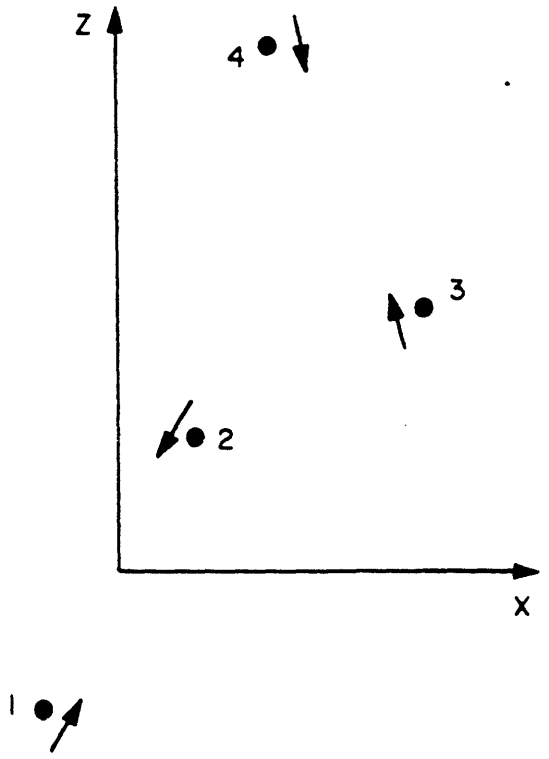

Figure 3-2. Electronic charge distribution for the atomic basis.

crystal is invariant under a mirror reflection in the XZ plane. The dipole configuration associated with the atomic basis shown in Figure 3-2 complies with the symmetry elements of the Ccmb group. The dipoles associated with a single molecule are placed antiparallel to each other because the center of mass of each molecule is a center of inversion for the whole crystal. The orientation of the atomic dipoles 3 and 4 with respect to the atomic dipoles 1 and 2 is dictated by the Ag symmetry element of the Ccmb group (12). The dipole distribution is invariant under any of the symmetry operations of the Ccmb group. Each dipole in the lattice is characterized by four parameters; a dipole moment, dipole orientation, dipole angular and radial positions relative to a fixed corrdinate system. In Figure 3-2, the origin of the coordinate system is taken to coincide with the center of mass of one of the molecules in the basis. If one considers atom 2 of the basis, the dipole moment is given as μ, the dipole orientation is represented by ϕ, the dipole angular position is designated by γ and the dipole radial position as d/2. The charge distribution in the whole lattice is constructed using the charge symmetry of the atomic basis shown in Figure 3-2. Thus the electrostatic interactions in the crystal are accounted for by the interatomic dipole-dipole interaction in the present potential model. In general the dipole-dipole interaction is given by

$$U_{ij} = \frac{\vec{\mu}_i \cdot \vec{\mu}_j - 3(\vec{n}\cdot\vec{\mu}_i)(\vec{n}\cdot\vec{\mu}_j)}{\left|\vec{r}_i - \vec{r}_j\right|^3} \qquad (3.1)$$

where U_{ij} is the energy of interaction, μ_i and μ_j are the dipole moments, $\vec{r}_i$ and $\vec{r}_j$ are the position vectors of the two interacting dipoles and $\vec{n}$ is given as

$$\vec{n} = \frac{\vec{r}_i - \vec{r}_j}{\left|\vec{r}_i - \vec{r}_j\right|} \qquad (3.2)$$

The dispersion-repulsion forces are given by two potential functions. The intramolecular interactions are represented by a Morse type potential written in terms of three parameters as

$$V_{ij} = D[1-\exp(-\beta(R_{ij}-R_E))]^2 \qquad (3.3)$$

where V_{ij} is the interatomic interaction energy for a given molecule, R_{ij} is the separation distance between the two constituent atoms, D is the dissociation energy referred to the minimum, β is a constant which determines the curvature of the function near the minimum and R_E is the equilibrium length of the free molecule. It should be noted however, that since the dipole-dipole interaction is taken in addition to the Morse interaction for a given intramolecular bond, the value of "D" for a given free halogen molecule is expected to be different from the tabulated dissociation energy. The other interatomic intermolecular interactions

are represented by a Buckingham-6 potential. The interaction energy is written in terms of three parameters as

$$V_{ij} = - \frac{A}{R_{ij}^6} + Be^{-\alpha R_{ij}} \qquad (3.4)$$

where V_{ij} is the interaction energy between two given atoms i and j, R_{ij} is the separation distance between them. A, B and α are constants of the potential determined by the particular crystal under study.

The potential model we are postulating involves ten parameters. Four parameters are determined by the electrostatic interatomic interactions characterizing the dipole properties for a given halogen. Three parameters are determined by the intramolecular bond and the last three are determined by the intermolecular interactions. The ten parameters of the potential model are calculated by fitting the potential to the observed static and dynamic properties of each halogen crystal as discussed in the next section.

III. DETERMINATION OF THE POTENTIAL PARAMETERS

The ten parameters appearing in the potential model discussed in the previous section are determined by fitting the potential model to the static and dynamic properties of the halogen crystal under consideration. The static properties constitute the resultant forces on an atom in the X and Z directions, Figure 3-2, and the cohesive energy of the crystal lattice. The resultant forces F_x and F_z

are determined in undimensional units by scaling them to the magnitude of the maximum force acting on that atom. The cohesive energy of the crystal lattice is equated to the experimental heat of sublimation neglecting the entropic contribution to the latter. The dynamic properties studied are the experimental nine zone-center frequencies for each of the halogen crystals measured by infrared and Raman scattering techniques. In the case of chlorine and bromine, the lowest A_u mode is not measured and a value is estimated for it from previous theoretical calculations (11,12). The dynamic and static properties of each of the halogen crystals were calculated and fitted to the experimental values using a nonlinear least square fitting algorithm. The lattice sums were carried over the twenty-nine adjacent neighbors of each atom, Figure 3-3. The scheme used for the fitting was to construct the lattice first in accordance with the Ccmb symmetry using the lattice parameters determined experimentally (10,11). The ten potential parameters in addition to the molecular length and angular inclination θ, Figure 3-3, are taken as twelve free fitting parameters. The static and dynamic properties of the crystal are calculated using these parameters and fitted to the twelve known properties of the crystal, nine constituting the zone-center frequencies in addition to two equilibrium conditions and the cohesive energy. The nonlinear least square fitting was carried out at an IBM 370 computer using the

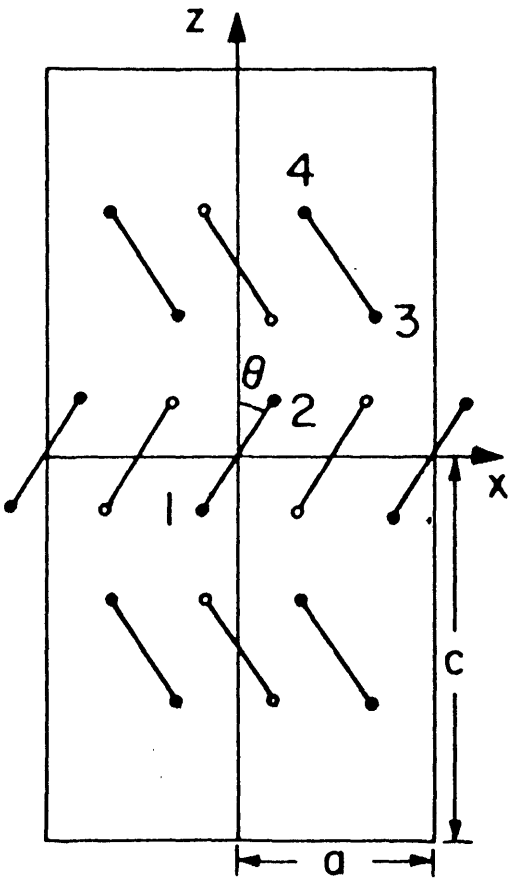

(a)

Figure 3-3(a). Structure of the halogen crystals. Full circles indicate molecules at y=0; open circles indicate molecules at $y = \pm \frac{b}{2}$.

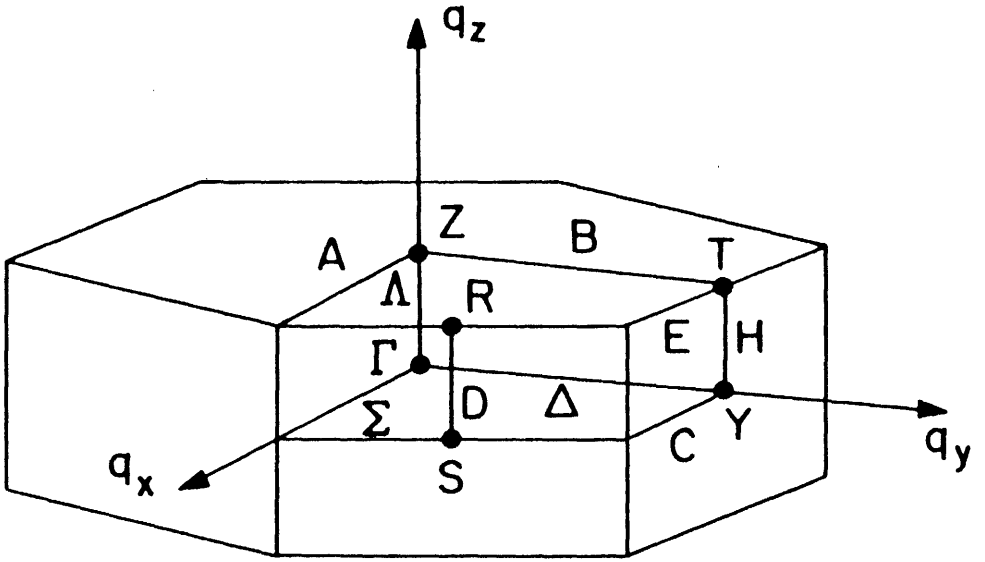

(b)

Figure 3-3(b). The Brillouin zone for the one-face centered orthorhombic lattice (a < b).

NL_2SOL algorithm (14). The average number of iterations needed was two hundred and the residue converged to an average value of 15%. It should be noted that the molecular quadrupole moment would have been an important physical property used in the fitting process. Due to the wide range of values reported in the literature, values of the quadrupole moments have been calculated using the determined potential parameters. The calculated quadrupole moments for each of the halogens are reported at the end of this section. The present potential model reproduces the dynamic and static properties of the halogen crystals with good accuracy. Table 3-1 compares the calculated properties with the experimental ones for each of the halogens. The internal modes A_g^2, B_{2g}^2 are all calculated to within 1% of the experimental values. All other optical modes fit the corresponding experimental ones to 10% accuracy, except for the B_{3g} mode. The largest discrepancy of the B_{3g} mode occurs in bromine with an 18% deviation from the experimental value. The cohesive energies calculated, fit the input values to 1% accuracy with proper adjustments made to take account of the temperature difference. The residual forces in the Z direction converge to an accuracy of less than 7% in all three crystals. As for the X direction, the convergence is within 14%. Overall the present potential model appears to account well for the type of interactions that exist in the halogen crystals. Table 3-2 lists the calculated

Table 3-1

Calculated Zone-Centre phonon frequencies, residual force components and cohesive energies for I_2, Br_2 and Cl_2. Experimental frequencies are given for comparison

	I_2		Br_2		CL_2	
Zone-centre phonon frequencies (cm^{-1})	Exp.	Calc.	Exp.	Calc.	Exp.	Calc.
F^1_{3u}		0.0		0.0		0.0
B_{2u}		0.0		0.0		0.0
B^1_{1u}		0.0		0.0		0.0
A_u	30.67	31.82	---	33.67	---	49.61
B^2_{1u}	40.00	39.67	49.00	47.84	62.00	62.25
B_{1g}	41.67	43.48	51.50	54.06	80.00	80.38
B_{3g}	57.67	48.37	70.50	57.33	96.00	84.91
B^2_{3u}	65.33	68.37	74.00	78.52	90.00	93.26
A^1_g	75.33	76.52	81.50	83.71	96.00	98.31
B^1_{2g}	87.33	79.52	95.00	86.45	112.00	102.19
B^2_{2g}	180.67	180.21	296.00	296.64	538.00	536.92
A^2_g	189.33	188.87	301.00	299.81	539.00	539.69
Cohesive Energy ($x10^7 J/Kg$ mole)	6.50	6.52	4.70	4.73	2.64	2.65
Residual force components (F_x,F_z)						
F_x	0.099		0.074		0.142	
F_z	0.037		0.069		0.015	

Table 3-2

Potential parameters, molecular length and orientation for I_2, Br_2 and Cl_2.

	I_2		Br_2		Cl_2	
D ($x10^{-12}$erg/mol)	0.28		4.94		2.73	
β ($\AA^{-1}$)	2.08		1.30		2.24	
R_E($\AA$)	3.03		2.62		2.34	
A ($x10^{-9}$erg/mol $\AA^6$)	11.48		4.95		2.58	
B ($x10^{-9}$erg/mol)	3.64		2.53		1.47	
α ($\AA^{-1}$)	1.78		1.93		1.96	
μ (e$\AA$)	1.35		0.91		0.73	
γ^c	-0.27		0.55		0.53	
ϕ^c	-2.54		-2.73		3.30	
d ($\AA$)	2.93		3.02		2.86	
l ($\AA$)	2.74	(2.71[a])	2.59	(2.32[a])	2.33	(1.99[a])
θ^c	0.61	(0.56[a])	0.68	(0.56[a])	0.64	(0.56[a])

* e = 4.80 x 10^{-10} esu

a Experimental values as given in references [10,11].

potential parameters, molecular length and orientation for the three halogens. One notes that the dipole heads are oriented towards the centre of mass of the molecule as shown in Figure 3-2. This indicates that the center of negative charge is closer to the outer ends of the molecule in agreement with the free molecule charge distribution predicted by our model in Section II. The calculated molecular lengths all agree with the experimental lengths to within 0.34Å.

Figure 3-4 shows the total intermolecular potential for two interacting atoms; the potential is plotted for the [100] direction. The main feature is that the repulsive dipole-dipole interaction increases the value of the interaction energy compared to the Buckingham-6 case. In the case of chlorine, the overall effect is that the negative potential minimum in the curve disappears and the potential energy approaches zero as R_{ij} increases. This feature of the potential has a profound effect on the shape of the acoustic dispersion curves and will be dealt with extensively in the next section.

The quadrupole moments of the halogen molecules have been evaluated using the calculated dipole moments. The tensorial components of the quadrupole moment are written as,

$$\Theta_{\alpha\beta} = \frac{1}{2}\int \rho(3r_\alpha r_\beta - r^2\delta_{\alpha\beta})d\tau \qquad (3.5)$$

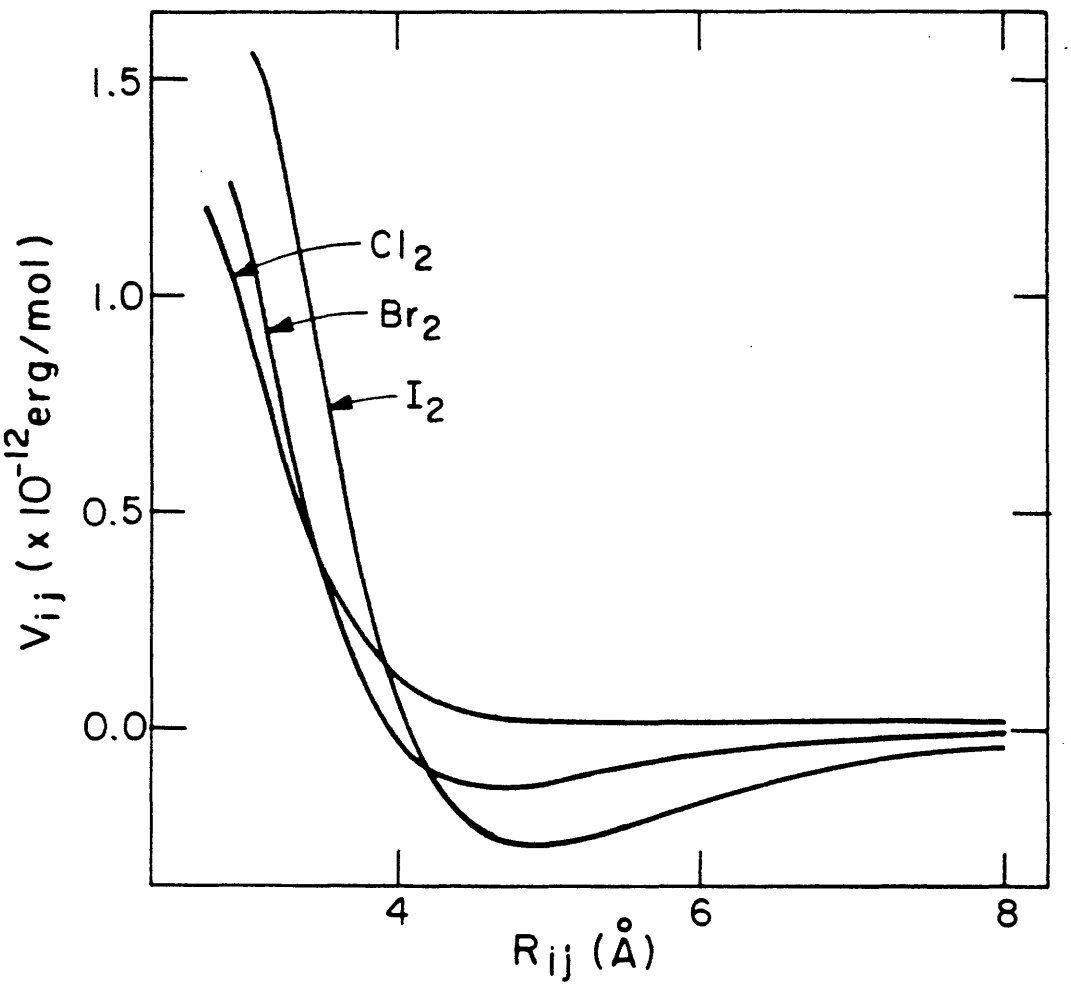

Figure 3-4. Potential profile for an atomic pair along the [100] direction.

where ρ is the charge density and the integral over τ is a surface integral. The moments are given relative to an origin at the center of mass of the molecule. The α direction is taken to coincide with the line joining the centers of the two dipoles and is designated as r. The β direction is taken to be perpendicular to the α direction and is designated as Θ. Table 3-3 lists the components of the quadrupole tensor in addition to the product μxd. Values of the quadrupole moments reported in the literature are given for comparison (15,16,17).

IV. DISCUSSION

The potential model seems to be a good description of the type of interactions that exist in the halogen crystals. The experimental Raman and infrared frequencies measured at the zone-center, for all three halogens, have been reproduced with good accuracy. Figure 3-5 compares the calculated phonon dispersion curves for iodine with the experimental points as measured by Smith et al. (7,8) for the Λ and Δ directions. The internal vibrational modes fit the measured experimental points to a good accuracy in both directions. For the Λ direction, the theoretical acoustic branches reproduce the experimental points within the experimental accuracy. Only two experimental acoustic branches are reported for the Δ direction and the theoretical calculations reproduce them with good accuracy. A discrepancy is noted

Table 3-3

Quadrupole moments for Iodine, bromine and chlorine.

Quadrupole moment $\times 10^{-26}$ esu cm^2	I_2	Br_2	Cl_2
Θ_{rr}	-23.97	-25.73	-18.77
$\Theta_{\theta\theta}$	11.98	12.86	9.38
$\Theta_{r\theta}$	21.91	-3.76	-5.49
μd	18.87	13.10	10.07
Reported Values for $\Theta_{\theta\theta}$		8.2 [16]	6.14[15], 4.2[17]

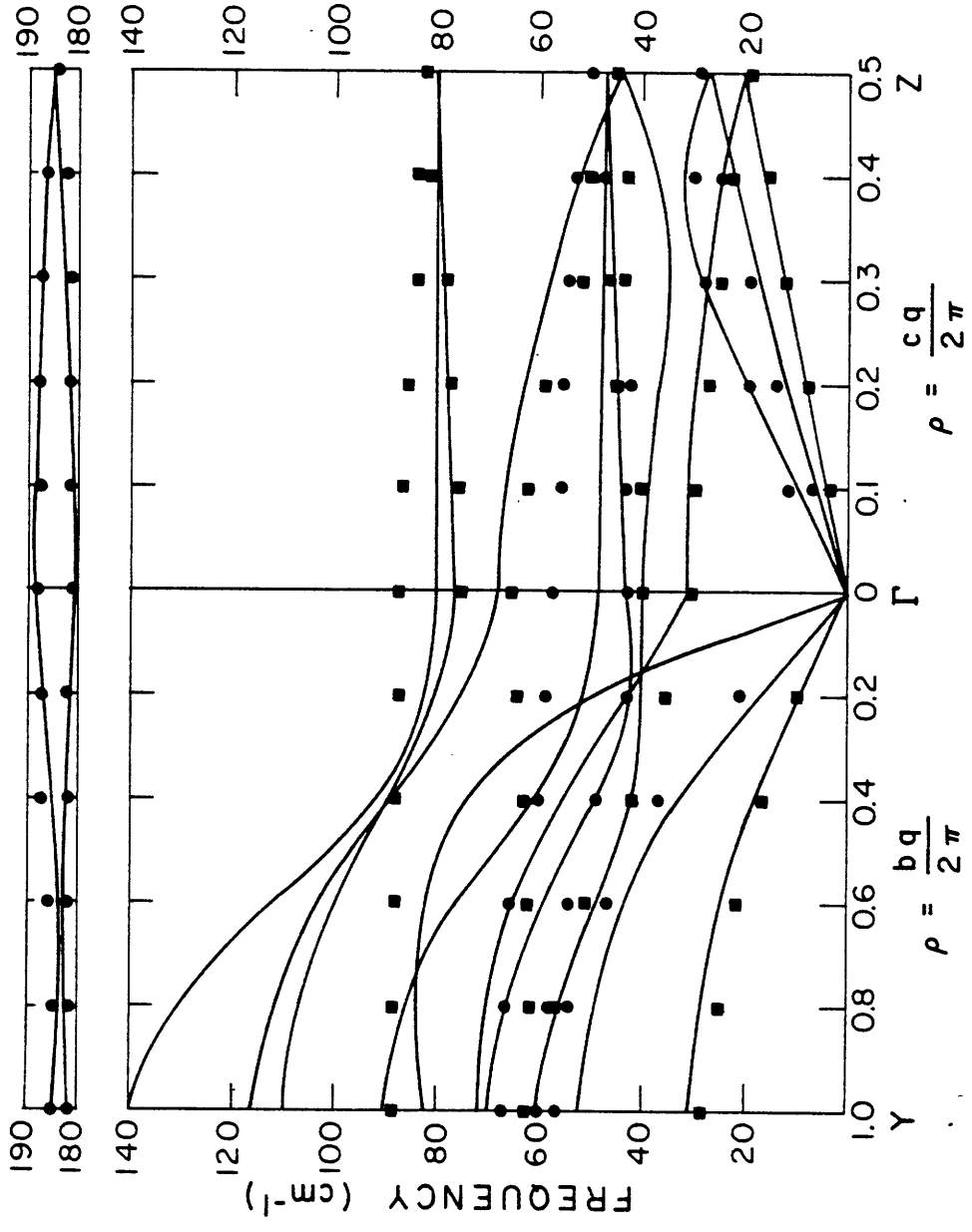

Figure 3-5. Dispersion curves for the Λ and Δ directions in iodine. Experimental points are indicated by black squares and circles ■, ●. Full curves indicate theoretical calculations.

between the experimental and theoretical points for the $\Lambda_1(B_{1u})$ branch. This is attributed to the presence of spurious effects in the measurements of that branch. The overall agreement between the experimental and theoretical points is good for the other optical branches. For the Δ direction there are two optical branches which have not been reported. The agreement between theory and experiment looks good for the lowest three optical branches $\Delta_2(A_u)$, $\Delta_3(B_{1u})$ and $\Delta_4(B_{1g})$. However, for the higher optical branches $\Delta_2(B_{2g})$ and $\Delta_4(B_{3u})$, comparison between theoretical calculations and experimental points indicate quite a discrepancy. Judgment on the behavior of the two remaining optical branches is not possible due to the lack of experimental data. In general agreement between the experimental and theoretical calculations is good for the Λ direction. There is partial agreement between theory and experiment for the Δ direction, however final judgment on the behavior of the theoretical calculations for that direction is possible only when the experimental data set is complete. Figures 3-6, 3-7, and 3-8 show the phonon dispersion curves for chlorine, bromine and iodine along the Σ, Δ and Λ directions respectively. The group symmetry tables for the points Σ, Δ and Y are given in Table 3-5. The character tables for points Γ, Λ and Z are already given in our previous work. The main features in the phonon dispersion curves are the same for all three halogens. However, the curves

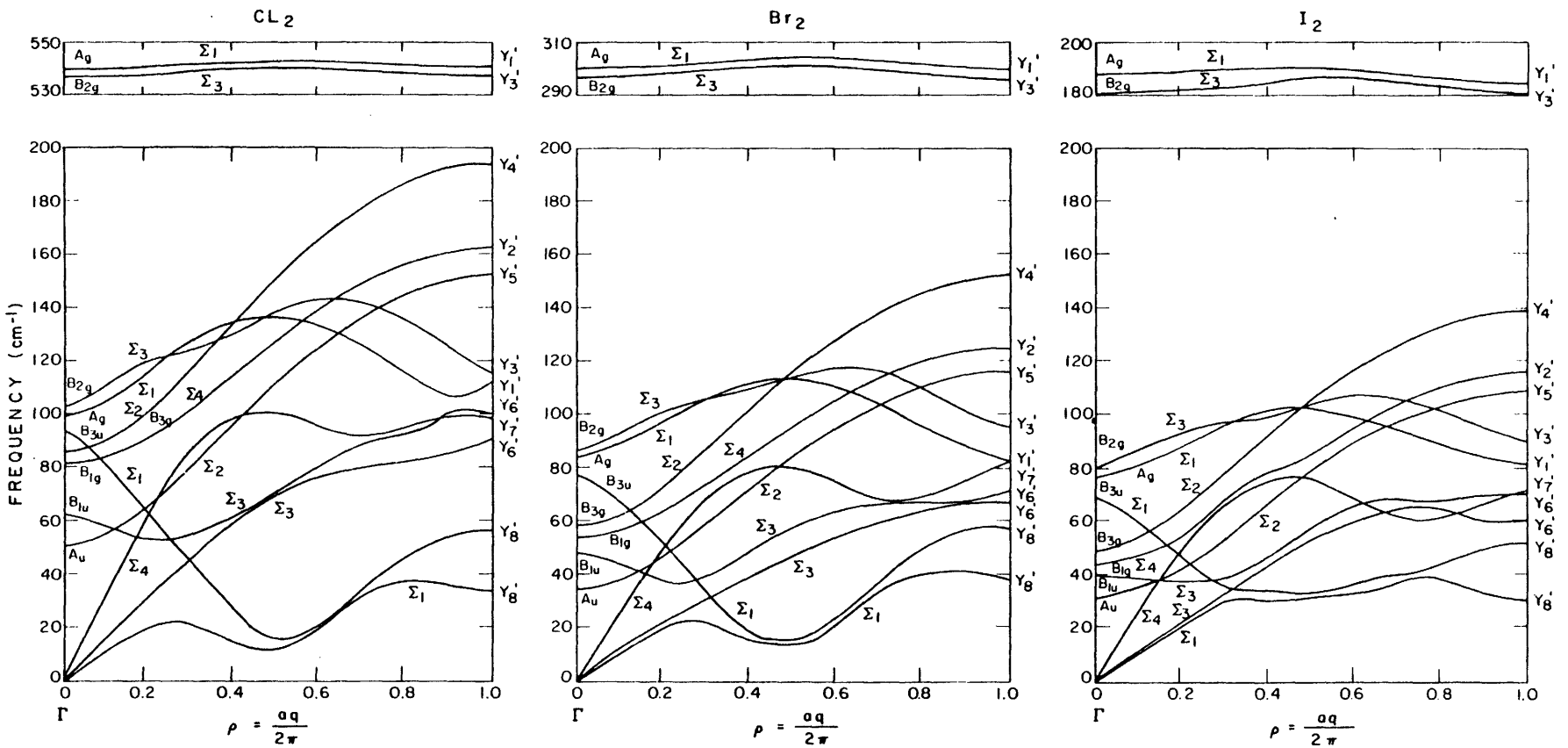

Figure 3-6. Dispersion curves for the Σ direction in chlorine, bromine and iodine. Symmetry assignments are given in detail in Table 3-5.

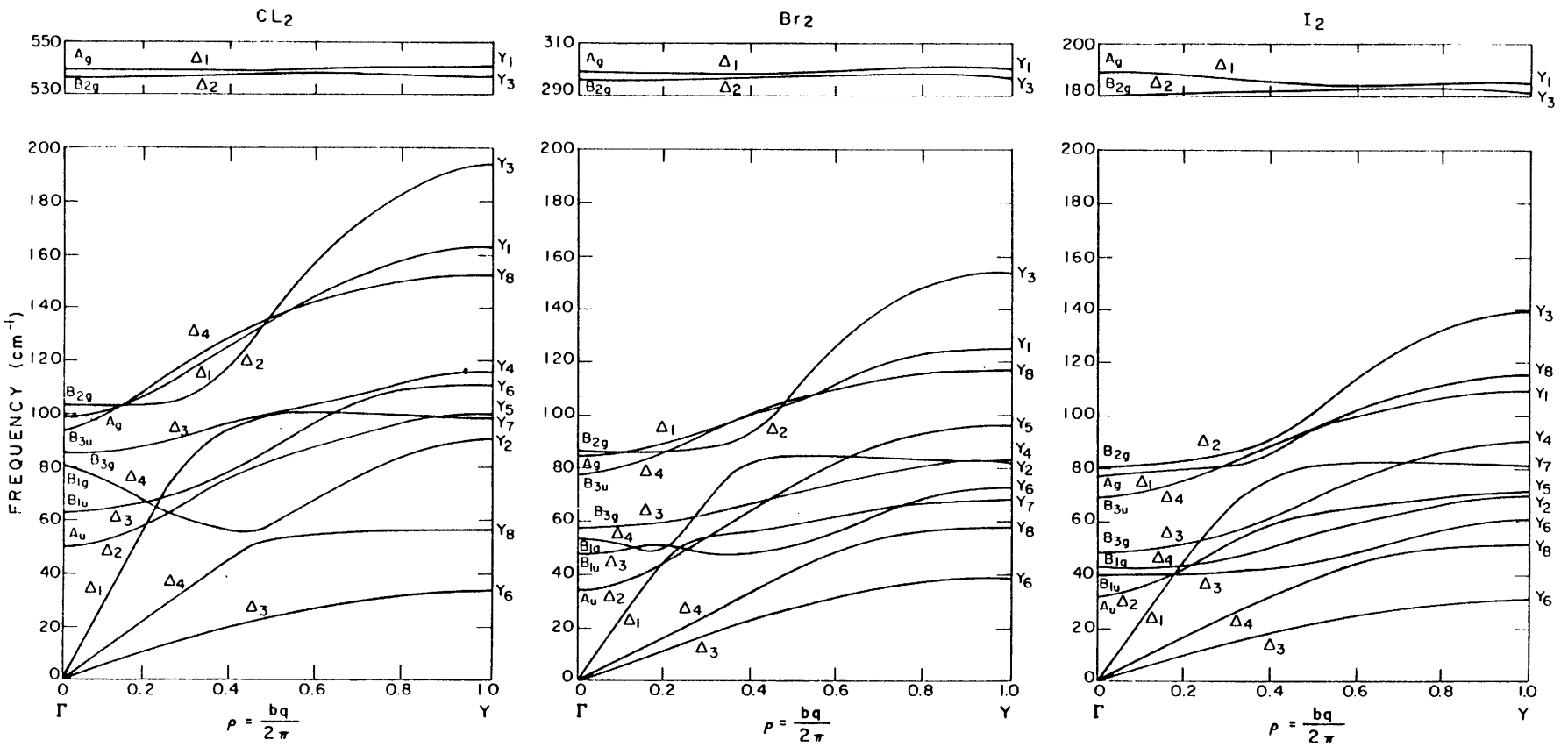

Figure 3-7. Dispersion curves for the Δ direction in chlorine, bromine and iodine. Symmetry assignments are given in detail in Table 3-5.

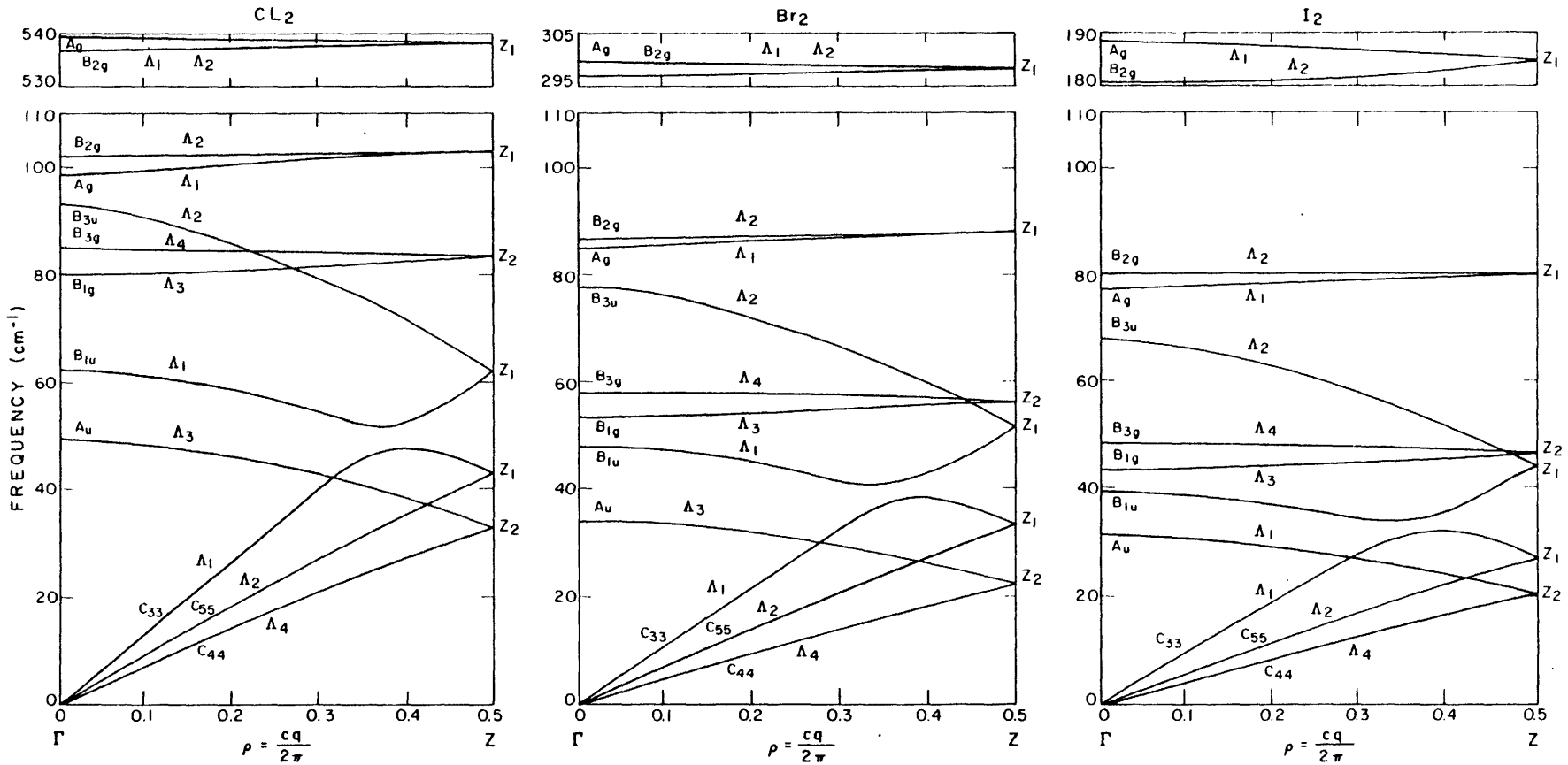

Figure 3-8. Dispersion curves for the Λ direction in chlorine, bromime and iodine. Symmetry assignments are given in detail in reference (12).

tend to compress as one shifts from chlorine to bromine to iodine due to the larger value of bond strengths in chlorine as compared to that of bromine and iodine.

One noteworthy feature is the occurrence of a valley in the Σ_1 acoustic branch, in chlorine and bromine and less apparently in iodine, with a minimum in the middle of the Brillouin zone. The wavelength of the longitudinal wave propagating through the crystal is equal to 2a. Thus atoms located near opposite corners of the orthorhombic lattice, being separated by a distance a, will be propagating with 180° phase difference relative to each other. Since the dipole-dipole interaction in this case is repulsive, the overall effect would be to decrease the attractive dispersion-repulsion forces, Figure 3-4, and thus soften the phonons at this particular wavelength. A deviation in either direction from that wavelength would indicate a shift from the 180° phase difference in which atoms near the corners of the orthorhombic lattice will move with a certain phase factor relative to each other. This will tend to decrease the effect of the repulsive dipole-dipole interaction, and thus increase the magnitude of the attractive dispersion-repulsion forces. The corresponding phonon frequencies will increase due to the larger value of the force constants. Hence one can conclude that a minimum in the phonon dispersion curves would occur at the middle point of the Brillouin zone corresponding to a wavelength of 2a, and with the phonon

frequency increasing as one shifts in either direction from the minimum. This feature is more obvious in chlorine and bromine as compared to iodine. This is explained by noting that the restoring forces are smaller in chlorine and bromine than in iodine. By referring to Figure 3-4, one notes that in the cases of chlorine and bromine the potential becomes rather flattened beyond a = 4.48 Å; and thus the restoring forces tend to be small. This effect is more pronounced in chlorine and hence it tends to show the steepest valley for the acoustic Σ_1 phonon dispersion curve. However, in the case of iodine, at a distance of a = 4.686 Å the attractive dispersion-repulsion forces tend to be more dominant as compared to the dipole-dipole repulsive interaction. The elastic constants for the Λ direction have been calculated from the slopes of the acoustic branches, Figure 3-8. Table 3-4 compares those values with the ones calculated using the force constant model (12) for each of the three halogens. Agreement between the new elastic constants calculated using the potential model and neutron experimental data is better than that using the force constant model. This is due to the limited number of force constants used to construct the phonon dispersion curves in the Λ direction. The number of force constants used is ten which is the same as that used to reproduce the zone-center frequencies, hence larger discrepancy is expected to arise in the latter case. Comparison of the two sets of phonon dispersion curves for iodine; the first using the present potential model and the

Table 3-4

Elastic constants for iodine, bromine and chlorine along the Λ direction*

Elastic Constant $\times 10^{11}$ dyne/cm^2	I_2	Br_2	Cl_2
C_{44}	0.87(0.51)	0.65(0.35)	0.65(0.48)
C_{55}	1.55(1.84)	1.46(1.59)	1.16(1.08)
C_{33}	4.14(4.72)	3.53(3.31)	2.33(2.71)

*Values in brackets as quoted in reference [12].

Table 3-5

Character tables for points Δ, Σ and Y.

(a) $\Delta(0, \frac{2\pi}{b}\mu, 0)$, $-1 < \mu < 1$

	E	$\{\bar{x}y\bar{z}\|000\}$	$\{\bar{x}yz\|\frac{1}{2}0\frac{1}{2}\}$	$\{xy\bar{z}\|\frac{1}{2}0\frac{1}{2}\}$	χ
Δ_1	1	1	1	1	3
Δ_2	1	1	-1	-1	3
Δ_3	1	-1	1	-1	3
Δ_4	1	-1	-1	1	3

(b) $\Sigma(\frac{2\pi}{a}\mu, 0, 0)$, $-1 < \mu < 1$

	E	$\{x\bar{y}\bar{z}\|\frac{1}{2}0\frac{1}{2}\}$	$\{x\bar{y}z\|000\}$	$\{xy\bar{z}\|\frac{1}{2}0\frac{1}{2}\}$	χ
Σ_1	1	$\exp(i\pi\mu)$	1	$\exp(i\pi\mu)$	4
Σ_2	1	$\exp(i\pi\mu)$	-1	$-\exp(i\pi\mu)$	2
Σ_3	1	$-\exp(i\pi\mu)$	1	$-\exp(i\pi\mu)$	4
Σ_4	1	$-\exp(i\pi\mu)$	-1	$\exp(i\pi\mu)$	2

Table 3-5 (continued)

(c) $Y(0, \frac{2\pi}{b}, 0)$

	E	$\{\bar{x}\bar{y}z\|\frac{1}{2}0\frac{1}{2}\}$	$\{\bar{x}y\bar{z}\|000\}$	$\{x\bar{y}\bar{z}\|\frac{1}{2}0\frac{1}{2}\}$	$\{\bar{x}\bar{y}\bar{z}\|000\}$	$\{xy\bar{z}\|\frac{1}{2}0\frac{1}{2}\}$	$\{x\bar{y}z\|000\}$	$\{\bar{x}yz\|\frac{1}{2}0\frac{1}{2}\}$	χ
Y_1	1	1	1	1	1	1	1	1	2
Y_2	1	1	-1	-1	1	1	-1	-1	1
Y_3	1	-1	1	-1	1	-1	1	-1	2
Y_4	1	-1	-1	1	1	-1	-1	1	1
Y_5	1	1	1	1	-1	-1	-1	-1	1
Y_6	1	1	-1	-1	-1	-1	1	1	2
Y_7	1	-1	1	-1	-1	1	-1	1	1
Y_8	1	-1	-1	1	-1	1	1	-1	2

second adopting the force constant model (12), with the experimental measurement indicates better agreement in the latter case. However, one should remember the fact that in the latter case, phonon dispersion curves are fitted to the experimental points by assigning determined values to the different force constants. A true test of the physical meaning of such a force constant model is to construct a potential function which will generate these force constants. In the force constant model, one is bound by the availability of experimental data along different symmetry directions in order to evaluate the force constants in that model. However, in the present potential model, having determined the potential parameters at the zone-center, the phonon dispersion curves along different symmetry directions are calculated using the same parameters. This enables one to test the validity of the experimental data measured, and also to predict phonon dispersion curves along other directions which have not been determined experimentally. The accuracy of the potential model may be improved by fitting it to additional physical properties such as the elastic constants or molecular quadrupole moments.

V. CONCLUSION

The present potential model reproduces the dynamic and static properties of each of the three halogens with reasonable accuracy. This indicates that the electrostatic charge interactions should be taken into account in addition to the

central dispersion-repulsion forces. In the present potential model the charge distribution around each atom is represented by a dipole located in the vicinity of the nuclear center. In reality the charge distribution is more complicated and the present model can be improved by inclusion of separate localized charge centers. This inclusion would take into account higher order interactions such as quadrupole-quadrupole interactions and will further improve the accuracy of the model. However, improvement of the present model is conditional to the generation of more experimental data. The molecular quadrupole moments and the nine characteristic elastic constants of the orthorhombic lattice should be taken as physical properties that have to be fitted by the potential parameters. These will generate better information on the nature of the interplanar forces. Another improvement on the model can be achieved by placing two smaller negative charges around the molecular center to represent the σ electronic convalent bond. The generation of experimental phonon dispersion curves along the Σ, Δ and Λ directions for chlorine and bromine as well as the Σ direction for iodine will further refine the model. It will be of great interest to pursue the measurement of the soft phonons in the Σ_1 acoustic branch for chlorine and bromine, by either measuring the whole branch or by measuring coherent inelastic scattering at the vicinity of the $|\vec{q}|$ point. If measurements confirm the same behavior as the one predicted by theory,

then the present phenomenon is very significant because it is an example of a soft phonon occurring in the middle of the Brillouin zone.

VI. REFERENCES

1. Nyburg, S.C. 1964 J. Chem Phys. 40, 2493-2501.
2. Nyburg S.C., and Wong-Ng, W. 1979 Proc. R. Soc. Lond. A. 367, 29-45.
3. Suzuki, M., Yokoyamma, T., and Ito, M. 1969 J. Chem. Phys. 50, 3392-98.
4. Suzuki, M., Yokoyamma, T., and Ito, M. 1969 J. Chem. Phys. 51, 1929-31.
5. English, P.S. and Leech, J.W. 1973 Chem. Phys. Lett. 23, 24-27.
6. Dumas, G.G., Vovelle, F., and Viennot, J.P. 1974 Mol. Phys. 28, 1345-57.
7. Smith, H.G., Nielson, M., and Clark, C.B. 1975 Chem. Phys. Lett. 33, 75-78.
8. Smith, H.G., Nielson, M., and Clark, C.B. 1974 ORNL-5028, 109-110.
9. Leech, J.W., and Pawely, G.S. 1976 Mol. Phys. 31, 1663-68.
10. Pasternak, A., Anderson, A., and Leech, J.W. 1977 J. Phys. C: Solid St. Phys. 10, 3261-71.
11. Pasternak, A., Anderson, A., and Leech, J.W. 1978 J. Phys. C: Solid St. Phys. 11, 1563-72.
12. Toukan, K., and Chen, S.H. 1981 Mol. Phys. 44, 693-707.
13. Gamba, Z., Bonadeo, H. 1981 J. Chem. Phys. 75, 5059-66.
14. Dennis, J.E., Gay, D.M., and Welsch, R.E. 1979 MRC Tech. Summary Report #2010, Univ. of Wisconsin-Madison.

15. Stogryn, D.E., and Stogryn, A.P. 1966 Mol. Phys. 11, 371-93.

16. Gopala Rao, R.V., and Joarder, R.N. 1978 Phys. Lett. 67A, 67-70.

17. King, A.O. 1969 J. Chem. Phys. 51, 1262-64.

Chapter 4

MOLECULAR DYNAMICS SIMULATION STUDY OF STABILITY IN ATOMIC LATTICES

I. INTRODUCTION

Physical systems in equilibrium generally exist in the structure that minimizes their free energy. A thermodynamic system not in equilibrium will evolve naturally in the direction that minimizes its free energy. If an absolute free energy minimum exists, the system will move towards that state and equilibrate there once having located that minimum. If the system can exist in more than one equilibrium state, then the system will tend to drift towards the state with the lowest value of the free energy. A clear view of this concept is given by the following example. Suppose a given system can exist in two unique states, that may correspond to two different structures, say A and B. A plot of the free energy of the two structures versus a given property of the system X, say pressure is illustrated in the following schematic;

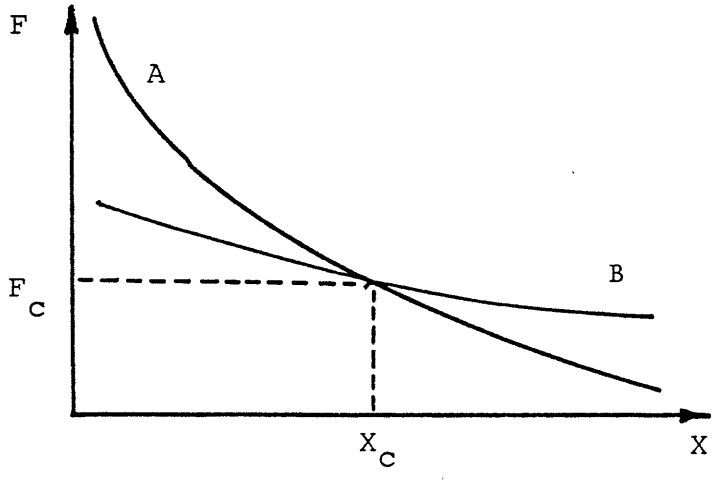

For X below X_c, the system having the structure A is at best in a metastable state because there is another structure of lower energy. This means that there is a potential difference that tries to drive the system from A to B. Whether such a transition can occur depends on the local potential barrier that the system A has to overcome. With a suitable perturbation of the system in state A, it may be moved to the lower free energy structure B. Thus, the system starts with a given structure at a certain energy and gradually changes its structure to the one corresponding to the lower free energy. If on the other hand the system is in state B for some X below X_c, then one is able to induce a structural phase transition from B to A by gradually increasing the value of X beyond the critical value X_c. The system in this case will trace the lower free energy curve and reside in the structure that corresponds to the lower free energy. Thus for such a system, one is able to investigate structural stability and phase transition.

Such phenomena may be studied using computer molecular dynamics or Monte Carlo simulation. With computer molecular dynamics, the time evolution of the system is traced from its initial to its final state. Probing thermodynamic variables such as temperature, pressure, enthalpy and internal energy to detect any structural transformation is possible through this technique. A general survey of the method is found in the articles by Beeler (1), Kushick and

Berne (2) and Erpenbeck and Wood (3). In Monte Carlo simulation, a study of the stochastic properties of the system is possible to detect any transition. Wood (4) and Binder (5) give a thorough review of the method in their articles. However, we will be looking at computer molecular dynamics only in this chapter.

The basic idea underlying such a technique is the simulation of the system using periodic flexible boundary conditions. The use of periodic boundary conditions allows one to study bulk properties with a small number of particles. The main assumption is that the bulk of the system is just a replica of the simulation cell. The term flexible boundary is applied here to indicate that the boundaries of the system can change shape as well as volume. This is opposed to periodic fixed boundary in which the system preserves its volume and shape through out the simulation. Conventional molecular dynamics has been usually carried out with fixed boundaries. Andersen (6) modified the method to study systems under constant pressure by introducing the volume of the system as an additional dynamical variable. A generalization of Andersen's idea has been carried out by Parrinello and Rahman (7) in which the shape as well as the volume of the simulation cell may vary with time. In this method the boundaries of the system are able to adjust themselves in such a manner that will balance the internal and external stresses applied on them. Thus the simulation cell is able

to expand, contract or change shape according to the net stress applied on it. In conjunction with that, the internal structure of the system will be rearranging itself in such a manner that will minimize its free energy and balance the net stress on the boundary. Parrinello and Rahman (8) have shown an FCC→HCP transition in Ni under compression by applying this technique.

In this chapter we will be considering specifically atomic systems in two dimensions. It is well known that the triangular HCP structure is the most stable one in two dimensions for a Lennard-Jones system. Hence any crystal structure different from the triangular one will evolve into the latter if no constraints are present. We will be looking first at Lennard-Jones atomic systems to investigate such structural transformations. Later a study of Hooke's Law crystals (9) to investigate possible structural phase transitions is carried out. For such systems two structures, triangular and square, coexist at particular densities. A transition from one structure to the other is sought using computer molecular dynamics with flexible boundary conditions. The merit of this technique as compared to the fixed boundary system in molecular dynamics is the flexibility in the shape of the simulation cell which allows the system to move more easily into a new state. Such a transformation might not be possible at all with a fixed boundary having a rigid constraint. Also such transformations can be studied using smaller systems in the former case. To explain such a technique we will first

give a brief idea of molecular dynamics and then develop the formalism underlying the flexible boundary systems.

Molecular dynamics is a method for studying classical statistical mechanics of well defined systems through a numerical solution of Newton's equations of motion. A set of N classical particles have coordinates $\vec{r}_i$, velocities $\dot{\vec{r}}_i$ and masses m_i, $i = 1,\ldots,N$. The particles interact through a potential $V_N(\vec{r}_1,\ldots,\vec{r}_N)$ which, in most cases is taken to be a pair potential of the form:

$$V_N = \frac{1}{2} \sum_i \sum_{j \neq i} \phi(r_{ij}) \qquad (4.1)$$

where $r_{ij} = |\vec{r}_{ij}| = |\vec{r}_i - \vec{r}_j|$.

For such potentials, Newton's equations of motion reduce to

$$m_i \ddot{\vec{r}}_i = - \sum_{j \neq i} \frac{1}{r_{ij}} \frac{d\phi}{dr_{ij}} \vec{r}_{ij}, \quad i = 1,\ldots,N \qquad (4.2)$$

and are solved numerically. As the system evolves in time it eventually reaches equilibrium conditions in its dynamical and structural properties; the statistical averages of interest are calculated from $\vec{r}_i(t)$ and $\dot{\vec{r}}_i(t)$, $i=1,\ldots,N$ as temporal averages over the trajectory of the system in its phase space. For practical reasons N is restricted to at most a few thousand. However to simulate a bulk system the common practice is to use periodic boundary conditions. These

are obtained by periodically repeating a unit cell of volume Ω containing the N particles by suitable translations. As a consequence of V_N being a function of r_{ij} only (Eq. (4.1)), the solution of Eq. (4.2) conserves the total energy E of the system; thus the statistical ensemble generated in a conventional MD calculation is a (Ω,E,N) ensemble or a micro-canonical ensemble. A thorough description of this method is discussed in a book by Hansen and McDonald (10).

The restriction that the MD cell be kept constant in volume and shape severely restricts the applicability of the method to problems involving volume changes or crystal structure transformations; in such transformations changes in the volume and shape of the cell play an essential role. Andersen (6) developed a scheme for MD simulation in which the cell volume can change but not its shape. Thus crystal structure transformations are inhibited because of the suppression of the essential fluctuations namely those in the shape of the MD cell. However in the method proposed by Parrinello and Rahman (7), an extra degree of flexibility is introduced which allows for a change in the shape of the MD cell. As before the system consists of N particles in a cell that is periodically repeated to fill all space. However, the cell can have an arbitrary shape and volume being completely described by three vectors $\vec{a}$, $\vec{b}$, $\vec{c}$ that span the edges of the MD cell. The vectors $\vec{a}$, $\vec{b}$, $\vec{c}$

can have different lengths and arbitrary mutual orientations. An alternative description is obtained by arranging the vectors as $\{\vec{a}, \vec{b}, \vec{c}\}$ to form a 3x3 matrix $\underset{\simeq}{h}$ whose columns are, in order, the components of $\vec{a}$, $\vec{b}$, and $\vec{c}$. The volume is given by

$$\Omega = ||\underset{\simeq}{h}|| = \vec{a}\cdot(\vec{b}\times\vec{c}) \tag{4.3}$$

The position $\vec{r}_i$ of a particle i can be written in terms of $\underset{\simeq}{h}$ and a column vector $\vec{s}_i$, with components ε_i, η_i, ρ_i as

$$\vec{r}_i = \underset{\simeq}{h}\vec{s}_i = \rho_i\vec{a}+\eta_i\vec{b}+\rho_i\vec{c} \tag{4.4}$$

Obviously $0 \leq \varepsilon_i, \eta_i, \rho_i \leq 1$ is the range of variation of the numbers ε_i, η_i, ρ_i, i=1,...,N. The images of $\vec{s}_i$ are at $\vec{s}_i+(\lambda,\mu,\nu)$ where λ, μ, ν are integers from $-\infty$ to $+\infty$. Considering two atoms i and j in the lattice, the square of the distance between i and j is given by

$$r_{ij}^2 = (\vec{s}_i-\vec{s}_j)' \underset{\simeq}{G} (\vec{s}_i-\vec{s}_j) \tag{4.5}$$

where $(\vec{s}_i-\vec{s}_j)'$ is the transpose of the given vector and the tensor $\underset{\simeq}{G}$ is

$$\underset{\simeq}{G} = \underset{\simeq}{h}'\underset{\simeq}{h} \tag{4.6}$$

The reciprocal lattice space is spanned by the vectors

$$\frac{2\pi}{\Omega}\{\vec{b}\times\vec{c}, \vec{c}\times\vec{a}, \vec{a}\times\vec{b}\} = \frac{2\pi}{\Omega}\underset{\simeq}{g} \tag{4.7}$$

The matrix $\underset{\simeq}{\sigma} = \Omega \underset{\simeq}{h}'^{-1}$ represents the surface area of the given MD cell.

In such a system the number of dynamical variables studied is 3N + 9; the usual set of 3N dynamical variables that describe the positions of the N particles, in addition to the 9 components of $\underset{\simeq}{h}$. The time evolution of the 3N + 9 variables is obtained from the Lagrangian

$$L = \frac{1}{2} \sum_{i=1}^{N} m_i \dot{\vec{s}}_i \underset{\simeq}{G}' \dot{\vec{s}}_i - \sum_{i=1}^{N} \sum_{j>i}^{N} \phi(r_{ij})$$

$$+ \frac{1}{2} W \mathrm{Tr} \dot{\underset{\simeq}{h}}' \dot{\underset{\simeq}{h}} - p\Omega \qquad (4.8)$$

The first term represents the total kinetic energy of the N particles in the MD cell. The second term represents the total potential energy of the N particle system. The third term represents the kinetic energy stored in the boundary of the MD cell and the last term is the hydrostatic energy of the system. From Eq.(4.8) the equations of motion are easily derived to give

$$\ddot{\vec{s}}_i = - \sum_{j \neq i} \frac{1}{m_i} \frac{\phi'}{r_{ij}} (\vec{s}_i - \vec{s}_j) - \underset{\simeq}{G}^{-1} \dot{\underset{\simeq}{G}} \dot{\vec{s}}_i, \; i=1,\ldots,N \qquad (4.9)$$

$$W \ddot{\underset{\simeq}{h}} = (\underset{\simeq}{\pi} - p\underset{\simeq}{I}) \underset{\simeq}{\sigma}, \qquad (4.10)$$

where using the usual dyadic notation, and writing $\vec{v}_i = \underline{\underline{h}}\dot{\vec{s}}_i$,

$$\Omega \underline{\underline{\pi}} = \sum_i m_i \vec{v}_i \vec{v}_i - \sum_i \sum_{j>i} \frac{\phi'}{r_{ij}} \vec{r}_{ij} \vec{r}_{ij} \qquad (4.11)$$

One should note that the actual velocity of the ith particle is $\vec{v}_i = \underline{\underline{h}}\dot{\vec{s}}_i + \dot{\underline{\underline{h}}}\vec{s}_i$. However, assuming that the frequency of the boundary fluctuation is much smaller than that of the particle oscillations, the second term may be dropped out when compared to the first term. The internal pressure of the system is a function of its internal fabric; its value can be obtained as 1/3 of the trace of the average of $\underline{\underline{\pi}}$. Equation (4.11) gives the internal microscopic stress tensor $\underline{\underline{\pi}}$ which is made up of the contributions to the internal stress from the particle momenta and forces. The first term is the kinetic contribution and its average value is directly proportional to the temperature of the system. The second term is the virial and is determined by the internal structure and potential of the system. Later we can see how one can drive the system through its internal pressure by exciting any of its constituent components. The first component can be excited by direct heating and the second by introducing internal shear in the structure. Equation (4.10) indicates that the temporal changes in $\underline{\underline{h}}$ i.e. in the shape and size of the MD cell are driven by the difference between $\underline{\underline{\pi}}$ and the external pressure p, and that this imbalance acts across the outer faces $\underline{\underline{\sigma}}$ of the MD cell. From

Eq.(4.10) it is seen that the mass W determines the relaxation time for recovery from an imbalance between the external pressure and the internal stress. Hence W can be thought of as the boundary mass determining the inertia of the system under applied stress. In our calculations W is chosen on the basis of computational convenience. However, the equilibrium properties of the system are not changed, being independent of the masses of its constituent parts.

The corresponding Hamiltonian for the system is derived from the Lagrangian Eq. (4.8) as

$$H = \sum_i \frac{1}{2} m_i |\vec{v}_i|^2 + \sum_i \sum_{j>i} \phi(r_{ij}) + \frac{1}{2} W \mathrm{Tr} \dot{\underset{\simeq}{h}} \dot{\underset{\simeq}{h}} + p\Omega \qquad (4.12)$$

Since the system is not subject to time dependent external forces this is a constant of the motion. Hence the Lagrangian Eq. (4.8) generates a (p,*H*,N) ensemble. In equilibrium, at temperature T, $9/2\ k_B T$ is contributed by the term with W and $3N/2\ k_B T$ by the other kinetic terms. If the number of particles is large, say several hundred, then one finds that the constant of motion *H* is nothing but the enthalpy

$$H = E + p\Omega \qquad (4.13)$$

where

$$E = \sum_i \frac{1}{2} m_i |\vec{v}_i|^2 + \sum_i \sum_{j>i} \phi(r_{ij}) \qquad (4.14)$$

Hence the Lagrangian Eq. (4.8) generates a (p,H,N) ensemble.

In Section II, we will discuss a simple illustration of the technique in a one dimensional system. Uniform expansion upon heating of a one dimensional atomic chain will be discussed. In Section III, transformations from square to triangular structure will be studied for a two dimensional Lennard-Jones system. It serves as a clear illustration of how a system evolves in time by seeking the minimum free energy structure, which is the triangular HCP structure for a two dimensional system. In Section IV, a piece-wise linear force potential model is investigated. For such a potential, both square and triangular structures coexist in a range of densities. A structural phase transition under the effect of applied hydrostatic pressure is sought by applying this technique.

II. ONE DIMENSIONAL CHAIN

The simplest system to study using the flexible boundary method is a one dimensional chain of atoms. We will examine the behavior of the chain upon heating to demonstrate the uniform expansion of the system under constant pressure. It should be mentioned that such a study is not possible with conventional molecular dynamics using fixed boundary conditions. The merit with the flexible boundary technique is that upon heating, the internal pressure of the system rises beyond its equilibrium value due to the increase in the instantaneous kinetic contribution of the internal stress tensor. With the boundary being flexible, the system is able to expand and equilibrate the net pressure on the surface by decreasing the virial contribution of the internal stress tensor. However, with a fixed boundary, the net result will be an increase in the internal pressure of the system with a net stress being exerted on its boundaries.

In the one dimensional case, the equations of motion take the following simple form.

$$L = \frac{1}{2} \sum_{i=1}^{N} m_i (h\dot{s}_i)^2 - \sum_{i=1}^{N} \sum_{j>i}^{N} \phi(r_{ij}) + \frac{1}{2} W\dot{h}^2 - ph \qquad (4.15)$$

$$\ddot{s}_i = - \sum_{j \neq i} \frac{1}{m_i} \frac{\phi'}{r_{ij}} (s_i - s_j) - \frac{2\dot{h}}{h} \dot{s}_i, \quad i=1,\ldots,N \qquad (4.16)$$

$$W\ddot{h} = (\pi - p) \tag{4.17}$$

and

$$h\pi = \sum_i m_i v_i^2 - \sum_i \sum_{j>i} r_{ij}\phi' \tag{4.18}$$

where h, G and π are scalars in this case. The variable h in the above equations corresponds to the chain length. We considered a system of ten equally displaced particles interacting through a Lennard-Jones potential. Periodic boundary conditions were applied and the simulation was started at zero external pressure and a lattice spacing corresponding to the minimum potential energy. Physical properties were scaled to nondimensional units using Lennard-Jones parameters according to the following scheme;

$$\begin{aligned} \phi^* &= \phi / 4\varepsilon \\ r^* &= r/\sigma \\ \Delta t^* &= \left(\frac{4\varepsilon}{m\sigma^2}\right)^{1/2} \Delta t \end{aligned} \tag{4.19}$$

The * indicates the scaled quantities. The parameters ε and σ correspond to the potential depth and zero crossing point of the Lennard-Jones system respectively. The quantity ϕ represents energy and might correspond to either kinetic or potential energy. The variables r and Δt correspond to length and time respectively. With W=4, the temperature was raised to 0.05 in nondimensional units, corresponding to 24^{o}K say, in the case of argon. The simulation was started with a time step size Δt^*=0.05, which is equivalent to 5.4×10^{-14} sec for argon and run for 25,000 time steps. Figure 4-1

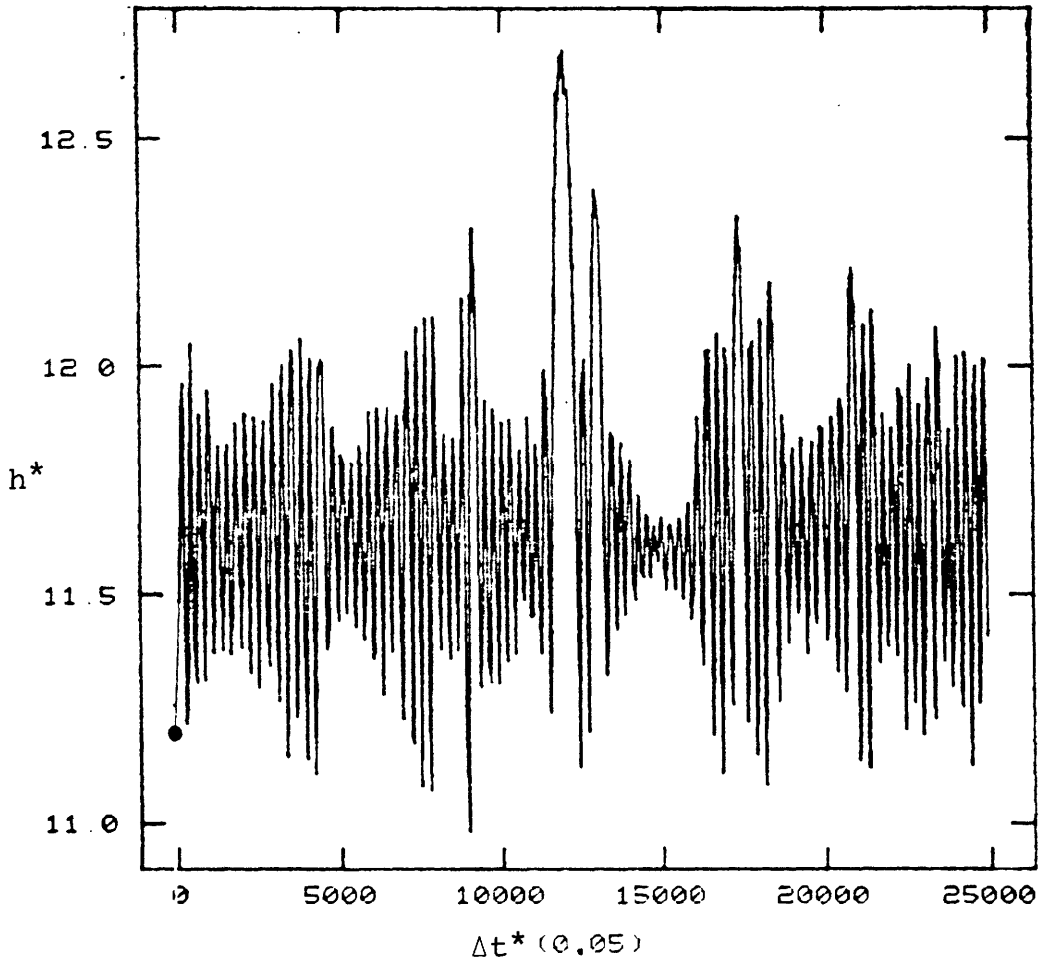

Figure 4-1. Instantaneous chain length as a function of time. Initial value of simulation is indicated by a black circle.

shows a plot of the instantaneous chain length as a function of time. After a few thousand time steps, the chain length oscillates around a mean which is larger than its initial value. This indicates that the chain has undergone expansion upon heating. The behavior of the temperature is interesting to study. In Figure 4-2, one notes that the temperature quickly decreases from its initial value trying to reach its new equilibrium value. In such cases, one expects the system to equilibrate at a final value equal to half its initial value based on the statistical equipartition theorem and assuming a harmonic system. However, in this case one notes that the final equilibrium value is smaller than half the initial value by 25%. The difference is attributed to the vibrational energy in the boundary which is not damped out. This aspect is actually one of the weaknesses of this method where one notes that the boundary keeps on oscillating with no apparent damping to reach its average value. Thus the fictitious boundary will carry some energy as it vibrates which is an undesirable feature. This may be attributed to the approximation noted earlier in the first section. Neglecting the term $\dot{h}s$ in the calculation of the velocity v removes the damping term in the equation for boundary motion. The net result of which is the continuous oscillation of the boundary around its equilibrium position.

Since the system is homogeneous, with all particles having the same mass and being equally displaced from one

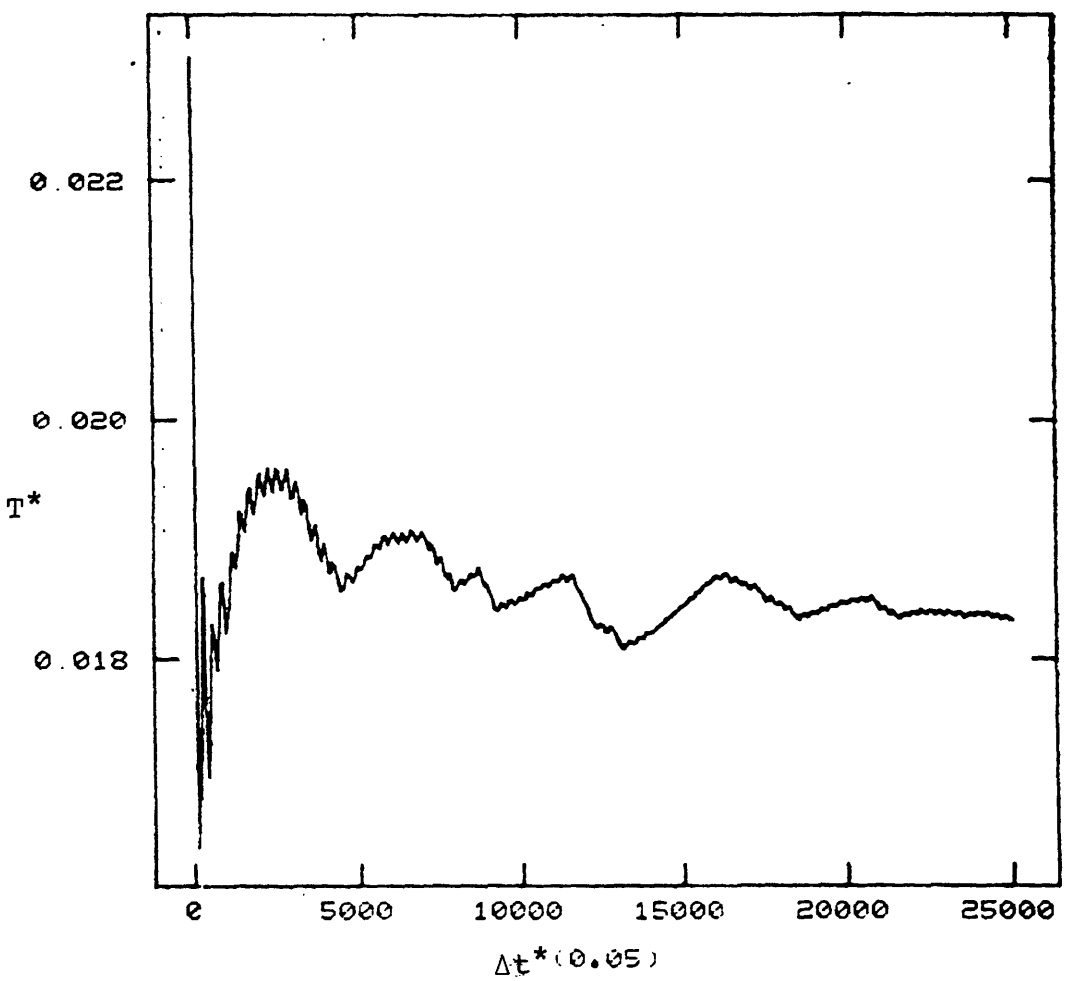

Figure 4-2. Average temperature as a function of time. Initial value of T*=0.05.

another in the initial configuration, it is expected to undergo uniform expansion upon heating. Figure 4-3 shows a typical plot of s, the relative position for a given particle in the chain. As noted, the particle oscillates around its initial position keeping the same value throughout the simulation. The behavior of all other particles in the simulation cell is similar. This indicates that the chain expands with all particles maintaining their same average relative position throughout the process, indicating uniform behavior as expected. The constant of motion in this process is the total energy rather than the enthalpy, the external pressure being zero. The total energy in this case is the sum of internal potential energy, the kinetic energy of the particles and the boundary kinetic energy. Figure 4-4 shows a plot of the instantaneous total energy of the chain. The energy oscillates around a mean value which is constant throughout the simulation. The percentage deviation in the instantaneous value does not exceed a value of 0.75 from the mean. A noteworthy aspect is to mention that the simulation time step size is determined by the energy constancy. For a given simulation, one looks for the optimum value of time step that preserves energy constancy within the desired limits and minimizes the number of time steps needed for the whole process.

Thus the flexible boundary method allows one to study such systems smoothly and with relative ease. One might

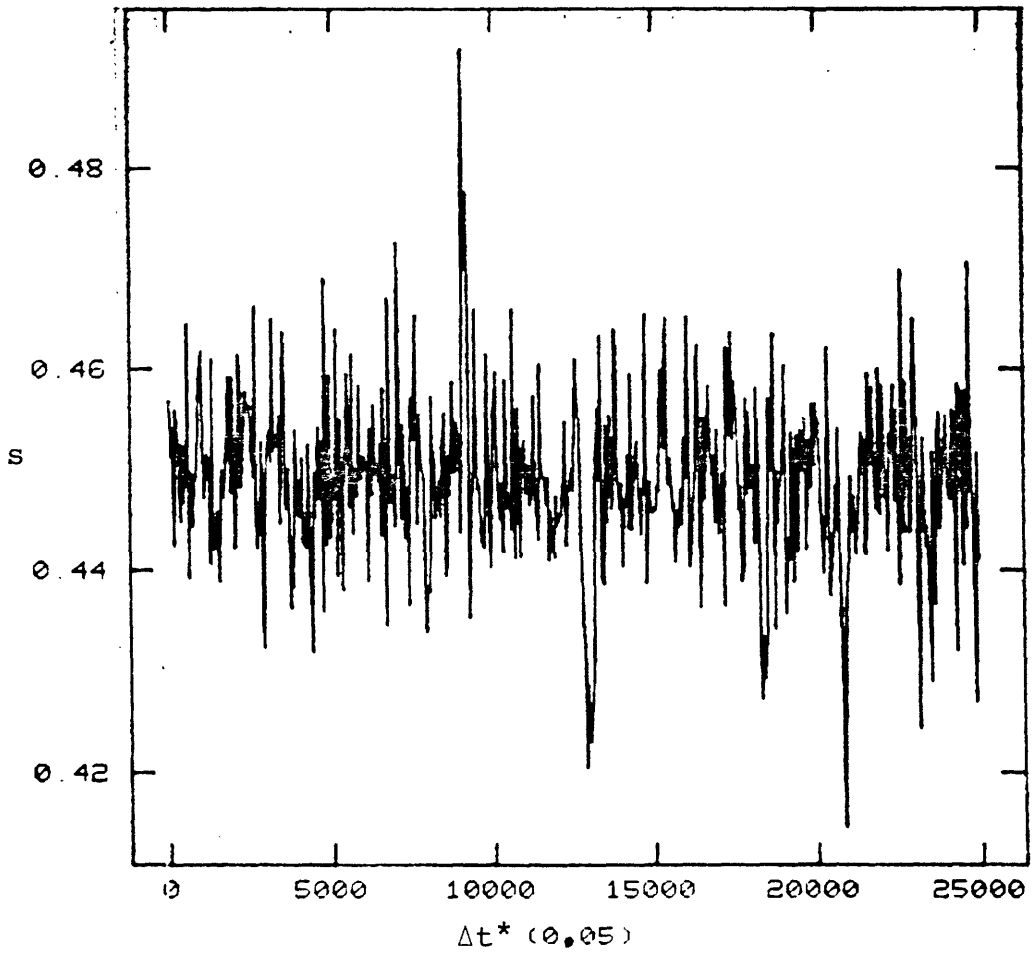

Figure 4-3. Instantaneous relative position s for a given particle as a function of time.

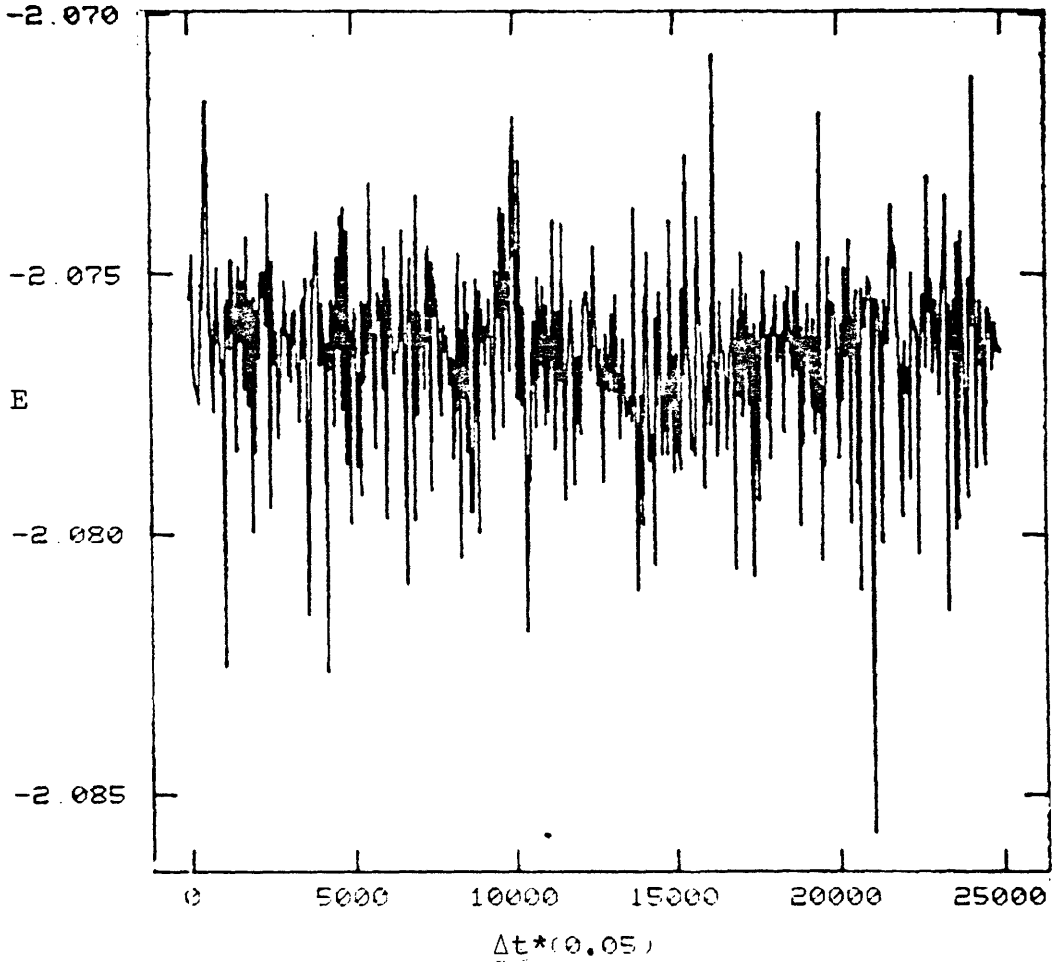

Figure 4-4. Instantaneous total energy as a function of time.

actually determine the coefficients of expansion as a function of temperature for real physical systems by this technique.

III. TWO DIMENSIONAL LENNARD-JONES SYSTEMS

The two dimensional Lennard-Jones system is a very interesting case to study for the wide use of Lennard-Jones potentials in many atomic and molecular systems. It is well established that the triangular structure is the most stable one for such a potential. The reason for that is the high symmetry that this structure possesses. With the six-fold axis symmetry that such a structure has, it makes it the highest order possible symmetry structure. Consequently, a given atom in the structure will have the largest number of close nearest neighbors, being six in this case. With an attractive potential, the triangular structure will have the lowest potential energy and thus be the most stable one compared to other lower symmetry structures. Hence, as discussed in Section I any crystal structure which is different from the triangular one will seek to go to it in order to achieve the minimum energy. We will consider in this section a square lattice as a specific example and study its time evolution as it undergoes such a transition. But before we do that, the formalism for the two dimensional flexible boundary condition will be first established.

The equations governing the individual motion of each of the particles and the boundary motion still retain the

form given by Equations (4.8)-(4.11). The matrix $\underset{\simeq}{h}$ takes on the following form in this case;

$$\underset{\simeq}{h} = \begin{bmatrix} a_x & b_x \\ a_y & b_y \end{bmatrix} \tag{4.20}$$

The four components of $\underset{\simeq}{h}$ relative to the fixed coordinate system are illustrated in the following schematic;

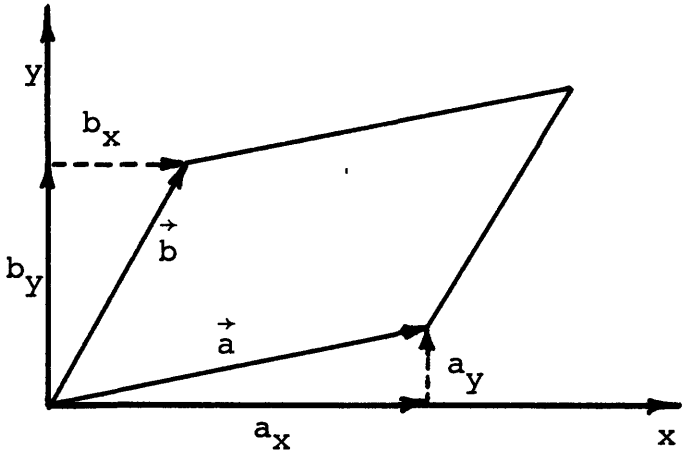

Periodic boundary conditions are applied here by displacing the simulation cell by multiples of the time dependent vectors $\vec{a}$ and $\vec{b}$. This is to be contrasted with the rigid boundary case where images are constructed by adding constant vectors $\vec{a}$ and $\vec{b}$ to the atomic coordinates in the simulation cell.

We considered a system of 36 particles with a square structure located in a square simulation cell. Since we are operating at temperatures close to $0^{o}K$, potential energies rather than free energies are compared. Figure 4-5 shows a plot of the potential energies for both structures as a function of the closest interatomic spacing, d. The minimum

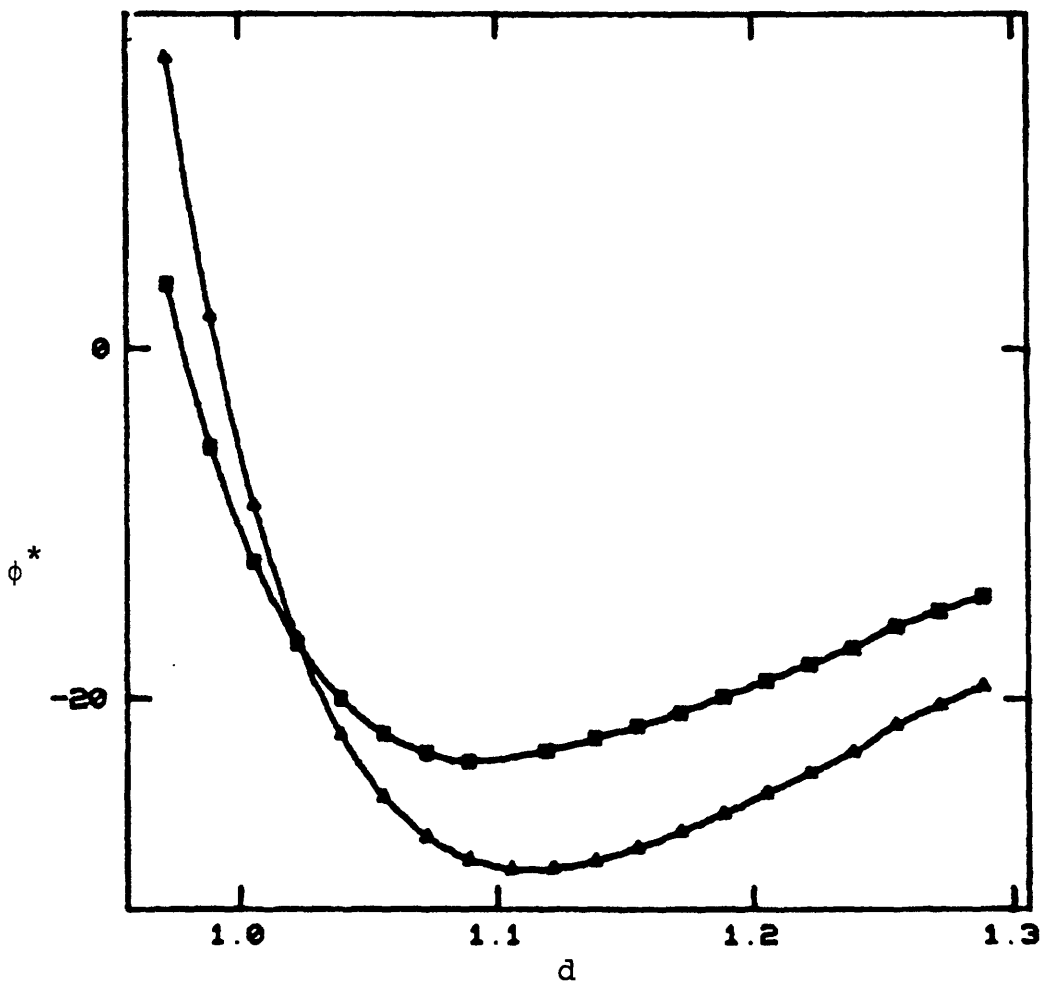

Figure 4-5. Potential energy curves for square and triangular structures as a function of interatomic spacing for a 36 particle system.

of the square structure occurs at an interatomic spacing of 1.0977 while that for the triangular occurs at a value equal to 1.1412. The larger shift in the square case from the nominal value of $(2)^{1/6}$ is due to the fact that second neighbor interactions are more pronounced in the square structure. One notes that the triangular structure has the lowest energy in the vicinity of this point. The corresponding plots as a function of pressure are given in Figure 4-6. The minima in the potential curves occur at zero pressure as expected. The interesting feature about such plots is that since the simulation is carried out isobarically, one expects a transition from one point on any of the potential curves to its vertical projection on the other curve corresponding to the other structure.

Thus as explained in Section I, if one starts with a square structure at any given pressure, it is expected that a transition would take place to a triangular one at the same pressure, the potential energy difference being the driving force in this case. To induce such a transition, any of the internal stress components may be excited. Heating of the system or internal shear introduced by breaking the system symmetry are two means of starting such a transition.

A simulation starting with a square structure at zero pressure was initiated by heating the system to a scaled temperature $T^*=0.05$. With $W=4$ and $\Delta t^*=0.005$ the system was run for 6000 time steps. As the system evolved in time

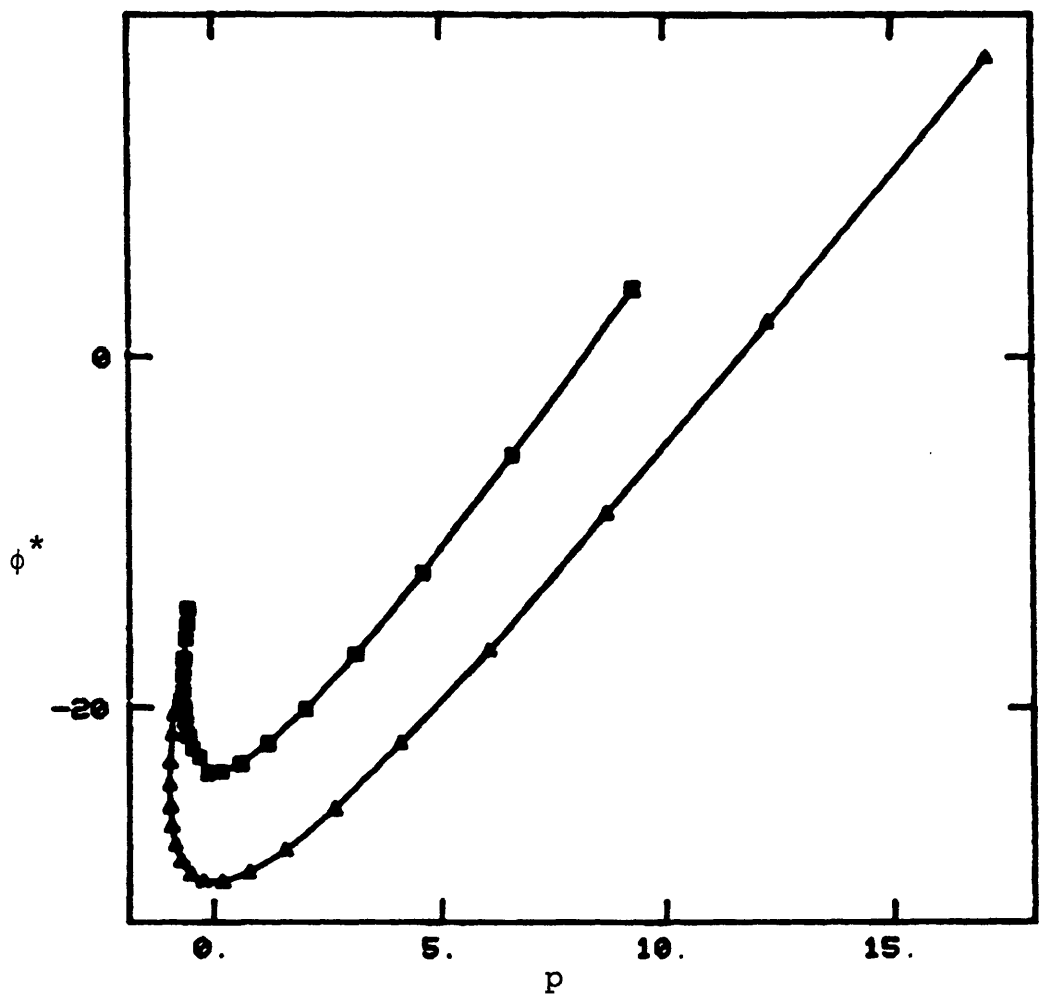

Figure 4-6. Potential energy curves for square and triangular structures as a function of pressure for a 36 particle system.

sharp transitions in the system properties were noticed. Figure 4-7 shows a plot of the potential energy of the system as a function of time. One notes the sharp drop in the potential energy after the first few hundred time steps indicating that the system is seeking a lower minimum energy structure. After several thousand time steps, the system appears to have located that minimum and is undergoing some fluctuations around its new average value. The behavior of the temperature is interesting to notice. Figure 4-8 shows the temperature time evolution. In the first few hundred time steps, the temperature decreases trying to go to half its initial value as mentioned in Section II. However, with the sudden surge of energy into the system due to the sharp drop in its potential energy, the system quickly heats up and equilibrates at a higher temperature corresponding to the new equilibrium structure. The force initiating such a transition is the internal stress in the system. At equilibrium one expects a balance between the internal and external pressures of the system. Since the simulation was started by heating up the system, this creates an imbalance between the net internal stress and the external applied pressure, being zero in this case. Figure 4-9 shows a plot of the net stress tensor "ST" taken as $\frac{1}{2}$ Tr $\underset{\simeq}{\pi}$ $\underset{\simeq}{\sigma}$ as a function of time. The initial value of "ST" is -1.8, implying an excess external pressure. As one traces the time evolution of the system, one notes that "ST" oscillates around a new equilibrium value

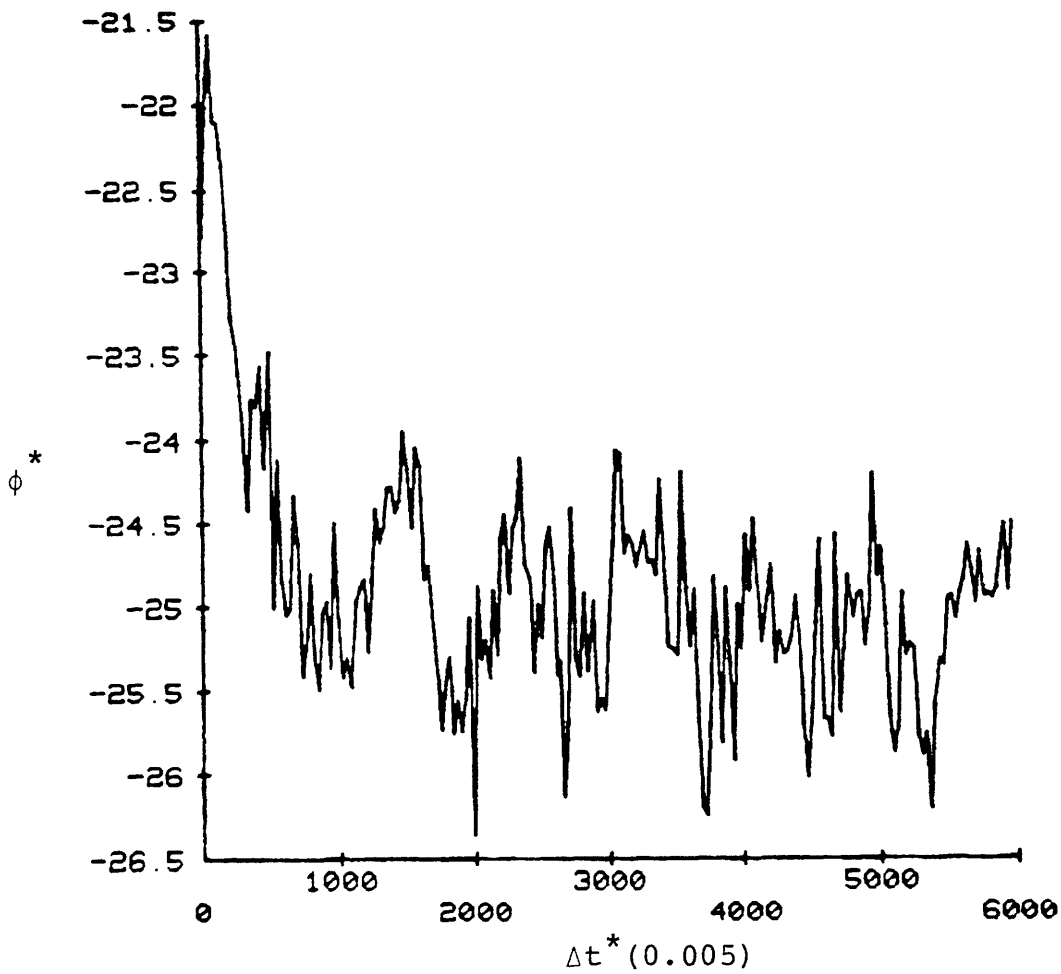

Figure 4-7. Potential energy of the system as a function of time.

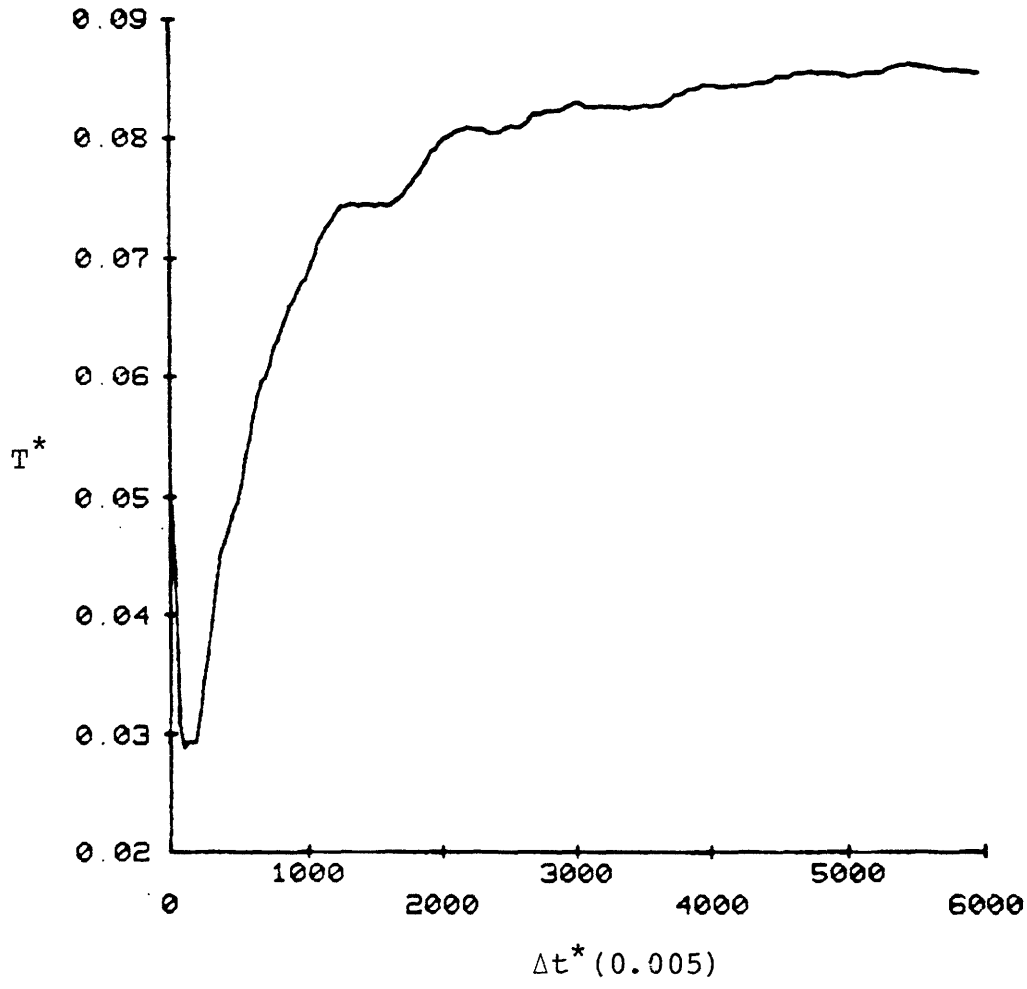

Figure 4-8. Scaled temperature as a function of time.

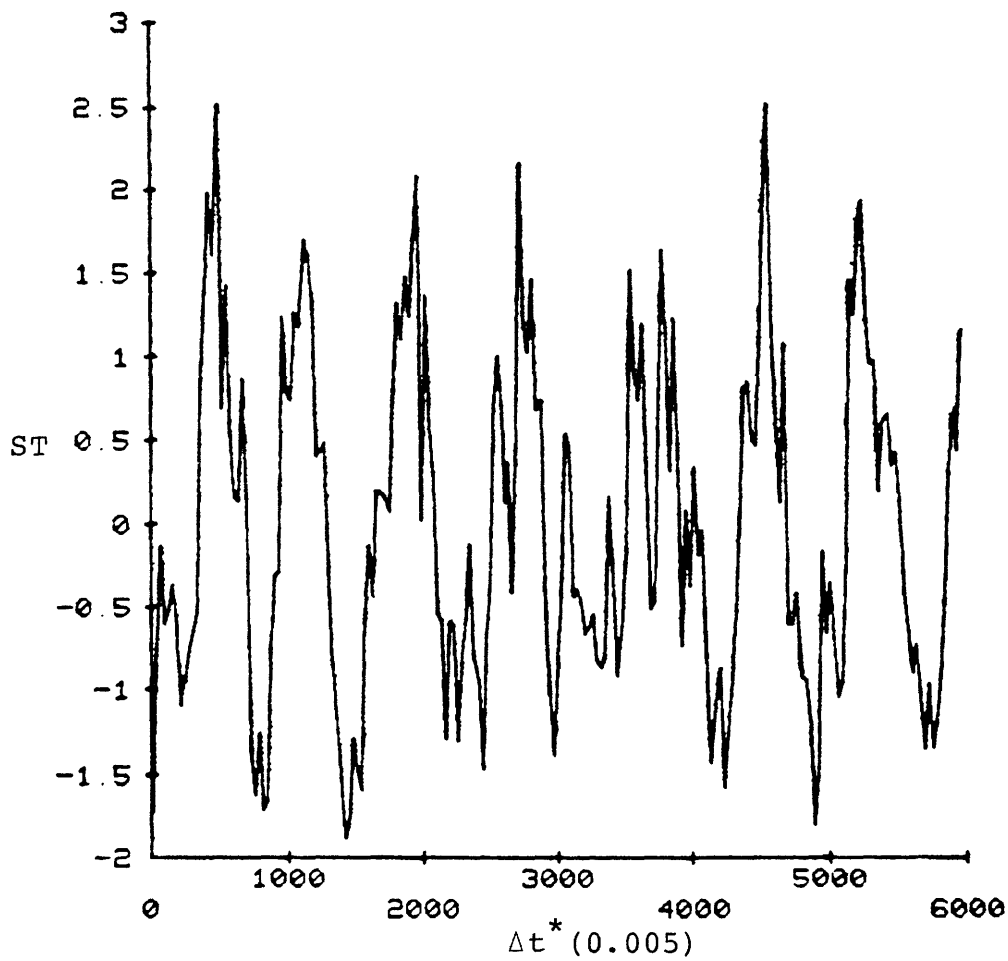

Figure 4-9. Net internal stress as a function of time.

very close to zero, implying that the balance between the external and internal pressure has been restored. The initial internal stress is negative since the simulation was started with an interatomic spacing slightly larger than that corresponding to the minimum.

A very interesting aspect to look at is the final particle configuration of the system. Figure 4-10 shows the initial square structure at the beginning of the simulation. Figure 4-11 shows the final structure of the system at the end of the simulation. One can clearly observe the final equilateral triangles formed by the particles indicating the final transition to a triangular structure. One interesting feature to note is the change in the shape of the simulation cell after such a transition. It is seen that there is relative compression in the vertical dimension accompanied by a relative expansion in the horizontal length a_x. Figure 4-12 shows the time evolution of b_y where one sees that it has shrunk from an initial value of 6.73 to a new average value of 6.05. Figure 4-13 shows the time behavior of a_x where an expansion from an initial value of 6.73 to a new equilibrium value of 7.0 has taken place. This is a very notable feature to consider. To accommodate such a transition, the simulation cell changed its shape from a perfect square to an elongated rectangle. Such a change can be well understood by considering the following schematic.

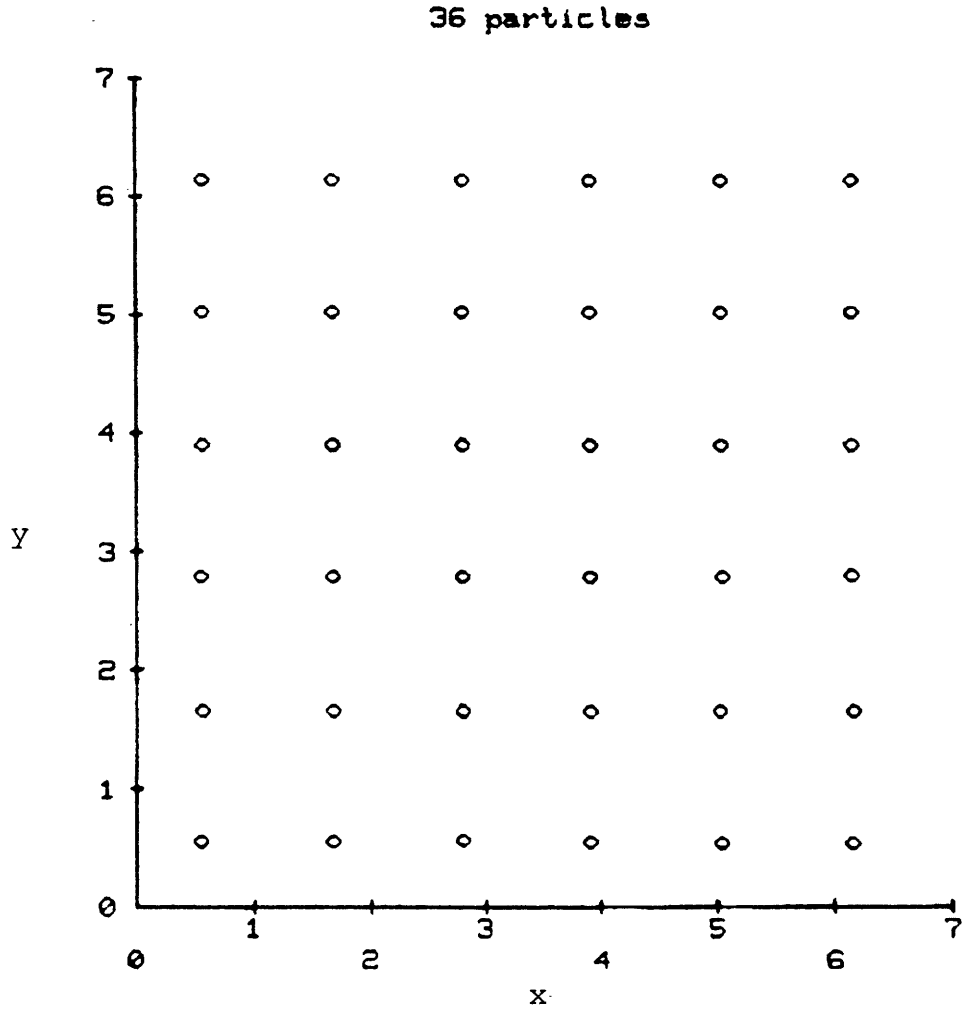

Figure 4-10. Initial square lattice at the beginning of the simulation.

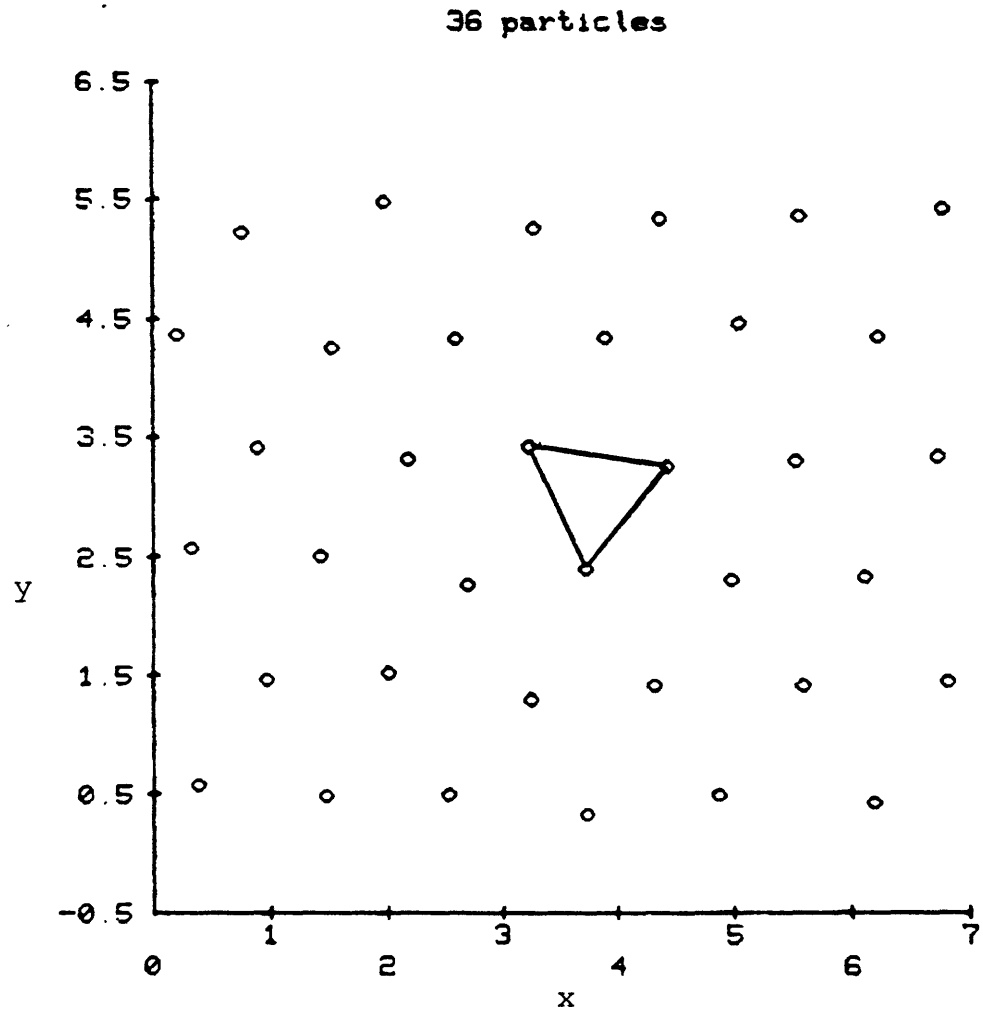

Figure 4-11. Final triangular lattice at the end of the simulation.

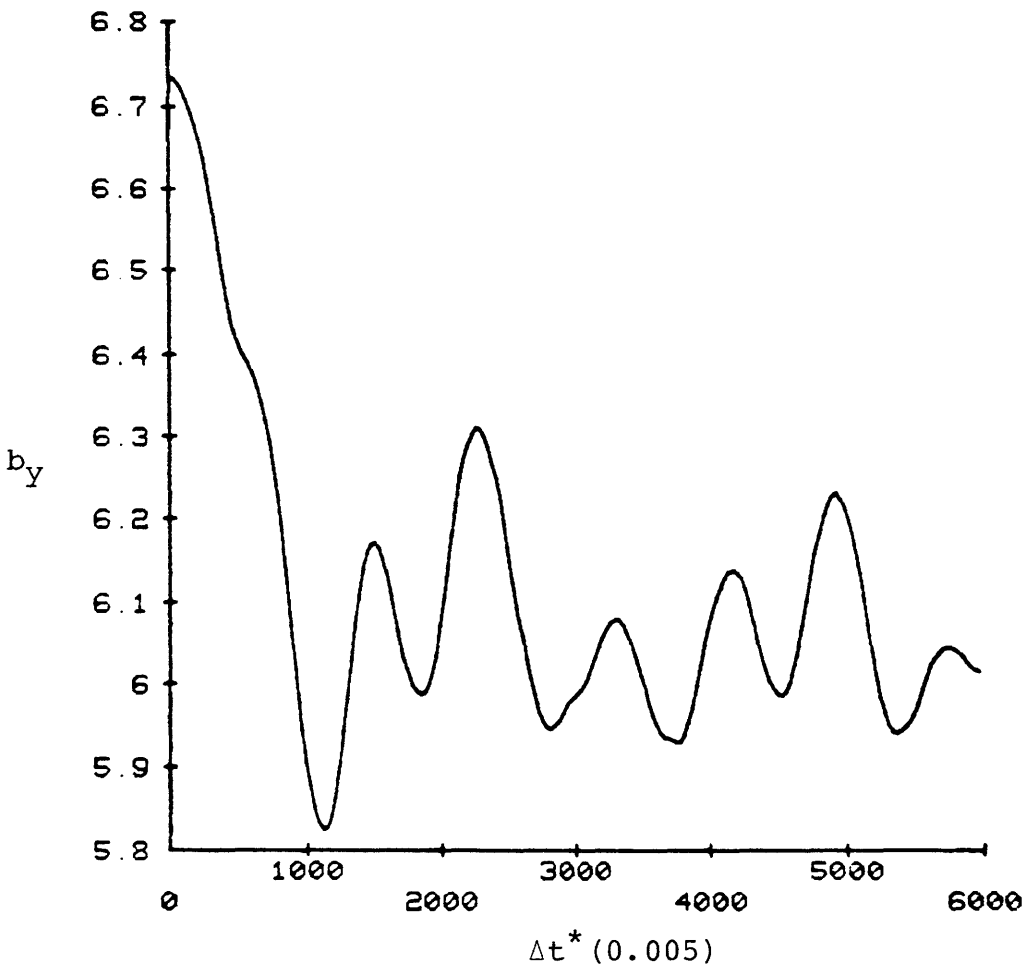

Figure 4-12. Time evolution of simulation cell length, b_y.

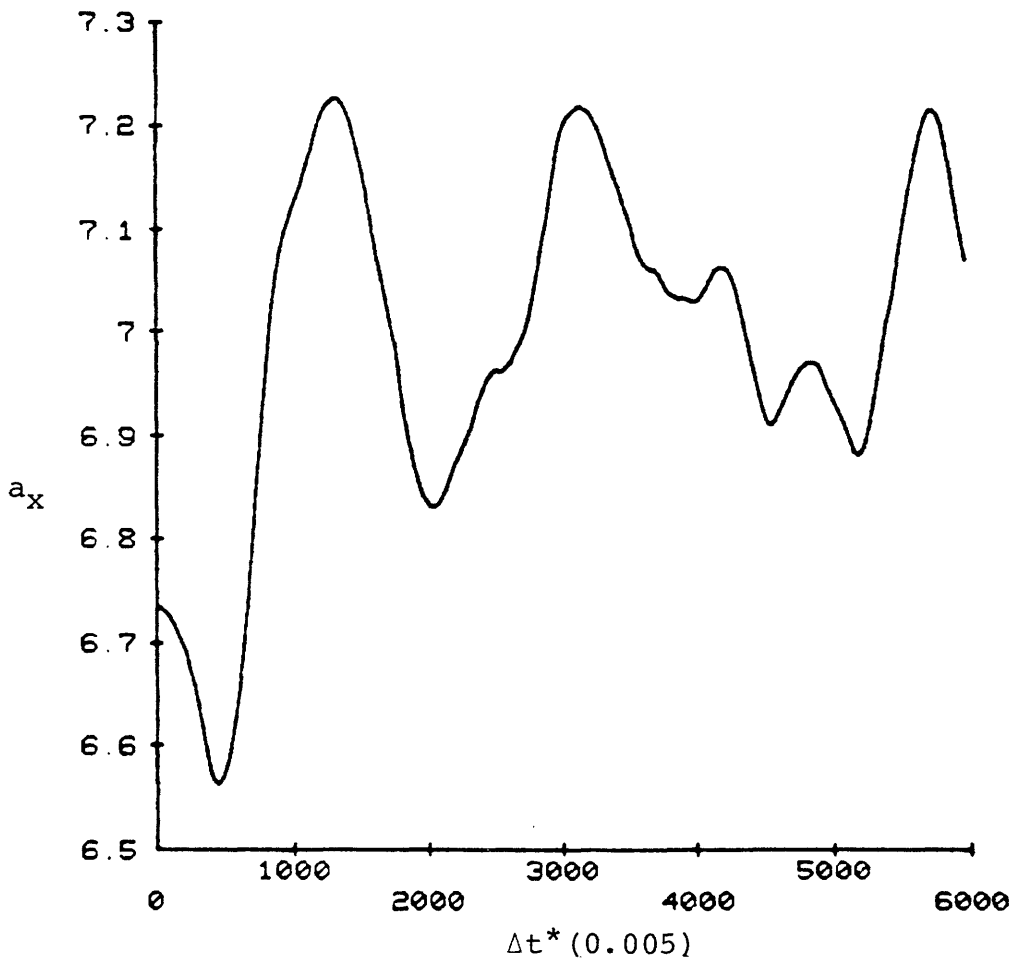

Figure 4-13. Time evolution of simulation cell length, a_x.

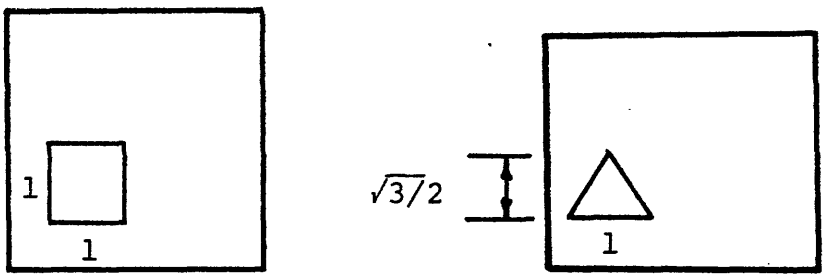

Since the height of an equilateral triangle is equal to 0.866 of its length, the cell has undergone such a change in its shape to satisfy this condition. The final ratio of the new average length of its boundaries 6.05/7=0.864 clearly indicates such a transition.

IV. HOOKE'S LAW CRYSTALS

A study of a piece-wise-linear force potential model is investigated in this section to seek structural phase transitions. A structural phase transition based on static energy calculations under the effect of hydrostatic pressure is reported by Hoover and Ladd (9). The potential is two piece-wise linear with three independent parameters; K, d_o, ω, of the form;

$$U(r) = \begin{cases} (1/2)K(r-d_o)^2 - K\omega^2 , & r<d_o+\omega \\ -(1/2)K(r-d_o-2\omega)^2, & d_o+\omega<r<d_o+2\omega \\ 0 , & d_o+2\omega<r \end{cases} \qquad (4.21)$$

Figure 4-14 shows a plot of U(r) and -U'(r) as a function of r. The force derived from this potential is continuous.

However its derivative is discontinuous at $r=d_o+\omega$. This aspect has a profound effect on the phase diagram of the model which will be discussed later in more detail. The force saturates at small values of r reaching a value of $K\left[\frac{d_o^2}{2}-\omega^2\right]$ in the limit r=0. This indicates that this potential has a soft repulsive core in contrast to a Lennard-Jones system where the potential takes a hard sphere behavior at small values of r.

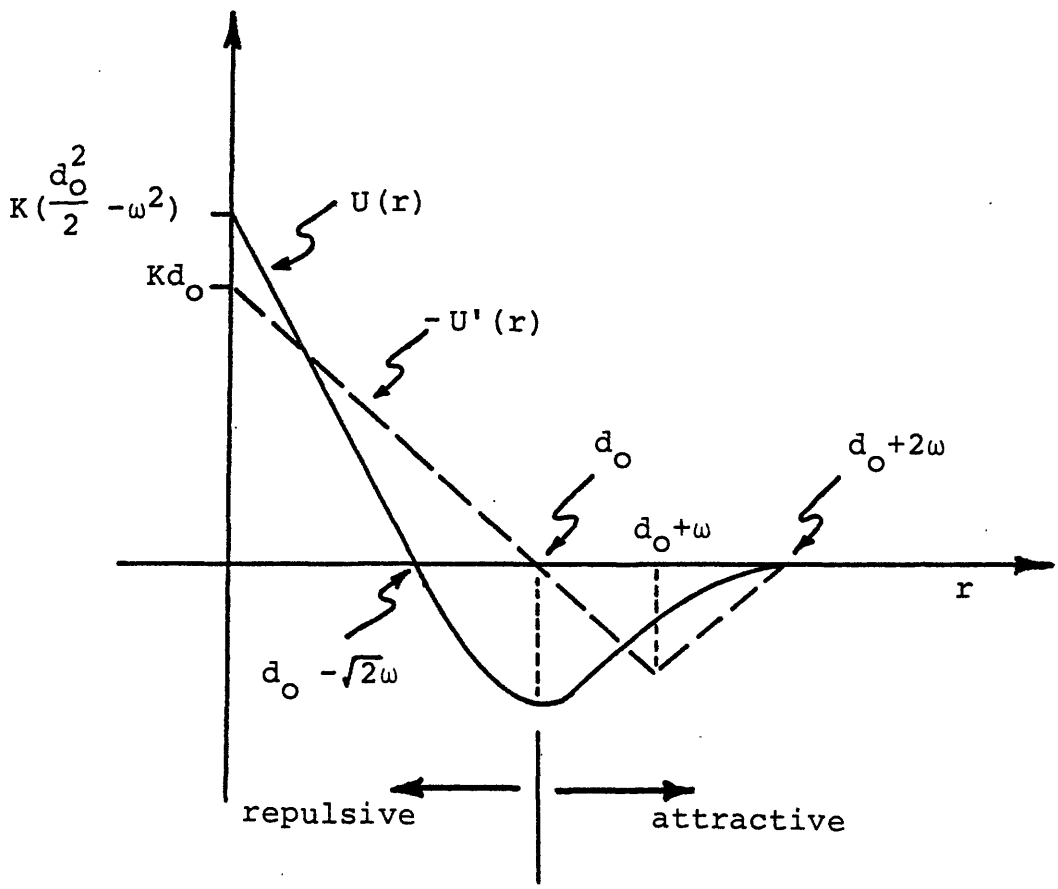

Figure 4-14. Plot of U(r) and -U'(r) as a function of r.

For all values of r less than $d_o+\omega$ (where the width ω is typically 0.15 d_o), this potential is equivalent to a purely harmonic Hooke's-law interaction. The reduced density $\rho^* = V_o/V$, where the two dimensional stress-free "volume" is $(3/4)^{\frac{1}{2}}Nd_o^2$. This V_o is exactly the volume occupied by N hard disks of diameter d_o in a close-packed triangular lattice. For a potential width ω=0.15 d_o, second-neighbor interactions would need to be included for densities greater than 1.78 in a triangular lattice.

According to Ladd and Hoover (9) a static calculation of energies for the piecewise-linear-force model, Eq. (4.21), with ω=0.15 d_o indicates a first-order triangular-to-square lattice transition at a pressure of 0.21 K with coexisting densities of 1.25 and 1.53. The square lattice, which is always unstable with just nearest-neighbor forces, is stabilized by second-neighbor interactions. Although we found that this is generally true based on static calculations, a transition from triangular to a square structure is not easily established. Figure 4-15 shows a plot of the potential energy for a 36 particle system as a function of nearest interatomic spacing, d. Indeed one can see that the square structure has the lower energy compared to the triangular one for $0.5<\frac{d}{d_o}<0.84$. Consider, for example, a density of 1.50. The nearest neighbor spacing is then 0.8165 d_o in the triangular lattice and 0.7598 d_o in the square lattice. With ω=0.15 d_o the second neighbors (at 1.4142 d_o in the triangular

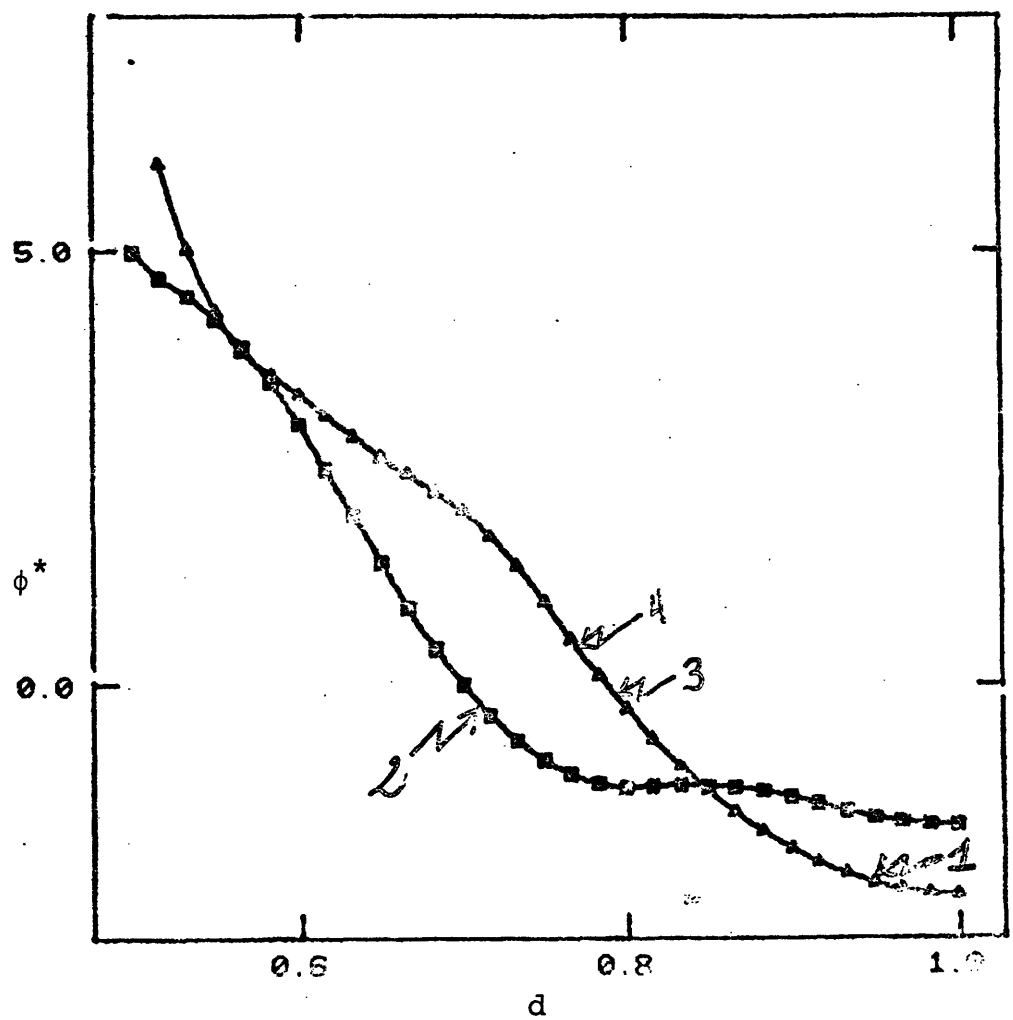

Figure 4-15. Potential energy of a thirty-six particle system as a function of nearest interatomic spacing, d.

case and 1.0745 d_o in the square case) lie within the range of the potential 1.3 d_o only in the square-lattice case. The energy per particle is $-0.0170\ Kd_o^2$ in the triangular case and $-0.0268\ Kd_o^2$ in the square case.

For densities $\rho^*>1$ and taking interactions up to the second nearest neighbor the pressure p derived as $\frac{1}{2}\ Tr(\underset{\simeq}{\pi})$, Eq. (4.11) is, for a triangular lattice,

$$p = \frac{\sqrt{3}}{d}\left[U_1'(d) + \sqrt{3}U_2'(\sqrt{3}d)\right] \tag{4.22}$$

and, for a square lattice,

$$p = \frac{1}{d}\left[U_1'(d) + \sqrt{2}U_2'(\sqrt{2}d)\right] \tag{4.23}$$

where U_1' and U_2' indicate potential derivatives evaluated for first and second nearest neighbors respectively. Similar formulas apply for higher densities with further neighbor interactions taken into account. Firugre 4-16 shows a plot of the total potential energy for a 36 particle system as a function of pressure in the range $0.5<d/d_o<1.0$. Sharp breaks in the behavior of the curve do occur at some specific points. We will specifically consider the points A and B labeled in the curves and discuss their significance at this point. Point A corresponds to an interatomic spacing $d = 0.75\ d_o$. At such a spacing the second nearest neighbor is at a distance of $1.30\ d_o$, which is the interaction range of the potential. Thus a break in the pressure curve is expected at this point due to the inclusion of an attractive

part to the potential opposing the repulsive interaction of the first nearest neighbor. Point B corresponds to an interatomic spacing $d = 0.66\ d_o$. At such a spacing the second nearest neighbor is at a distance of $1.15\ d_o$, where a break in the force behavior occurs. At this point, the force reverses its trend and starts increasing for smaller interatomic spacing indicating a sudden increase in the total pressure p of the system. Other sharp changes in the behavior of the curve can be explained by taking note of further interactions like third and fourth nearest neighbors. The interesting feature about this curve is that at a given pressure p, the system can exist in more than two unique states. At a pressure of $p = 0.4$, the system can exist in three distinct triangular structures corresponding to three different densities and another three distinct square structures as seen in Figure 4-16. Thus, for isobaric simulations, starting with a given high energy structure, the system can fall into more than one metastable state. This makes such structural phase transitions harder to observe with the system having different channels it can go through, some of which lead to a structure with the same symmetry.

We performed several simulations to study such a system. Table 4-1 gives a list of the major simulation runs which are also labeled in Figure 4-15. The simulations were all started at the corresponding equilibrium pressures for the

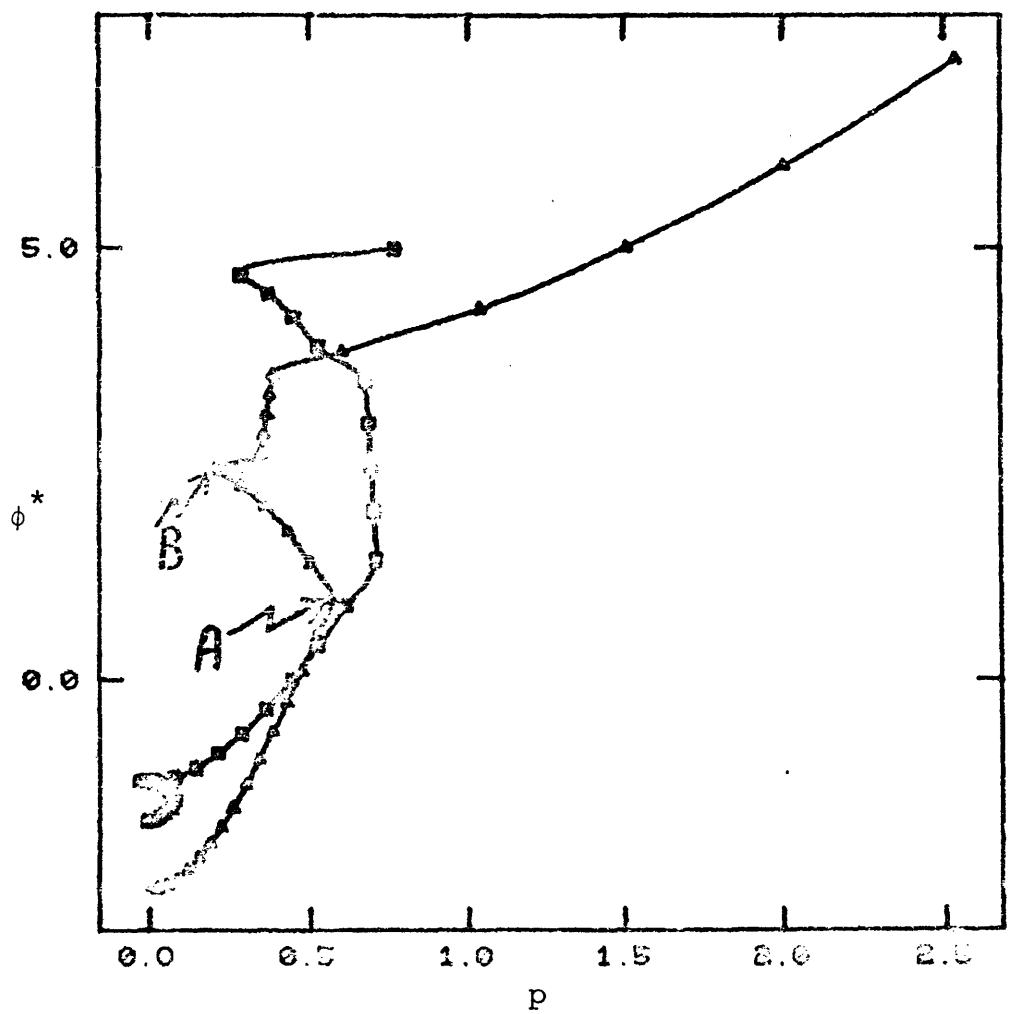

Figure 4-16. Potential energy of a thirty-six particle system as a function of the equilibrium pressure, p.

Table 4-1. Simulation runs for Hooke's law interaction

Simulation Number	Structure	d	ρ*	p*	T*
1	△	0.953	1.10	0.085	$5x10^{-5}$
2	□	0.703	1.75	0.422	$5x10^{-5}$
3	△	0.791	1.60	0.458	$5x10^{-5}$
4	△	0.749	1.78	0.576	$5x10^{-5}$

particular density considered. Simulation (1) established the stability of the triangular structure at ρ*=1.1. Since this is the lower energy structure this is expected. Figure 4-17 shows the average temperature, T*, behavior as a function of time. As noted the average temperature quickly equilibrates at half the initial value with the triangular structure being preserved. Simulation (2) established the stability of the square structure at ρ*=1.75. Figure 4-18 shows a similar behavior to that discussed previously. The average temperature quickly reaches a new equilibrium at half its initial value with the square structure being preserved. Simulation (3) was started with the triangular structure at a corresponding density ρ*=1.6. Based on the potential energy curves, the triangular structure is metastable at this density and one would expect it to roll out if the system is suitably perturbed. Figure 4-19 shows the average temperature behavior as a function of time. The temperature quickly equilibrates at half its initial value preserving the triangular structure.

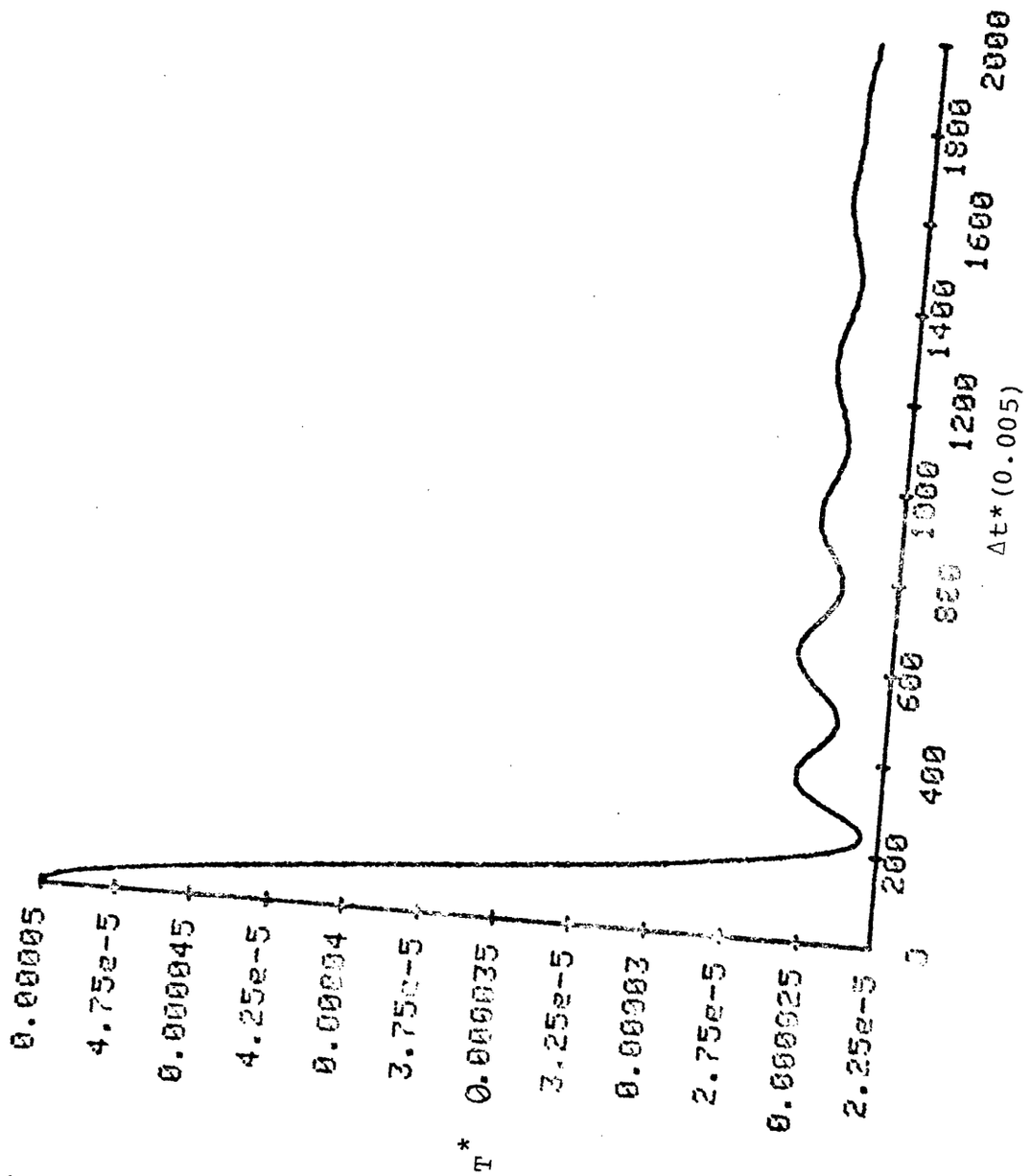

Figure 4-17. Average temperature as a function of time for simulation (1).

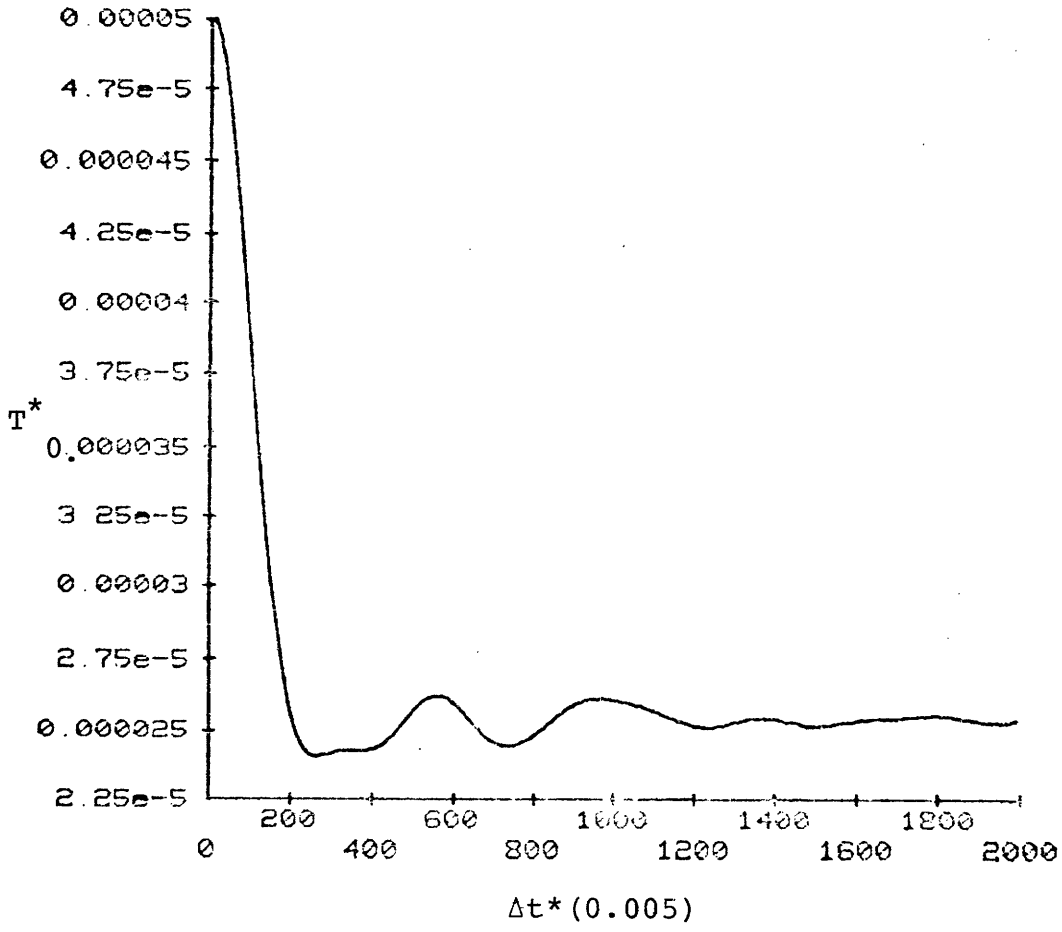

Figure 4-18. Average temperature as a function of time for simulation (2).

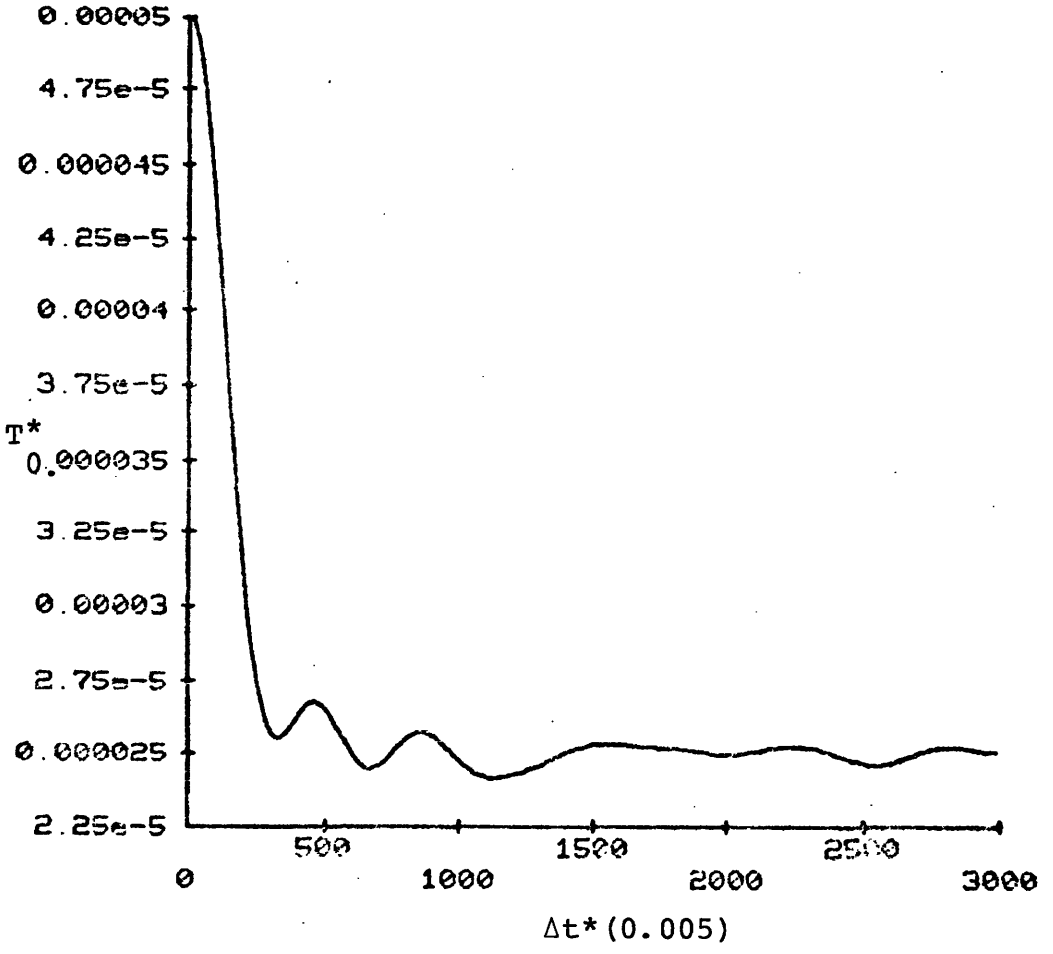

Figure 4-19. Average temperature as a function of time for simulation (3) .

This indicates that the potential barrier that the system has to cross before it reaches the lower square energy structure is rather significant. This is to be contrasted with the Lennard-Jones case, Section III, where a small perturbation was able to roll the system out of the metastable square structure and bring it to the lower energy triangular structure. This indicates that transitions with the piece-wise linear force model potential are not easily attained. Since such structural transitions depend mainly on the number of neighbors interacting with a given atom in the lattice, rather than on the potential form, it is expected that the system will have more difficulty in locating the lower energy structures that have the given particular neighbor configuration.

Simulation (4) was carried out at a density $\rho^*=1.78$. This density is of interest because second-neighbor interactions start to be included at such a density for a triangular lattice. Figure 4-20 shows the potential energy behavior as a function of time. One notes that the potential energy starts decreasing after 500 time steps and then starts suddenly increasing indicating melting. Monitoring the temperature behavior, Figure 4-21, indicates that the temperature maintains its constancy for the first 400 time steps and increases rapidly in the next 100 time steps. This indicates that the system is seeking a lower energy structure being unstable at the present one. So the potential energy decreases first trying to reach a more stable structure. Not

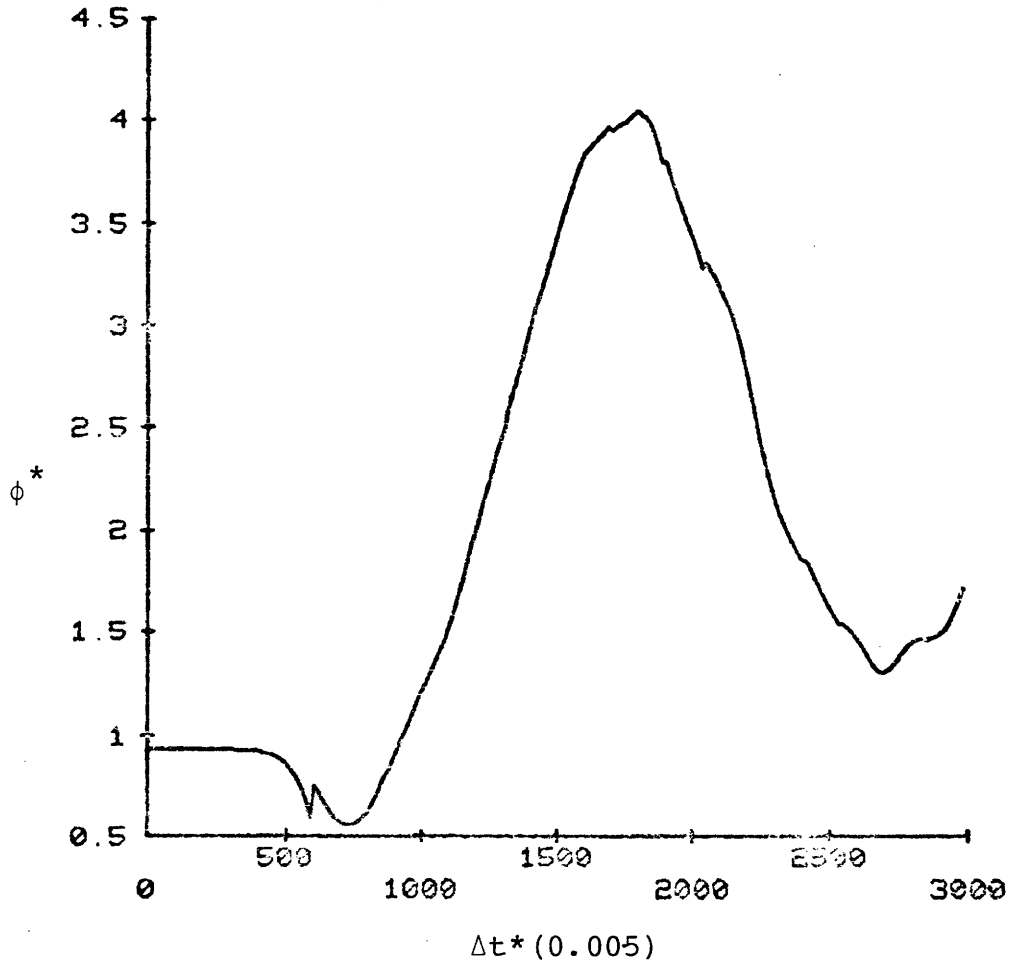

Figure 4-20. Potential energy of the system as a function of time for simulation (4) .

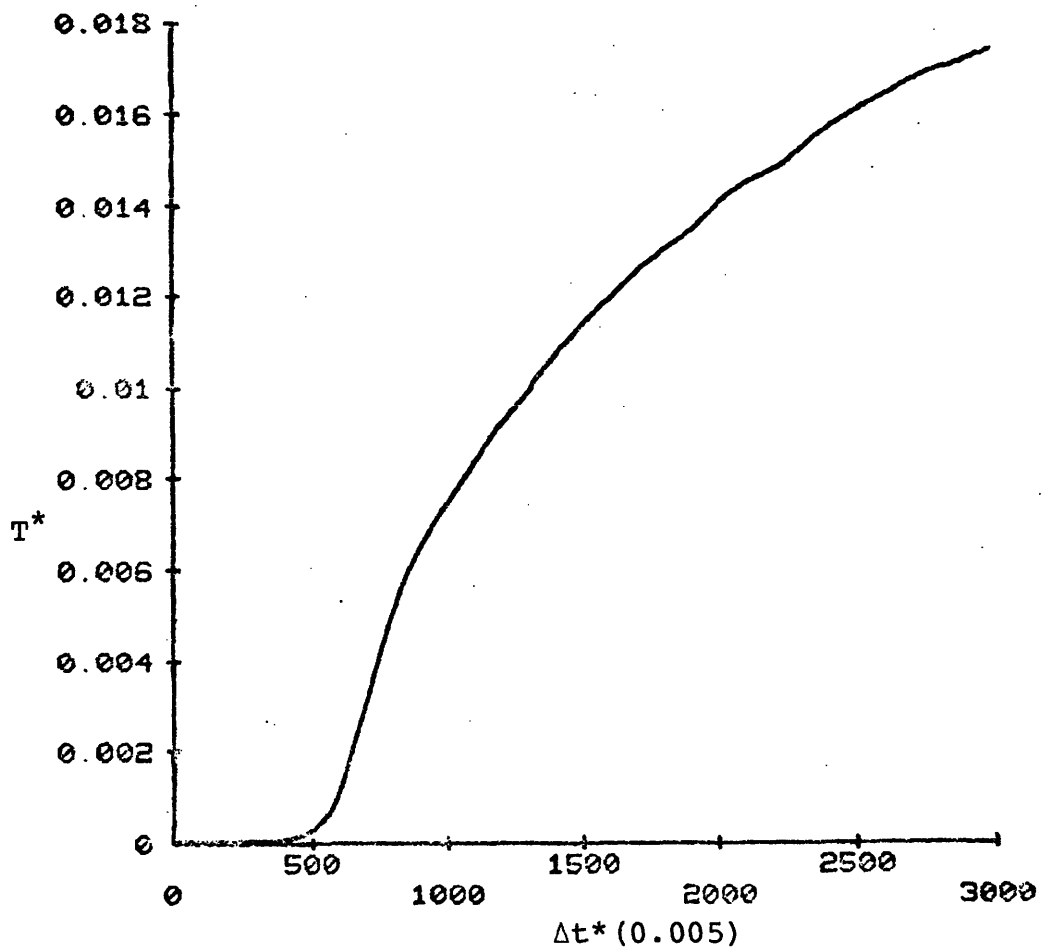

Figure 4-21. Average temperature as a function of time for simulation (4) .

able to locate that structure the system, with a sudden surge of energy, heats up and melts trying to reach a new equilibrium position.

The study of the piece-wise-linear force model given in this section indicates possible transitions from triangular to square structures and vice versa at a certain density range. Based on potential energy curves, Figure 4-15, one can expect to go from one structure to the other by perturbing the system properly. However, a more detailed study shows high nonlinearity in system properties using such a simple potential. As shown by Figure 4-16, the system can exist in more than one density at a particular pressure with the same structure. This feature is rather nonphysical indicating no unique equation of state. Such systems can be expected to have mechanical soft-mode instabilities over a wide density range. One is clearly indicated by Ladd and Hoover (9) at a density of 1.78. This makes the study of phase transitions in such a system rather difficult due to the presence of the highly unstable modes present in the system properties.

V. CONCLUSION

The periodic flexible boundary method for carrying out computer simulations appears to be a strong technique for investigating a broad new type of interesting physical problems. Structural stability and phase transitions are the most prominent for such studies. As we have noted the method was

a success in accounting for the well known stable triangular structure for a Lennard-Jones atomic system. The time evolution of the system was monitored thoroughly and a transition from the square to the triangular structure was detected.

Results for the piece-wise-linear force model indicate that the study of such a system to observe a transition is still possible if one neglects interactions beyond the second-nearest neighbor to smooth out the nonlinear effects in the phase diagram. The merit of this technique is its ability to simulate transitions under constant pressure which allows one to have a considerable control on the system behavior. Phase transitions in molecular systems can also be studied using such a technique. With the simulation cell being flexible in shape as well as volume, rotational and structural phase transitions are possible to investigate for such systems.

VI. REFERENCES

1. Beeler, J.R., Advances in Materials Research, ed. Herman, H.H., Wiley, New York, Vol. 4 1970.

2. Kushick, J. and Berne, B.J., Statistical Mechanics Part B; Time Dependent Processes, ed. Berne, B.J., Plenum Press, New York 1977.

3. Erpenbeck, J.J. and Wood, W.W., Statistical Mechanics Part B; Time Dependent Processes, ed. Berne, B.J., Plenum Press, New York 1977.

4. Wood, W.W., Physics of Simple Liquids, ed. Temperley, H. N.V., Rowlinson, J.S. and Rushbrooke, G.S., North-Holland, Amsterdam 1968.

5. Binder, K., Monte Carlo Methods in Statistical Physics, Springer, Berlin 1979.

6. Andersen, H.C., J. Chem. Phys. 72, 2384, 1980.

7. Parrinello, M. and Rahman, A., Phys. Rev. Letters 45, 1196, 1980.

8. Parrinello, M. and Rahman, A., J. Appl. Physics 52(12), 7182, 1981.

9. Ladd, A.J.C., Hoover, W.G., J. Chem. Phys. 74, 1337, 1981.

10. Hansen, J.P. and McDonald, I.R., Theory of Simple Liquids, Academic Press, London 1976.

Chapter 5

SUMMARY AND CONCLUSIONS

Our study indicates that the halogen crystals span a spectrum in their type of interactive forces. While iodine shows an interatomic interaction, chlorine shows a molecular behavior and bromine has both atomic and molecular properties. Charge interactions play a major role in removing the inherent instability in conventional isotropic central force potentials. This clearly indicates that interactions in the halogen crystals have an anisotropic character. Since an actual theoretical solution for the charge distribution in the halogen crystals is formidable at this stage, it can be approximated by a set of monopoles suitably placed near the nuclear centers. Computer molecular dynamics can play a very active role in such studies. The determination of minimum free energy structures for a given potential model at a finite temperature could be performed using flexible boundary conditions at constant pressure. Any future work in this field would be more valuable if utilized in the generation of more experimental data. In particular, the measurement of quadrupole moments, elastic constants, and phonon dispersion curves in iodine, bromine and chlorine would greatly enhance the theoretical work in this field.

The study of structural stability and phase transitions by computer molecular dynamics with flexible boundary conditions looks to be a very promising field. M. Parrinello

and A. Rahman have already demonstrated an FCC→HCP transition in nickel and $B_1 \rightarrow B_2$ transition in K^+Cl^- by applying this technique. Our work has shown a square to triangular transition for a two dimensional Lennard-Jones system. Possible transitions in Hooke's-Law crystals; square to triangular and vice versa should be sought. However, one should work in the density range $1<\rho^*<1.75$ to avoid the multiplicity of structure at higher density ranges. Transitions under the effect of applied shear are a possible route to follow in future work. This method could also be used in the study of structural and rotational phase transitions in molecular systems. Improvement of this technique should be pursued by damping the boundary motion. Inclusion of the term $\dot{\underline{\underline{h}}}\vec{s}$ in the velocity calculation would make the formalism more complete.